NDOT Research Report

Report No: RDT 97-019

IN-SITU STIFFNESS and DAMPING of SPREAD FOOTIMGS and PILE FOUNDATIONS in BRIDGES in NORTHERN NEVADA

August 2001

Prepared by Research Division
Nevada Department of Transportation
1263 South Stewart Street
Carson City, Nevada 89712

NEVADA DOT

TECHNICAL REPORT DOCUMENTATION PAGE

Report No. **RDT 97-019**	2. Government Accession No.	3. Recipient's Catalog No.
4. Title and Subtitle **In-Situ Stiffness and Damping of Spread Footings and Pile Foundations in Bridges in Northern Nevada**	5. Report Date **October 1997**	
	6. Performing Organization Code	
7. Author(s) **M. Saiidi, I. Darwish, G. Norris, E. Maragakis**	8. Performing Organization Report No.	
9. Performing Organization Name and Address **Department of Civil Engineering** **University of Nevada, Reno** **Reno, Nevada 89557**	10. Work Unit No.	
	11. Contract or Grant No. P498-94	
12. Sponsoring Agency Name and Address **Nevada Department of Transportation** **1263 South Stewart** **Carson City, Nevada 89712**	13. Type or Report and Period Covered January 1995 - To October 1997	
	14. Sponsoring Agency Code **NDOT**	

15. Supplementary Notes

16. Abstract

This report presents the results of an experimental and analytical study, which was conducted on three footings of an existing bridge in order to determine their in-situ stiffness. The bridge is located on Interstate 80 south east of Verdi, Nevada. Six tests were conducted by shaking each footing in the longitudinal and the short direction. Each footing was subjected to sinusoidal vibration force, which was applied through an eccentric mass shaker. Twenty-three accelerometers were used to measure the response of the soil, bridge footings, and the bent cap of the bridge during shaking.

A three-dimensional finite element model of the last two spans of the bridge was developed using computer program COSMOS//M. Then, a linear response history analysis was performed to determine the steady state acceleration response of the three footings. During the analysis, the soil-footing interaction was modeled using a spring-dashpot model. Several refinements were applied to the response history analysis until the predicted steady state peak acceleration at the footing level matched the measured steady state peak acceleration on the corresponding footing during the dynamic field test.

A design guideline and recommendations, which provide the basis for the computation of footing stiffness using spring models, were developed based on the experimental and the analytical results.

17. Key Words	18. Distribution Statement		
In-Situ Footing Stiffness, Footings, COSMOS/M, +	**Unrestricted. This document is available through the National Technical Information Service, Springfield, VA 21161**		
19. Security Classif is report) **Unclassified**	20. Security Classif. (of this page) **Unclassified**	21. No. Of Pages 155	22. Price

Abstract

This report presents the results of an experimental and analytical study, which was conducted on three footings of an existing bridge in order to determine their in-situ stiffnesses. The bridge is located on Interstate 80 south east of Verdi, Nevada. Six tests were conducted by shaking each footing in the longitudinal and the short direction. Each footing was subjected to sinusoidal vibration force, which was applied through an eccentric mass shaker. Twenty-three accelerometers were used to measure the response of the soil, bridge footings, and the bent cap of the bridge during shaking.

A three-dimensional finite element model of the last two spans of the bridge was developed using computer program *COSMOS/M*. Then, a linear response history analysis was performed to determine the steady state acceleration response of the three footings. During the analysis, the soil-footing interaction was modeled using a spring-dashpot model. Several refinements were applied to the response history analysis until the predicted steady state peak acceleration at the footing level matched the measured steady state peak acceleration on the corresponding footing during the dynamic field test.

A design guideline and recommendations, which provide the basis for the computation of footing stiffness using spring models, were developed based on the experimental and the analytical results.

Acknowledgments

This research was conducted under a grant from the Nevada Department of Transportation. The opinions expressed in this research belong solely to the authors and do not necessarily represent the views of the Nevada Department of Transportation (NDOT).

The authors would like to express their appreciation to Messrs. Mike Mayberry, Matt Randall, Cory Caywood, and Frank Martinovic, civil engineering students at UNR, for their assistance during the field testing. Special thanks are due Mr. Hernan Perez, a former graduate student at UNR, for conducting the geotechnical laboratory testing.

Mr. Jesus Pedroarena, the Civil Engineering Technician is also thanked for his valuable assistance in instrumenting and testing the bridge.

Table of Contents

List of Tables

List of Figures

Chapter 1

Introduction

1.1 Background

In evaluating the response of bridges to earthquakes, it is normally assumed that the bridge structure is fixed to a rigid base to which the free-field motion is applied (motion occurred at the soil-foundation interface in the absence of the structure). However, the response of a bridge to an earthquake is significantly affected by the ground condition at the bridge site due to soil-structure interaction. The structure always interacts with the surrounding soil, and therefore, increasing the system flexibility. This may produce an increase in structure response in one case and decrease in another, depending on the properties of the structure, the soil properties, and the earthquake excitation. Knowing the footing stiffness allows for better modelling of soil-structure interaction.

Spring-dashpot models and finite element models are used to represent the soil-footing system. Finite element models can provide realistic means of representing the soil under the foundation. This is mainly because they consider the nonlinear effects of the soil, the effects of foundation embedment, and variation of soil properties with depth. However, modeling the soil-structure system using finite element models is time consuming and impractical in most cases. As a result, simple models of spring-dashpot, which also account for these

In general, it is desirable to design bridges with fundamental periods of vibration larger than the predominant period of the seismic input in order to ensure that the bridge will escape the frequency range where the earthquake has greatest power (Fig. 1.1). Coupling between the structure and its supporting soil leads to a system that is characterized by a longer fundamental period (softer system) than the same structure with fixed bases. Therefore, consideration of soil-structure interaction, in general, will always tend to produce a decrease in the acceleration response (Fig. 1.1), and thus, provide an additional factor of safety. On the other hand, the elongation of the period of vibration of a bridge tends to increase the bridge displacement, compared to similar bridges with fixed bases. In this case, including the flexibility of footings in the analysis, may increase the required spacing between adjacent bridges in order to prevent pounding damage. In addition, it may increase the effect of the secondary forces in columns, associated with P-Δ effects, and therefore, decrease the lateral load capacity of the bridge columns (Fig. 1.2).

Soil-structure interaction consists of two distinct effects: kinematic interaction and inertial interaction[6, 7]. Kinematic interaction occurs when the free-field motions are constrained by the presence of the foundations. Kinematic interaction effects are generally insignificant when the wavelengths in the free-field motions are greater than the dimensions of the foundation[6]. In this case, the foundation will have very little effect on the soil, and the foundation motions will

be the same as the free-field motions. Inertial interaction arises due to the transmission of inertia forces from the structure to the soil during an earthquake. These forces induce a deformation in the soil in addition to the one existing in the free field. Veletsos and Prasad[42] reported that kinematic interaction and inertial interaction may significantly affect the responses of systems in the medium- and high-frequency regions. However, the inertial interaction effects are greatly more important than kinematic interaction effects. In this study, only the inertial interaction was accounted for. This is because in the dynamic field testing, the soil is strained by the inertia forces from the structure.

1.2 Previous Work

There are several analytical and experimental researches that have been conducted in order to compute the dynamic stiffness and the seismic response of footings.

Dobry and Gazetas[8] conducted an analytical study to compute the effective dynamic stiffness and dashpot coefficients for arbitrarily shaped, rigid surface machine foundations placed on homogeneous and deep soil deposits. In their study, they proposed a method in the form of simple algebraic formulas and dimensionless charts, which can be used to compute the foundation stiffness and the radiation damping coefficients for the all modes of vibration. The proposed method was based on a comprehensive compilation of several analytical studies.

The method is applicable to different foundation shapes, including circular, strip, and rectangular footings. In this method, the footing stiffness coefficients depend on the frequency of loading but are independent of the variation of soil shear modulus with shear strain. This is mainly because in machine vibration problems, very small strains are expected in the soil. The results of this study confirmed that both frequency and foundation shape have significant effects on the dynamic foundation stiffness and on the foundation damping, with the effect being greater for long foundations and saturated soils.

Dobry et al.[9] used the results of twenty-one free vibration tests on surface model footings to verify their analytical method presented in Ref. 8. In the experimental program, seven concrete blocks of identical contact surface areas (A = 110 in^2 = 710 cm^2) and heights (h = 18 in. = 45.7 cm) were cast-in-place on the surface of a moist, dense sand and were subjected to vertical, torsional and rocking vibrations. Two of the footings were circular, one was square, and three were rectangular. Initially, all the footings had similar total weights, W = 180 lb. (800.7 N). In addition, the tests were repeated after attaching symmetrical weights, for total foundation weights of W = 240 lb. (1067.6 N) and W = 300 lb. (1334.5 N). This was done in order to change the natural frequencies of each footing without varying its geometry. With the seven concrete blocks, twenty-one different free vibration tests were performed in each mode. All footings were placed on top of cylindrical mass of uniform, moist, dense sand 5 ft (1.5 m) deep and 10 ft (3 m) in

diameter. Close agreement was found between the predicted and measured frequencies in all cases, and also between damping ratios in the vertical and torsional vibrations. In addition, the results of the vibration tests provided a strong support for the analytical method presented in Ref. 8.

Levine and Scott[27] developed a simplified method to find the rotational boundary stiffnesses, which represent the foundation of a structure and its surrounding soil. This method was applied to the Meloland Road overpass, for which records were obtained during the 1979 Imperial Valley earthquake. This bridge is a two-span continuous reinforced concrete structure supported on a single column pier. The bridge has an integral abutment. A very simple 3-D beam model for the bridge was constructed. To represent the boundary conditions of the model, rotational springs at the ends of the deck and at the pier base were used. No translational springs were used since the measured translational motions of the abutments and at the column base were used as the input earthquake excitation. The purpose of the study was to compare the actual dynamic properties of the bridge with those predicted with the simple model. The seismic response characteristics and the dynamic properties of the bridge were determined using a system identification technique developed by Beck[2]. This technique, which was applied to the array of the strong motion measurements, yielded an excellent fit to the measured motions of the bridge. A sensitivity analysis was also performed on the rotational boundary springs to study their effect on the dynamic response of the

bridge. In this study, it was concluded that the modal frequencies of the finite element model with rotational boundary springs compared well with the results obtained through system identification, even though a simplified model was used. The authors also recommended applying their simplified method for the computation of the rotational foundation stiffnesses in conjunction with system identification techniques to strong motion records in order to obtain boundary spring models for the foundations. The results of the sensitivity analysis indicated that varying the rotational stiffnesses of the pier about the transverse and the longitudinal axes of the bridge affected the pier deflection but only changed the transverse deck mode. However, changing the rotational stiffness of the pier about the vertical axis of the bridge did not have any effect on either the vertical or transverse mode.

Vrontinos[45] constructed a 3-D finite element model of the Meloland Road overpass, which was subjected to an earthquake in 1979. The model used 3-D line beam elements to represent the superstructure, and a 3-D array of spring elements at each of the abutments and at the pier foundations support to capture the soil-structure interaction. The main objectives of this study were to use the results obtained from a quick-release field testing of the bridge[12] in order to obtain the dynamic stiffnesses at the bridge abutments and pier foundations, and to calibrate the model based on the dynamic test results and the strong motion records obtained at the bridge site during the 1979 Imperial Valley earthquake.

A system identification technique was performed by fitting the model to a complete series of measured static and dynamic response data collected during full-scale quick-release ram field tests[12]. The study also included fitting the calibrated model to the bridge earthquake response records collected during the 1979 earthquake. The study obtained the effective values of the soil springs (stiffnesses) and several additional bridge structural design parameters controlling the bridge response under earthquake loading. The results of the system identification study showed that the linear finite element model was adequate in capturing the non-linear behavior of the bridge at low to moderate vibration amplitude. Also, a high damping ratio value of 22.6 % was obtained from the system identification study using the response records. The high damping ratio value was attributed to the damping soil behavior of the abutment backfill.

Another study was performed to verify the sensitivity of the response to different soil spring values. In this study, all the soil spring values at both the abutments and the pier foundation were taken as a single group of springs. The values of all the springs were then varied at the same time and by the same percentage amount. They were set equal to 0.1, 0.5, 0.75, 1.5, and 5.0 times their optimum values obtained from the system identification technique. The results of this part of the study indicated that the variations of soil springs have a significant effect on the deformations of the bridge. The deck displacements and rotations showed a large increase or decrease depending on the soil springs. A decrease in

the values of soil springs by 50 % led to an increase of up to about 80 % in the maximum deck displacements.

1.3 Objective and Scope

The main objective of this study was to develop a simple and rational procedure for the computation of stiffness for spread footings supporting bridges.

The focus of the study was on three rectangular footings of an existing bridge located on Interstate 80 south east of Verdi, Nevada. Each footing was subjected to dynamic forces through an eccentric mass shaker once in the long and then in the short direction of the footing. The test results and the analytical studies conducted on the three existing footings were used to recommend a simple integrated procedure to compute the footing stiffness.

1.4 Research Significance

Soil-structure interaction can significantly affect the dynamic response of bridges. This research provides an effective means to enhance the computation of footing stiffness. The approach recommended in this study is more realistic and consistent than other methods. It includes means of accounting for the strain-dependence of the soil shear modulus and other important factors such as footing embedment and presence of bedrock, which significantly affect the soil-structure interaction.

Chapter 2

Experimental Studies

2.1 Introduction

The experimental program included the shaker testing of three existing spread footings of an eleven-span steel girder bridge. The bridge is located on Interstate 80 south east of Verdi, Nevada. Each footing was subjected to sinusoidal vibration through an eccentric mass shaker in both directions of the footing. The shaker was attached to the footing through high strength bolts that were anchored to the footing. In addition, accelerometers were used to measure the response of the soil, bridge footings, and the bent cap of the bridge during shaking.

This chapter includes the bridge description, equipment, instrumentation, and testing procedure used in experimental program.

2.2 Bridge Description

The bridge tested as part of this research (IR 080-WA 5.45 G-772 W) is located on the Interstate 80 south east of Verdi. The bridge, shown in Fig. 2.1, consists of an eleven-span steel girder superstructure with an overall length of 974.25 ft (297 m) measured from the center of WB1 to the center of WB12, and a total width of 43 ft (13.10 m). The steel girders are continuous over bents WB3,

WB4, and WB5 (Fig. 2.1). However, they are simply supported over the other bents. The bridge carries two lanes of westbound traffic over a railroad crossing and the Truckee River. There is no skewness except at the last five bents of the bridge (bent WB8 to bent WB12 in Fig. 2.1), where the bridge is skewed at an angle of 35 degrees.

As shown in Fig. 2.2, the superstructure consists of seven built-up steel girders, which are equally spaced at 6'-4" (1.90 m) on center. The steel girders have depths and plate thickness that vary over the span of the bridge. The concrete deck is 7 inches (180 mm) thick.

The focus of the study was on the footings of bent WB11 shown in Fig. 2.3. Each column was retrofitted for earthquakes by using a 1/2-inch (13 mm) thick circular steel jacket with an inner diameter of 5'-1" (1549 mm). The steel jacket has a height of 21'-8" (6604 mm). A 2-inch (50 mm) gap was left between the top of the steel jacket and the bottom of the bent cap and between the bottom of the jacket and the top of the footing. The columns are rigidly connected to their footings. The footings are embedded 5.5 ft (1676 mm) into the soil, where the depth of embedment is measured from the grade level to the bottom of the footings. The bent cap was also retrofitted by increasing its length and width, and by adding shear keys between the steel girders to restrain their lateral movements (Figs. 2.3 and 2.4). According to AASHTO[47], the bridge is located in a seismic area with a maximum acceleration coefficient, A, of 0.37.

2.3 Test Setup

A shaker system model "MK-12.8A-4600" by Anco Engineers, Inc.[20], was used during the test to apply sinusoidal vibration to the footings. It consists of an eccentric mass, a drive motor, a frequency inverter with a remote operator's station, interconnecting cabling, and flexible shafting. The mass shaker consists of matched sets of eccentric weights that rotate in opposite directions about parallel vertical shafts. Two match sets of weights are provided with the shaker, a 4,600 lb-in. (520 KN-mm) eccentric mass set and a 980 lb-in. (111 KN-mm) eccentric mass set. Each set consists of six weights; three of these weights form a left stack and the other three form a right stack. Eccentricity of the shaker is continuously adjustable over the ranges 0-980 lb-in. (0-111 KN-mm) and 0-4,600 lb-in. (0-520 KN-mm).

During the test, a 4,600 lb-in. (520 KN-mm) eccentric set of weights was used to achieve higher forces at low frequencies. With the large weight set installed, the force output is limited to 10,000 lb. (44.5 KN) continuously, and 20,000 lb (89 KN) intermittently at frequencies less than 10 Hz. The direction of the force vector resulting from the shaker operation can also be adjusted to any direction in a horizontal plane by rotating the left set of weights relative to the right set.

The following expression was used to relate the output force to running speed and eccentricity[20]:

$$WR = \frac{F}{0.102(X)f^2} \text{ lb - in.}$$
$$WR = \frac{F}{0.004(X)f^2} \text{ KN - mm} \qquad (2.1)$$

where WR is the maximum eccentricity (lb-in. or KN-mm), F is the output force (lb or KN), X is a fraction of maximum eccentricity, and f is the running speed (Hz). Since it was decided to use the 20,000 lb. (89 KN) maximum force capacity of the shaker with the 4,600 lb-in. (520 KN-mm) moment, a maximum running speed of 6.5 Hz was achieved during the test. Figure 2.20 shows the maximum operating limits for the mass shaker.

The shaker was attached to each footing by a 1-in. (25 mm) thick A36 steel base plate and stud-type anchors (Fig. 2.5). The mass shaker was attached to the base plate by ten 5/6-in. (21 mm) diameter Grade B7 studs that were welded to the base plate. Each stud had a length of 6-in. (152 mm) above the top surface of the base plate. The base plate was attached to each footing through ten 1.0-in. (254 mm) diameter Grade B7 stud-type anchors (Fig. 2.5). The anchor bolts were 24-in. (610 mm) embedded into the footing. A high-strength epoxy adhesive was used to anchor the studs to the footings. A 1/2-in. (13 mm) thick gypsum cement grout (hydrostone) was used between the base plate and the footing for leveling.

Twenty-three accelerometers model "FBA-11" by Kinemetrics, Inc. were used to measure the soil, bridge footings, and bent cap response during the test. The accelerometers have a full range of 4g and a sensitivity of 0.0008g, where "g"

is the gravity acceleration. To get clear sinusoidal acceleration during the test, the attenuator settings of the accelerometers were adjusted at 12 dB. This setting was predetermined before starting the test by running the mass shaker, which was attached to one of the footings at 6.5 Hz. Then, the attenuator setting was changed until it was possible to measure a clear sinusoidal response. Appendix A shows the analog sensitivity for the accelerometers used during the dynamic field testing.

In order to calculate the peak recorded acceleration in "g", the following equation was used:

$$A_{max} = \frac{4\,a}{2.5\left(2^{n-1}\right)} \tag{2.2}$$

where A is the peak recorded acceleration (g), a is the peak recorded amplitude (volts), and n is a number corresponding to the attenuator setting.

Eighteen ground acceleration stations measuring 8" x 4" (203 mm x 102 mm) located on the soil around the footings were used during the test. Those stations were used to mount the accelerometers that measure the soil acceleration response during the test. Figure 2.6 shows the layout of the ground acceleration stations. Six tests were conducted by shaking each footing once in the long and then in the short direction of the footing. Each test was repeated at least twice to have redundancies in the data.

During each test, eight accelerometers were mounted on pre-assigned ground stations (active ground stations) to measure the soil response. The accelerometers were flush with the soil surface. The eight accelerometers were

moved from one set of ground stations to another, depending on the footing being tested. Figure 2.7 shows the ground accelerometer location and numbering during the test of footing I in the longitudinal direction of the footing.

Twelve accelerometers were mounted on the surface of the three footings to measure the acceleration response of the footings during the tests. The top surface of three footings was exposed by removing the overburden soil that was 2 ft (610 mm). However, the soil was left intact between the sides of the footings and the surrounding soil. On each footing, two accelerometers were used to measure the footing acceleration in the longitudinal direction of the footing, while the other two accelerometers were used to measure the footing acceleration in the short direction of the footing. The accelerometers were located at 3 inches (76 mm) from the mid-sides of the footings. However, accelerometers located on the side of the eccentric mass shaker (east side of footings) were mounted at 3 inches (76 mm) from the short and long edges of the footings. Figure 2.8 shows the location and numbering of footing accelerometers during the test of footing I in the longitudinal direction.

To measure the acceleration response of the bent cap, three accelerometers were used. Two accelerometers were mounted on the far right side of the bent cap; one to measure the acceleration in the longitudinal direction of the bent cap, and the other to measure the acceleration in the transverse direction. However, on the far-left side of the bent cap, only one accelerometer was used to measure the

response in the short direction of the cap. Figure 2.9 shows the location and the numbering of bent cap accelerometers. The bent cap accelerometer location did not change during different shaker tests. Figures 2.7 through 2.19 show the numbering and the location of ground and footing accelerometers used during the test of three footings in the longitudinal and the short directions of the footings.

2.4 Test Procedure

An operator station was used to control the shaker tests. The testing procedure was identical for all shaker runs. The first step was to gradually increase the frequency of the shaker until reaching a predetermined frequency of approximately 6.5 Hz. At this amplitude, the total cyclic force was approximately 20,000 lb. (89 KN). Then, the attenuator setting of the accelerometers was adjusted until a clear sinusoidal acceleration could be measured. Once there were no trucks crossing the bridge, the computer was triggered to record the test data for approximately two minutes. At least two sets of data were recorded during each test in order to check the collected data against errors. After each test, the locations of the eight ground accelerometers were changed according to their pre-assigned locations. In addition, the weights located inside the mass shaker were rotated to change the direction of shaking.

Chapter 3

Test Results

3.1 Introduction

The experimental program included testing of three footings of an existing bridge. The footings are rectangular and measure 13 ft (3.96 m) by 9 ft (2.74 m) and have a depth of 3-ft (914 mm). In addition, they are embedded 5.5 ft (1.67 m) into the soil. Each footing was subjected to a sinusoidal vibration force of amplitude of approximately 20,000 lb (89 KN) at a frequency of 6.5 Hz in the long and in the short direction of the footing. The dynamic forces were applied through an eccentric mass shaker that was mounted on the surface of the footing.

Twenty-three accelerometers were used to record soil, footings, and bent cap responses during the tests. For each footing and in each direction, soil response and the footing response are presented in this chapter. The measured responses represented the most important data recorded during each test, and were used to determine the dynamic footing stiffness, as presented in following chapters.

As mentioned in the previous chapter, the accelerometers used during the tests have a full range of 4g and a sensitivity of 0.0008g. Therefore, any accelerometer record with a peak of less than 0.0008g are not shown.

3.2 Bent Cap Response

Three accelerometers were installed on the bent cap during each test (bent WB11, Figs. 2.1 and 2.3). Two of the accelerometers were used to record accelerations in the longitudinal direction of the bridge, while the other was used to record accelerations in the transverse direction (Fig. 2.9).

During the test, accelerations recorded on the bent cap were very small and less than the sensitivity of the accelerometers. This was because shaking of the footing caused insignificant vibration of the bent cap. Also, the small accelerations recorded were mainly governed by the traffic crossing the bridge during the recording time. Therefore, the results of accelerations recorded on the bent cap were excluded from the test results and the analyses. This did not affect the main objective of the study, since the scope was on the acceleration response of the three existing footings and the determination of their in-situ stiffness corresponding to the applied dynamic force.

3.3 Shaking of Footings in the Longitudinal Direction

Footings I, II, and III were subjected to harmonic forces of 19.16 kips, (85.23 KN), 19.17 kips (87.6 KN), and 20.00 kips (89 KN), respectively, in the longitudinal direction of the footings. The forces were applied at frequencies of 6.19 Hz, 6.49 Hz, and 6.52 Hz, respectively. During the shaking of each footing, accelerometers mounted on soil, adjacent footings, and the bent cap recorded small

accelerations, and some of their peak values were less than the sensitivity of the accelerometers. However, accelerations recorded on the tested footings were adequate to predict the in-situ footing stiffness. Tables 3.1, 3.3, and 3.5 show maximum measured steady state acceleration response of soil and footings in the longitudinal direction.

3.3.1 Soil Response

Eight ground accelerometers were active during the shaking of each footing in the longitudinal direction (Fig. 2.7, 2.12, and, 2.16). Three accelerometers were directed perpendicular to each long side of the footing, and the other two accelerometers were directed perpendicular to the short side of the footing. The accelerometers were spaced at 5' (1524 mm) on center.

Figures 3.1, 3.3, and 3.5 show the measured peak steady state soil acceleration response during the testing of each footing in the longitudinal direction. During the test, ground accelerometers that were perpendicular to the direction of the applied force recorded very small accelerations. This was mainly due to the uncoupling of short and long direction vibration.

Ground accelerometers along the short sides of footings I, II, and III recorded maximum steady state acceleration amplitudes of 0.0023g (accelerometer DIL4), 0.0029g (accelerometer IIL4), and 0.0024g (accelerometer NIIIL4), respectively. However, accelerometers EILS, JIILS, and OIIIL5, which were,

located 5' (1524 mm) from accelerometers DIL4, IIL4, and NIIIL4, recorded maximum steady state acceleration amplitudes of 0.00088g, 0.0012g, and 0.001g, respectively. These were approximately 61 percent, 59 percent, and 58 percent less than the maximum steady state accelerations recorded by accelerometers DIL4, IIL4, and NIIIL4, respectively. The decrease in accelerations indicates the attenuation of accelerations with the distance from the vibration source. Accelerations recorded represent the soil response at the ground surface.

There was 26 percent increase in the measured peak steady state acceleration along the short side of footing II than the accelerations measured along the short side of footings I and III. The variation in the measured accelerations indicated that the soil along the longitudinal direction of footing II is slightly softer than the soil along the longitudinal direction of footings I and III. This is supported by the fact that the soil near the ground surface and under the footings are randomly mixed with cobbles, which vary in sizes from small to considerably large cobbles.

3.3.2 Footing Response

Figures 3.1, 3.3, and 3.5 show the maximum measured steady state acceleration response of footings I, II, and III, respectively, in the longitudinal direction of the footings.

During the shaking of each footing, accelerometers mounted on the other

two footings recorded very small accelerations. During the test of footings I and III, the two accelerometers mounted on the long sides of each footing recorded an equal maximum steady state acceleration of 0.0033g. However, during the test of footing II, they recorded an equal maximum steady state acceleration of 0.00355g. Therefore, there was a 7 percent increase in the measured peak steady state acceleration on footing II in the longitudinal direction than that measured on the other two footings.

The increase in the measured acceleration was mainly due the fact that the soil along the longitudinal direction of footing II is slightly softer than the soil along the longitudinal direction of footings I and III. This was also supported by the fact that the measured peak steady state acceleration along the short side of footing II is 26 percent more than the accelerations measured along the short side of footings I and III (Sec. 3.3.1).

3.4 Shaking of Footings in the Short Direction

Footings I, II, and III were subjected to harmonic forces of 18.90 kips (84 KN), 19.50 kips (86.7 KN), and19.50 kips (86.7 KN), respectively, in the short direction of the footings. The forces were applied at frequencies of 6.36 Hz, 6.45 Hz, and 6.45 Hz, respectively. Since the dynamic forces applied to the footings were small, accelerometers mounted on soil, adjacent footings, and the bent cap recorded small accelerations, and some of the peak values were less than the

sensitivity of the accelerometers. However, accelerations recorded on each of the tested footings were sufficiently large to predict the in-situ footing stiffness. Tables 3.2, 3.4, and 3.6 show the measured peak steady state acceleration response of soil and footings in the short direction.

3.4.1 Soil Response

Eight ground accelerometers were active during the shaking of each footing in the short direction (Figs. 2.10, 2.14, and, 2.18). Figures 3.2, 3.4, and 3.6 show the measured peak steady state soil acceleration response during the testing of each footing in the short direction. During the test, ground accelerometers that were perpendicular to the direction of the applied force recorded very small accelerations mainly due to the uncoupling of short and long direction vibration.

Notice the consistency between the measured peak steady state accelerations on the soil between the three footings during the shaking of the footings in the short direction (Figs. 3.2, 3.4, and 3.6). There were very small variations in the measured accelerations on the soils among the footings. This indicated that there were no significant changes in the soil properties along the short direction of the footings. However, the soil directly along the long sides of footing III was stiffer as indicated by the decrease in the measured peak steady state acceleration than the measured accelerations along the long sides of the other two footings. This was mainly because the soil along the south side of footing III

was directly exposed to the sunlight. This increases the capillary tension in the soil due to the high soil suction. The increase in the capillary tension can increase the effective stresses in the soil, and therefore, increase the soil shear modulus.

3.4.2 Footing Response

Figures 3.2, 3.4, and 3.6 show the measured peak steady state acceleration response of footings I, II, and III, respectively, in the short direction of the footings. The average measured peak steady state accelerations on footings I, II, and III were 0.00365g, 0.00365g, and 0.00325g, respectively. The average acceleration recorded on footing III was approximately 10 percent less than the average accelerations measured on footings I and II. This is in agreement with the fact the soil along the long sides of footing III was stiffer than the soil along the long sides of the other two footings (Sec. 3.4.1).

Note the difference between the recorded accelerations of the two accelerometers mounted on the short sides of each footing (Figs. 3.2, 3.4, and 3.6). This was mainly due to the torsional moments induced during the tests. To shake the footings in the short direction, it was not able to attach the shaker to the center of the footings due to the presence of the bridge columns. Therefore, the shaker was attached to the east sides of the footings and the dynamic forces were applied to the footings with an eccentricity of 53-in. (1346 mm), measured from the center of the shaker to the center of the column (Fig. 2.5). This induced a maximum

torsional moment of approximately 1023 kip-in. (115578 KN-mm) at the center of the column. The torsional moment led to the increase of the measured steady state acceleration on the east side of footings (side of the mass shaker) than those measured on the west side of the footings.

In the long direction of the footings, the measured average peak steady state accelerations for footings I, II, and III were 0.00126g, 0.0015g, and 0.00102g, respectively. There was no coupling between the long and short directions vibration during the testing of the three footings in the longitudinal direction. However, that coupling existed during the shaking of the footings in the short direction. This was mainly because of the torsional moments induced during the tests. These moments led to the excitation of the torsional and the rocking modes of vibration of the footings. Therefore, significant accelerations were recorded on long direction of the footings during the shaking in the short direction.

Chapter 4

In-Situ Soil Testing

4.1 Introduction

A modified version of the seismic down-hole method[3, 16] was used to measure the shear wave velocity at low-strain, $V_{s,\,max}$, of the soil directly under the footings of bent WB11 (Fig. 2.3). Four down-hole tests were conducted in order to check the accuracy of the measurements. Due to the difficulties of the field condition, only $V_{s,\,max}$ of the soil between footings I and II was measured. In addition, a subsurface exploration of the soil was performed in order to establish the top 5.5 ft (1.67 m) of the soil profile. This chapter includes the soil profile in addition to the description, the test setup, the test procedure, and the results of the in-situ soil testing.

4.2 Soil Profile

In order to establish the profile of the soil at the bridge site, a subsurface exploration was performed on the top 5.5 ft (1.67 m) of the soil directly by the south side of footing I (Fig. 4.1). Visual examination and the laboratory tests performed on the soil samples indicated that the first 3.5 ft (1.07 m) of the soil, measured from the ground surface, is composed of sandy clay with large cobbles. The next 2 ft (0.61 m) of the soil is composed of fine gravely sands mixed with

cobbles. The soil exploration was stopped at [illegible] reached. Figure 4.1 shows the soil profile and [illegible] at the bridge site.

4.3 The Seismic Down-hole Method

4.3.1 Test Description

The seismic down-hole method[3, 16] is [illegible] determining the variation with depth of the [illegible] at low strains (smaller than 10^{-5}). In this method [illegible] inside a borehole at a pre-determined depth [illegible] surface (Fig. 4.2). The source used to generate [illegible] travel time of an S wave between the source and [illegible] measuring the distance between the source and [illegible] wave velocity, $V_{s,\ max}$, and therefore, the [illegible] determined.

The down-hole method needs only one [illegible] wave velocity of the soil. However, in this case [illegible] time is required. To measure the variation of [illegible] several receivers can be placed inside the bore[hole] wave velocities between the receivers can be [illegible] required for passage of the wave between the [illegible]

4.3.2 Test Setup

Figure 4.3 shows the test setup of the modified downehole test that was conducted in order to determine $V_{s,\ max}$ of the soil under the footings. Only two boreholes were used in the test. This was mainly due to the difficulties of the field condition. The soil at the bridge site was mixed with large cobbles, which led to difficulties in making several boreholes in the soil. Each borehole had a depth of 5.5-ft (1.67 m) measured from grade level. The bottom of the boreholes reached the level of the bottom of the footing.

Three geophones were used during the test. Two geophones were placed at the bottom of the boreholes; one in each hole (G_1 and G_2), while the third was placed in the soil directly by the long side of footing II (G_3) (Fig. 4.3). The geophones were securely coupled to the bottom of the boreholes. The geophones were placed very close to each other in order to avoid having cobbles in the soil between the geophones. During the boring of the two holes, a large cobble was found in the soil between the boreholes (G_1 and G_2). However, there were no cobbles noticed between geophones, G_2 and G_3.

During the test, the S waves were generated by striking the steel jacket placed on the column with a sledge hammer (modified seismic-downhole method). A computer was used to record the arrival times of the waves to the receivers (geophones). Since the wave velocities of the soil between the geophones were of interest, there was no need of precise recording of the trigger time.

4.3.3 Test Procedure

In order to check the accuracy of the measured $V_{s,\ max}$, four tests were conducted. During each test, the first step was to strike the steel jacket on the column with a sledge hammer. This was done in order to generate shear waves in the soil. At the same time, the computer was triggered to record the arrival times of the waves to the geophones. For tests 1 and 2, the east side and the west side of the column connected to footing I were struck, respectively (Fig. 4.3). For tests 3 and 4, the west side and the east side of the column connected to footing II were struck, respectively.

4.3.4 In-Situ Test Results

The results of the four tests were divided into two sets. Each set was used to determine $V_{s,\ max}$ of the soil between the geophones. The first set of data included the results of tests 1 and 2, while the second test included the results of tests 3 and 4.

For each set and for each geophone, the arrival time record from the first test in the set was superimposed on that record from the second test (Fig. 4.4). This was done in order to accurately determine the first arrival of the S wave to the geophone. Then, by calculating the time difference between the arrival of the waves to the geophones, the shear wave velocity of the soil was calculated.

For the two sets, the time difference between the arrival of the waves to geophones, G_1 and G_2 was 1.25 milli-seconds. However, the time difference between the arrival of the waves at geophones G_2 and G_3 was 2.7 milli-seconds. This corresponded to a shear wave velocity, $V_{s,\,max}$ of 3100 ft/sec (945 m/sec) for the soil between G_1 and G_2, and $V_{s,\,max}$ of 1048 ft/sec (319.5 m/sec) for the soil between G_2 and G_3. See the measured distances between the geophones shown in Fig. 4.3. Note that the measured values represented the shear wave velocities of the soil layer directly under the base of the footings and along their short direction. The large measured value of $V_{s,\,max}$ between G_1 and G_2 was mainly due to the presence of a large cobble between the two boreholes.

The soil shear modulus at low-strain, G_{max}, is related to the measured $V_{s,\,max}$ through the following equation[16]:

$$G_{max} = \rho V^2_{s,\,max} \tag{4.1}$$

where ρ is the mass density of the soil. For the very stiff soil under the footing, a soil unit weight of 135 pcf (20.8 KN/m^3) can be used[8]. Therefore, G_{max} of the soil can be determined as follow:

For soil between G_1 and G_2:

$$G_{max} = \frac{0.135}{32.2} * (3100)^2 * \frac{1}{144} = 280\ \text{Ksi}\ \ (1930\ \text{MPa}) \tag{4.2}$$

For soil between G_2 and G_3:

$$G_{max} = \frac{0.135}{32.2} * (1048)^2 * \frac{1}{144} = 32\ \text{Ksi}\ \ (221\ \text{MPa}) \tag{4.3}$$

The large value of G_{max} between G_1 and G_2 is due to the presence of a large cobble. Typically for rock, $V_{s,\ max}$ exceeds 6000 ft/sec (1800 m/sec)[31]. This indicates that the measured $V_{s,\ max}$ between G_1 and G_2 represents the shear wave velocity of the soil and a large cobble at that location. The G_{max} obtained between G_1 and G_2 was not representative of the overall soil condition at the footings, and therefore, excluded from the study. However, G_{max} for the soil between G_2 and G_3 was believed to be more representative of the soil condition and was used in the study.

4.4 Concluding Remarks

The shear wave velocity, $V_{s,\ max}$, was measured at the top of the "very stiff layer" shown in Fig. 4.1. According to the boring log of the bridge plans, this layer was described as "medium compact brown sandy gravel and decomposed granite with many cobbles and boulders". It was assumed that the measured shear wave velocity was reflective of the over 30 ft (9.10 m) depth of this layer atop bedrock.

The geophones were placed so close to each other in order to force the shear wave velocity to reflect on the interface with the lower (faster) layer. The problem with such close spacing was that the boulder found between geophones G_1 and G_2 led to an unreasonably large value of measured shear wave velocity.

Chapter 5

Analytical Study of In-Situ Footing Stiffness

5.1 Introduction

An analytical study was conducted to help determine the in-situ stiffness of the three existing footings of bent WB11 of "G-772 W" bridge. A three-dimensional finite element model of the last two spans of the bridge (Fig. 2.1) was constructed using an existing computer program. The columns, the bent cap, the superstructure, and the footings were modeled as linear elastic elements. This is because no nonlinear actions were expected due to the small dynamic forces applied to the existing footings in the dynamic field test. The soil-footing interaction was modeled in the computer program using a spring-dashpot model.

A response history analysis was performed to determine the acceleration response of the three footings. The analysis was refined until the predicted steady state peak acceleration at the footing level matched the measured steady state peak acceleration on the corresponding footing during the dynamic field test.

Two procedures were used to compute the footing stiffness: the Federal Highway Administration (FHWA) method[40] and Gazetas method[16]. The two methods adopt different approaches for the computation of footing stiffness and consider different parameters that affect the footing stiffness and the soil-structure response.

This chapter includes the description of the analytical model of the bridge, the approach used to determine the in-situ footing stiffness, and presents and discusses the results.

5.2 Computer Program

The analysis was performed using *COSMOS/M* version 1.75 software[30]. *COSMOS/M* is a three-dimensional finite element analysis package developed by Structural Research and Analysis Corporation for personal computers and workstations. The program includes modules to solve linear and nonlinear static and dynamic structural problems including response history analysis of structures.

The advanced dynamic module of the program is used for the solution of dynamic response problems such as modal response history, response spectra, response spectra generation, random vibration, steady state harmonic motion, and curve transformation. For the modal response history analysis, which was used in this study, the uncoupled modal equations of motion are solved using the step-by-step integration technique of the Wilson-θ[6] or the Newmark method[6]. In this study, the Newmark method was used for the response time history analysis.

The computer program is also capable of handling linear and nonlinear spring elements. For the spring element, two degrees of freedom (one translation and one rotation) are considered for each node in the element local coordinate system. The element has the capability to perform as a longitudinal and/or

torsional spring in one-, two-, or three-dimensional applications.

In the computer program, concentrated dampers at specified nodes can be modeled only in conjunction with the modal time history analysis option in addition to modal, Rayleigh, and composite damping options. Damper elements can be considered between any two nodes or any one node and the ground. The damping coefficient is defined in terms of its components along the global X-, Y-, and Z-directions. However, rotational (rocking or torsional) dampers are not considered in the computer program.

In *COSMOS/M*, load excitations may be applied as concentrated loads at specified nodes or as distributed pressure applied to specified element faces. Depending on the type of analysis, loads may have arbitrary patterns in the time or frequency domain. Forces can be defined in global or local coordinates. The evaluated response consists of displacements, velocities, accelerations, and stresses.

5.3 The Analytical Model

The finite element model of "G-772 W" bridge is shown in Fig. 5.1. Only the last two spans of the bridge (Fig. 2.1) were modeled in the computer program. This was mainly because the shaker loads were directly applied at locations where spring stiffness was of interest, and very little influence of the structure away from the footings was expected. The reason the bent and the adjacent spans were

modeled was to attempt to identify the in-situ properties of the columns and the bent cap as a side benefit of this study. The model (Fig. 5.1) consists of 54 nodes including 4 auxiliary nodes, 49 beam elements, and 9 spring elements (3 sets) at the base of the footings to model the footing-soil interaction. The displacements at the abutment (WB10) and at bent WB12 (Fig. 2.1) were restrained along the global X-, Y-, and Z-directions.

The superstructure was modeled as a continuous system over the bent because the 1-in. (25 mm) hinge gap between the girders was not expected to influence pier cap movements for the force levels used in this study. To model the boundary conditions at node 5 (Fig. 5.1), the rotations along the local y- and z-directions were released at the end of element 4 (nodes 4 to 5) and at the beginning of element 5 (nodes 5 to 6). The properties of the seven steel girders in the superstructure were lumped in one spine element (Fig. 5.1).

5.3.1 Element Properties

The section properties of the superstructure are listed in Table 5.1. The section properties shown are with respect to the local coordinates of the beam element (Fig. 5.1). The concrete deck was included in the calculation of the superstructure properties after it was converted into transformed steel. For the superstructure, the outer two girders had different cross section properties than the five inner girders. Also, within each girder, the thickness of the bottom flange

varied along the span of the bridge. A modulus of elasticity, E_S, of 29,000 Ksi (200,000 MPa) was used for steel, and a compressive strength, f'_C, of 5 Ksi (34.5MPa) was used for concrete. Appendices B and C show the procedures used to calculate the equivalent moment of inertia, I_{equiv}, and the equivalent polar moment of inertia, J_{equiv}, of the retrofitted part of the column, respectively.

The retrofitted bent cap was modeled using sixteen beam elements in order to adequately model the variation of the bent cap properties. The bent cap section properties are shown in Table 5.2. The parameters were found using the cap gross section. The section properties included the shear keys that were used to restrain the lateral movements of the steel girders.

A rigid beam element was used to link the superstructure to the bent cap. Also, the bent cap was linked to the columns through three linear-elastic rigid beam elements to account for high rigidity of the joint region (Fig. 5.1).

Each column was modeled using six beam elements. Four elements were used to model the part of the column with steel jacket. However, the other two beam elements were used to model the 2-in. (51 mm) gap left between the top of the jacket and the bottom of the bent cap, and between the bottom of the jacket and the top of the footing (unconfined part of the reinforced concrete column). Table 5.3 lists the typical column gross section properties for bent WB11.

Each footing was modeled using one beam element. The footing stiffness was modeled using three spring sets (Fig. 5.1). Each spring set consists of a

translational and a rotational stiffness spring. In addition, at the base of the each foundation (nodes 34, 42, and 50 in Fig. 5.1), a concentrated damper (dashpot) set was connected to the ground to model the radiation damping and the hysteretic damping of the soil in the three directions. The damper modeled the vertical and the sliding damping only. In this study, the rocking and torsion damping were not modeled, since *COSMOS/M* computer program does not support these types of damping. Computation of spring and dashpot coefficients is described in Sec. 5.4.3. Table 5.3 shows the footing gross section properties for bent WB11.

5.4 Approach to Problem

In order to accurately predict the in-situ footing stiffness through the finite element model, it was necessary to define all the factors and the variables that affect the soil-structure interaction, and therefore, the dynamic response of the bridge. A sensitivity study was performed on the important variables in order to measure their effects and exclude those that did not have any significant influence on the footing response.

In this study, linear spring-dashpot models were used to represent the soil-footing system and to model the soil-structure interaction. Finite element models can be a more accurate way of representing the soil under the foundation and the soil-structure interaction[11, 28, 29, 34, 36, 38, 39]. This is mainly due to the fact that finite element models consider the nonlinear effects of the soil, the effects of foundation

embedment, and variation of soil properties with depth. Also, they can consider the presence of adjacent structures and their effects on the soil-structure interaction of the structure under consideration (three-dimensional effects). However, modeling the soil-structure system using finite element models is time consuming. As a result, simple models of spring-dashpot are commonly used because they are sufficiently accurate[16, 24, 27, 40, 41, 46, 44].

In the analysis, soil-structure interaction was accounted for using the substructure method[6, 7]. In this method, the response of the footing was first analyzed without the superstructure, and the footing stiffness was computed using a spring-dashpot system. Then, a response history analysis of the bridge supported on this spring-dashpot system was performed in order to obtain the dynamic response of the bridge-foundation system for the applied dynamic loading.

In this study, a simple rational procedure, which accounts for many significant factors that affect the soil-structure interaction, was developed for the computation of spring stiffness for the footing-soil system. The procedure was developed from two methods that are commonly used in the analysis of the soil-structure interaction problems[16, 40]. Section 5.4.3 explains in more details the two methods.

A preliminary calculation, using the procedure developed in this study (Sec. 5.6 and Chapter 6) was conducted at the beginning of the analysis in order to determine the footing stiffness. The predicted footing stiffness and damping

coefficients were based on the footing and the soil properties. Then, a response history analysis was performed by applying a harmonic force to each footing in the finite element model. Each footing was subjected to a harmonic force equal to the harmonic force applied to the corresponding footing during the dynamic field test. The spring stiffness and the damping coefficients were refined until the predicted steady state peak acceleration at the footing level matched the measured steady state peak acceleration on the corresponding footing during the test.

5.4.1 Factors Affecting Soil-Structure Interaction

To improve the prediction of the in-situ stiffness of the three existing footings of bent WB11 (Fig. 2.3), several important factors, which influence the degree to which soil-structure interaction affects the response of the bridge were identified. The following factors were considered in the analytical study:

1. Column stiffness
2. Bent cap stiffness
3. Structural damping of the bridge
4. Radiation damping
5. Soil properties: soil shear modulus, Poisson's ratio, and material damping ratio
6. Embedment depth of footings in soil
7. Depth of soil deposit to bedrock
8. Variation of soil properties with depth (layering effect).

In the analysis, the first five factors were treated as variables. Then, a sensitivity analysis was performed in order to measure the effects of varying those variables on the dynamic response of the footings and on the computation of the in-situ footing stiffness (Sec. 5.7). The last three factors were identified and measured from the bridge plan and the boring log of the soil.

5.4.2 Soil Parameters

There are two important soil parameters that affect the footing stiffness: soil shear modulus, G_{max}, and Poisson's ratio, ν. In this study, these parameters were examined carefully in order to properly model the soil-footing interaction.

5.4.2.1 Soil Shear Modulus, G_{max}

One of the most important soil parameters that affect the soil-structure interaction is the maximum soil shear modulus (shear modulus at very low-strain), G_{max}, or the corresponding shear wave velocity, $V_{s,\ max}$. For all soils, the shear modulus is greatly influenced by the mean confining effective stress, $\overline{\sigma}_o$, and the void ratio, e. For clays, G_{max} is also influenced by the over-consolidation ratio, OCR.

The magnitude of the soil shear modulus is significantly affected by the cyclic shear strain induced in the soil. Plots of the modulus ratio G/G_{max} as functions of cyclic strain γ_c have become the traditional way of depicting the effect

of strain amplitude on cyclic shear stress behavior. Figure 5.2 shows the shear modulus reduction curve used in this study. The figure was adopted from Ref. 16, which summarizes recently published data for clays, sands, and gravels. The parameter I_p shown in Fig. 5.2 is the plasticity index of the soil. In this study, the curve for sandy soils was used because of the nature of the soil under the three footings at the bridge site (Chapter 4).

As shown in the previous chapter, a shear wave velocity, $V_{s,\ max}$ = 1048 ft/sec (319.5 m/sec) was measured at the base of the footings using the seismic down-hole test. This corresponded to a soil shear modulus, G_{max} = 32 Ksi (220.6 MPa). However, in the analysis, G_{max} was considered as an unknown variable. This was mainly done in order to compare the G_{max} predicted from the analysis with the measured soil shear modulus. The value of G_{max} was changed in the calculation of footing stiffness, until the predicted steady state peak acceleration at each of the footing level matched the measured steady state peak acceleration on the corresponding footing. Then, by using Fig. 5.2, G/G_{max} was determined at the shear strain level induced in the soil, and the predicted G_{max} was found.

5.4.2.2 Poisson's Ratio, ν

Poisson's ratio, ν, also affects the soil-structure interaction but shows little sensitivity to soil type, confining pressure, and void ratio[16]. However, several studies have indicated that the influence of ν is not of great significance in the

problem of soil-structure interaction, except in vertical and rocking oscillations in soils with ν close to 0.50[16]. At low strain levels, a ν close to 0.1 can be used[4]. Because of the small shear strain induced in the soil during the dynamic field test, $\nu = 0.1$ was used in the computation of footing stiffness.

5.4.3 Computation of Footing Stiffness

In this study, the computation of footing stiffness was mainly adopted from two available methods that use spring-dashpot models (lumped-parameter) for the modeling of soil-structure interaction. The first was the Federal Highway Administration (FHWA) method[40, 41]. The second method adopted in this study was compiled from several publications by different researches and was cited by Gazetas in Ref. 16. In this report, the second procedure is referred to as Gazetas method for ease of making reference. The following sections present a general background followed by a description of the two methods adopted in this study.

5.4.3.1 Theory of Computation of Footing Stiffness

In general, a rigid footing has six degrees of freedom, three translations and three rotations (Fig. 5.3). Usually, the rotations about the X and Y-axes are termed rocking and the Z-axis rotation is termed torsional or yawing.

For a vertical mode of oscillation, the dynamic equilibrium of the footing (Fig. 5.3) assuming a spring-dashpot model takes the form:

$$m\ddot{z} + C_z\dot{z} + K_z z = F_z(t) \tag{5.1}$$

Similarly, for sliding modes:

$$m\ddot{x} + C_x\dot{x} + K_x x = F_x(t) \tag{5.2}$$

$$m\ddot{y} + C_y\dot{y} + K_y y = F_y(t) \tag{5.3}$$

For a torsional mode:

$$I_{\theta z}\ddot{\theta} + C_{\theta z}\dot{\theta} + K_{\theta z}\theta = M_z(t) \tag{5.4}$$

For rocking modes:

$$I_{\theta x}\ddot{\theta} + C_{\theta x}\dot{\theta} + K_{\theta x}\theta = M_x(t) \tag{5.5}$$

$$I_{\theta y}\ddot{\theta} + C_{\theta y}\dot{\theta} + K_{\theta y}\theta = M_y(t) \tag{5.6}$$

where,

m = mass of the footing

$I_{\theta x}$, $I_{\theta y}$, $I_{\theta z}$ = mass moment of inertia of the footing about X, Y, and Z axes, respectively

$\ddot{x}$, $\ddot{y}$, $\ddot{z}$ = acceleration response of the footing in the X, Y, and Z axes, respectively

$\dot{x}$, $\dot{y}$, $\dot{z}$ = velocity response of the footing in the X, Y, and Z axes, respectively

x, y, z = displacement response of the footing in the X, Y, and Z axes, respectively

K_x, K_y, K_z = translational footing stiffness (spring constants) in the X, Y, and Z axes, respectively

$K_{\theta x}$, $K_{\theta y}$, $K_{\theta z}$ = rotational footing stiffness about X, Y, and Z axes, respectively

C_x, C_y, C_z = translational damping coefficient in the X, Y, and Z axes, respectively

$C_{\theta x}$, $C_{\theta y}$, $C_{\theta z}$ = rotational damping coefficient in the X, Y, and Z axes, respectively

F_x, F_y, F_z = applied dynamic forces in the X, Y, and Z axes, respectively

M_x, M_y, M_z = applied dynamic moments about X, Y, and Z-axes, respectively.

For embedded footings, horizontal forces along principal axes induce rotational in addition to translational vibrations[16, 41]. Therefore, two more "cross-coupling" horizontal rocking stiffnesses exist: $K_{x\theta y}$, $K_{y\theta x}$. The coupling is found due to the fact that the center of gravity of the foundation is above the center of pressure of the soil reactions. Therefore, if the foundation is translated horizontally, inertial forces arises at the center of gravity and a net moment at the foundation base is produced, and thus, rocking is initiated[34]. For shallow foundations, the cross-coupling effect is small and can be neglected[16, 41]. However, their contribution to the footing stiffness may need to be included for deeply embedded footings where the ratio of the depth of embedment to the equivalent footing diameter is greater than five[41]. In this study, the cross-coupling effect was neglected since the ratio of the depth of embedment to the equivalent footing diameter was approximately 0.9.

For a soil-footing system, the damping coefficients shown in the previous equations reflect two types of damping: radiation damping and material damping. Radiation damping is due to energy carried by waves spreading away from the footing. It is a function of the characteristics of the soil such as density, Poisson's

ratio, and soil shear modulus. It also depends on the frequency of loading and the depth of embedment of the foundation in the soil[16]. However, the material damping is due to energy dissipated by the inelastic action in the soil (hysteretic action) and is a strain-dependent. In general, radiation damping is considerably higher than the material damping of the soil[16].

For most soils and for well-designed vibrating machine foundations causing little straining of the soil mass, material damping ranges typically from 2 to 6 percent[8, 16]. In the analysis, and because of the small strains induced in the soil during the dynamic field testing, 5 percent material damping was considered for the soil. The spring constants and the damping coefficients used in the previous equations can be computed using different methods[16, 40]. Foundation damping (radiation and hysteretic) is not directly additive to the structural damping.

5.4.3.2 The Federal Highway Administration (FHWA) Method

The FHWA current procedure in soil-structure interaction analyses for footings involves solving for the response of a rigid footing on a semi-infinite elastic half space[40, 41]. In order to represent the footing stiffness, six equivalent springs are used: three translational and three rotational.

Spring constants for shallow rectangular footings are obtained by modifying the solution for circular surface footings on a semi-infinite elastic half space. In general, the stiffness of an embedded footing (assuming semi-infinite elastic half

space) can be expressed as follow[41]:

$$K = \alpha \, . \, \beta \, . \, K_o \tag{5.7}$$

where,

K_o = stiffness coefficient for the equivalent circular footing

α = foundation shape correction factor

β = foundation embedment factor.

To use Eq. 5.7, the stiffness coefficients for a circular surface footing (K_o) are determined according to the following equations:

For vertical translation:

$$K_z = \frac{4\,GR}{1 - \nu} \tag{5.8}$$

For horizontal translations:

$$K_x = K_y = \frac{8\,GR}{2 - \nu} \tag{5.9}$$

For torsional rotation:

$$K_{\theta z} = \frac{16\,GR^3}{3} \tag{5.10}$$

For rocking rotations:

$$K_{\theta x} = K_{\theta y} = \frac{8\,GR^3}{3\,(1 - \nu)} \tag{5.11}$$

where, G and ν are the shear modulus and Poisson's ratio for the elastic half space, respectively. R is the equivalent radius of the rectangular footing (Fig. 5.4).

The equivalent radius can be computed as follow[41]:

For translational modes:

$$R = \sqrt{\frac{4BL}{\pi}} \tag{5.12}$$

For rotational modes:

$$R = \left[\frac{4BL\left(4B^2 + 4L^2\right)}{6\pi}\right]^{1/4} \quad \text{(Z-axis torsion)} \tag{5.13}$$

$$R = \left[\frac{(2B)(2L)^3}{3\pi}\right]^{1/4} \quad \text{(X-axis rocking)} \tag{5.14}$$

$$R = \left[\frac{(2B)^3(2L)}{3\pi}\right]^{1/4} \quad \text{(Y-axis rocking)} \tag{5.15}$$

where L is one half the longer dimension of the footing and B is one half the shorter dimension of the footing (Fig. 5.4). The FHWA procedure accounts for dependence of the footing stiffness on strains induced in the soil, but ignores dependence of footing stiffness on the frequency of loading.

To establish the required soil parameters, in-situ testing and/or laboratory testing is recommended. The low strain shear modulus G_{max} may be obtained from correlation with the Standard Penetration Test (SPT) values or through geophysical tests. The FHWA also recommends using a shear modulus reduction curve similar to Fig. 5.2, in order to account for the change of soil shear modulus with the shear strains induced in the soil during an earthquake. For practical design purposes, the

FHWA suggests using $\nu = 0.35$ for cohesionless soils and $\nu = 0.45$ for cohesive soil[41].

Figure 5.5 shows the foundation shape correction factor, α, for all modes of vibration. The figure was adopted from Ref. 41 and can be used according to the coordinates shown in Fig. 5.4. Figure 18 in Ref. 41 can be used to determine the foundation embedment factor, β, for any mode of vibration. For simplicity, FHWA recommends ignoring the depth of soil overburden or the depth of excavation to the top of the footing surface in the computation of the embedment factor.

In the case where the top of the footing is below the grade level, the thickness of the footing, D (Fig. 5.4) can be used to calculate the embedment ratio (D/R) in determining the embedment factor, β. However, for embedment depth greater than five times the equivalent footing diameter, 2R (Fig. 5.4), FHWA recommends performing a special study to determine the appropriate depth of embedment[40].

The FHWA strongly recommends modeling of the foundation damping using viscous dampers that include both radiation and material damping[41]. Those viscous dampers are used in conjunction with the equivalent foundation stiffness. However, the FHWA does not suggest any procedure to calculate the damping coefficients and the contribution of foundation damping to the overall bridge response.

5.4.3.3 Gazetas Method

Gazetas[16] presented comprehensive yet simple procedures that can be used in the computation of spring and dashpot coefficients for the soil-structure interaction analyses. These procedures were mainly developed for assessing the vibration response of footings subjected to machine loads. They were based on the results of both rigorous and approximate formulations that have been compiled from several publications by Gazetas and other researchers[5, 8, 9, 10, 14, 15, 17, 18, 21, 22, 23, 25, 43, 44]. The procedure presented by Gazetas are in the form of simple algebraic formulas and dimensionless charts referring to all possible modes of vibration and covering several soil profiles and foundation geometries (circular, rectangular, and strip foundations).

In this method, the footing stiffness coefficients depend on the frequency of loading but are independent of the variation of soil shear modulus with shear strain. This is mainly because in machine vibration problems, footings are designed such that the amplitudes of all possible modes of vibration are limited to very small levels. In this case, soil in the immediate vicinity of the footings is subjected to very small strain (γ_c) levels, usually less than 10^{-5} percent[16].

In general, the dynamic stiffness of footings can be expressed as follow[16]:

$$\overline{K} = K \cdot k(\omega) \tag{5.16}$$

where,

$\overline{K}$ = dynamic stiffness of footing

K = static stiffness of footing

$k(\omega)$ = dynamic stiffness coefficient.

One of the advantages of this method is that it accounts for the presence of bedrock at shallow depths, instead of assuming a semi-infinite elastic half space (soil deposit extends to infinite depth). The presence of bedrock has the effect of increasing the footing stiffness more than that predicted assuming elastic half space. This is mainly due to the decrease in the depth of the deforming zone under the footings. This method also accounts for the radiation damping by using dashpot models. Soil hysteretic damping can be added to the radiation damping by using the following expression[16]:

$$\text{Total } C = \text{radiation } C(\omega) + \frac{2\overline{K}}{\omega}\beta_o \qquad (5.17)$$

where,

$C(\omega)$ = radiation damping coefficient

ω = load frequency

β_o = material damping ratio.

Tables 15.1 to 15.4 in Chapter 15 of Ref. 16 include the procedures for computing the dynamic footing stiffness and the radiation damping for surface and embedded foundations on a homogeneous half space and on a homogeneous stratum over bedrock.

The following is the procedure for computation of the dynamic footing stiffness for surface and embedded circular footings of radius R (Figs. 5.6 and

5.7), taking into consideration the presence of bedrock:

5.4.3.3.1 Surface Circular Footings on Soil Deposit over Bedrock

The static stiffness coefficients (K) of surface circular footings (Fig. 5.6) are computed as follow[34]:

$$K_z = \frac{4\,GR}{1-\nu}\left(1 + 1.3\frac{R}{H}\right) \tag{5.18}$$

$$K_x = K_y = \frac{8\,GR}{2-\nu}\left(1 + 0.5\frac{R}{H}\right) \tag{5.19}$$

$$K_{\theta z} = \frac{16}{3}GR^3\left(1 + 0.10\frac{R}{H}\right) \tag{5.20}$$

$$K_{\theta x} = K_{\theta y} = \frac{8\,GR^3}{3(1-\nu)}\left(1 + 0.17\frac{R}{H}\right) \tag{5.21}$$

where H is the depth of the soil to the bedrock (Fig. 5.6) and R is the radius of the circular footing.

The dynamic stiffness coefficient ($k(\omega)$) for each mode of oscillation is computed from charts which are presented in Ref. 16. The dynamic stiffness coefficient depends on the ratio of H/R and a dimensionless frequency factor, a_o:

$$a_o = \frac{\omega R}{V_s} \tag{5.22}$$

The radiation damping coefficient ($c(\omega)$), can be computed by following the procedures presented in Ref. 16.

5.4.3.3.2 Embedded Circular Footings on Soil Deposit over Bedrock

The static stiffness coefficients (K) of embedded circular footings (Fig. 5.7) are computed as follow[16]:

$$K_{z,emb} \cong K_{z,sur}\left(1 + 0.55\frac{d}{R}\right)\left[1 + \left(0.85 - 0.28\frac{D}{R}\right)\frac{D}{H - D}\right] \tag{5.23}$$

$$K_{x,emb} = K_{y,emb} \cong K_{x,sur}\left(1 + \frac{d}{R}\right)\left(1 + 1.25\frac{D}{H}\right) \tag{5.24}$$

$$K_{\theta z,emb} \cong K_{\theta z,sur}\left(1 + 2.67\frac{d}{R}\right) \tag{5.25}$$

$$K_{\theta x,emb} = K_{\theta y,emb} \cong K_{\theta x,sur}\left(1 + 2\frac{d}{R}\right)\left(1 + 0.65\frac{D}{H}\right) \tag{5.26}$$

where D is the embedment depth and d is the footing depth. Gazetas has mentioned that the above expressions were only crude approximations based on limited information[16]. The dynamic stiffness coefficient ($k(\omega)$) and the radiation damping coefficients ($c(\omega)$) for each mode of oscillation is computed from charts, which are presented in Ref. 16.

5.5 Comparison of FHWA and Gazetas Methods

The FHWA and Gazetas methods adopt two different approaches in computing the footing stiffness. The FHWA assumes that the stiffness depends on the level of strain induced in the soil during an earthquake (strain-dependent approach). However, Gazetas assumes that the stiffness of the footings depends

on the frequency of the applied dynamic load (frequency-dependent approach).

It was noticed that both methods are using the same form of solution for the static response of a surface rigid footing foundation on a semi-infinite half space. However, they are using different multipliers to account for the different shape of foundations, and the embedment effect. The presence of bedrock at shallow depths is accounted for only in the Gazetas method.

5.6 Proposed Approach

The objective of this study was to develop a simple procedure for the computation of footing stiffness, which accounts for different factors affecting the footing stiffness. The approach proposed in this study was a combination of the FHWA and Gazetas methods. The formulas for an embedded circular footing on a homogeneous soil over bedrock were used to compute the footing stiffnesses (Eqs. 5.23 to 5.26). The stiffness of the circular surface footing, given in Eqs. 5.23 to 5.26, were determined using Eqs. 5.18 to 5.21. The equivalent radius (R) shown in these equations was determined using Eqs. 5.12 to 5.15. Then, to correct for the foundation shape, the foundation shape correction factor (α) for different modes of oscillation was used (Fig. 5.5).

In the analysis, it was assumed that the footing stiffness is strain-dependent only, and therefore, Fig. 5.2 was used to account for the variation of shear modulus with shear strain. This assumption was made because the frequency of

the earthquake is considerably less than that produced by machine foundations, which was the focus of the Gazetas work.

From the boring log at the "G-772 W" bridge site, the depth of the soil to the bedrock (H) is 35 ft (10.67 m) which was used in the formulas. The following sections show the analytical procedure used to determine the in-situ footing stiffness.

5.7 Sensitivity Study

The main objective of the current study was to improve the prediction of the in-situ stiffness of the three existing footings of bent WB11 based on the results of the dynamic tests. This can be achieved by using system identification technique. To perform system identification, important variables have to be considered. Ordinarily, the most plausible values for these variables are found by matching the measured and calculated responses. Important variables are those that affect the response significantly.

Because in each of the field tests, the shaker load was applied at the location where the footing stiffness was of interest, it was suspected that the properties of structural components other than the footings would have significant effect on the response. The structural damping of the bridge, the foundation damping, the column stiffness, the bent cap stiffness, and the soil shear modulus were considered as potentially important factors that influence the response of the

bridge.

A sensitivity study was performed to measure the effects of varying these factors on the dynamic response of the footings. In the analysis, each factor was varied one at a time, while the others were kept constant.

5.7.1 Effect of Structural Damping of the Bridge

In general, an increase in the structural damping is always beneficial, inducing significant reduction of the dynamic response of the bridge. There are two common types of structural damping in bridges: Coulomb damping and hysteretic damping[33]. Coulomb damping (friction damping) occurs due to the joint movements in the bridge superstructure, friction at connections and support points or due to friction between the cracks of the reinforced concrete members. Coulomb damping is independent of velocity or displacement.

Hysteretic damping (energy dissipation) is represented by the area within the loops of the force-deformation response of the structure[6, 33]. It strongly depends on the hysteretic response of the bridge (ductility), and whether the response is linear or nonlinear during an earthquake.

Despite the two common types of damping, structural damping in bridges is always represented by an equivalent viscous damping (velocity proportional damping). This is done in order to conform to the simple mathematical form of the equation of motion[6]. The equivalent viscous damping values are chosen to

reflect all the possible damping contributions from the bridge structure. However, the determination of a value for analytical bridge models is difficult. This is due to the uncertainties and complexities of determining either Coulomb or hysteretic damping. For bridge structures, viscous damping ratios between 2% and 10% are commonly assumed[33].

To measure the effect of varying the structural damping of the bridge on the response of the three footings subjected to loads from the mass shaker, three damping ratios were chosen: ζ = 2%, 5%, and 10%. In the analysis, the gross moment of inertia of the columns and the bent cap were used. In addition, the measured soil shear modulus, G_{max} = 32 Ksi (221 MPa) was used in the computation of the footing stiffness coefficients.

Figures 5.8 and 5.9 show the effect of varying the structural damping ratios on the steady state peak acceleration response of footing I in the longitudinal and short directions. Similar responses were obtained for footings II and III. It was noticed that the damping ratio did not have any effect on the steady state acceleration response of the footings. This was mainly due to the fact that the dynamic loads were applied at the same locations where the steady state accelerations were determined. Therefore, very little influence of the structure away from the footings was expected.

For a damped system subjected to harmonic loading, the total response of the system consists of transient response, which damps out quickly, and a steady

state harmonic response, which continues for a longer time[6]. As shown in Fig. 5.10, the effect of damping on the steady state response is very small for $\beta \prec 0.25$ or $\beta \succ 2$, where β is the ratio of the applied loading frequency to the natural free vibration frequency of the system[6]. For the dynamic response of only one column and a footing of bent WB11 (ignoring the effect of the other two columns and footings), β is approximately 0.65. At $\beta = 0.65$, and for damping ratio between 0 and 20 percent, the effect of damping on the dynamic magnification factor (D) is small (Fig. 5.10). This also explains the negligible effect of damping on the steady state acceleration response of the footings. The dynamic magnification factor, D, shown in Fig. 5.10, is the ratio of the resultant harmonic response amplitude to the static displacement[6].

5.7.2 Effect of Foundation Damping

Foundation damping is represented by radiation damping and soil hysteretic damping. Radiation damping refers to the energy dissipation that takes place through the soil on which the structure is found. Radiation damping in the foundation generally leads to reduction in the response of the structure. In the analysis, the radiation damping was computed based on the procedure recommended by Gazetas[16]. The total foundation damping (radiation and 5 % hysteretic) was computed using Eq. 5.17.

In the computer model, the foundation damping was implemented using

dashpots at footing nodes (Fig. 5.1). Due to the limitation of the computer program *COSMOS/M*, the dashpots included the vertical and the sliding foundation damping only.

Figures 5.11 and 5.12 show the effect of the foundation damping on the steady state peak acceleration response of footing III, where the highest impact of the foundation damping was found. It was noticed that including the foundation damping did not significantly affect the response of the footings. Several factors contributed to this observation. First, radiation damping is significantly affected by the frequency of loading[16]. During the dynamic field test, small load frequencies were applied to the footings (approximately 6.5 Hz). This led to the significant reduction of the radiation damping. Second, for soil deposits over stiff material or bedrock, radiation damping is nonexistent or negligible for load frequencies less than the fundamental frequencies of the soil deposit[16]. This is due to the fact that no surface waves can exist in the soil deposit over bedrock at such low frequencies. In addition, the presence of bedrock prevents the waves from propagating downward, leading to the significant reduction of the radiation damping. This can be verified by computing the frequencies of the soil deposit for all modes of vibration. For the shearing modes of vibration (swaying and torsion), the fundamental frequency of the soil deposit, f_s, is[16]:

$$f_s = \frac{V_s}{4H} = \frac{1048}{4 \times 35} = 7.5 \text{ Hz} \tag{5.27}$$

where V_s is the measured shear wave velocity (V_s = 1048 ft/sec = 319.5 m/sec)

and H is the depth of the soil deposit to the bedrock (H = 35 ft = 10.7 m). For the compressing modes (vertical and rocking), the corresponding frequency, f_c, is[16]:

$$f_C \approx \frac{3.4}{\pi(1-\nu)} f_S \approx \frac{3.4}{\pi(1-0.1)} \times 7.5 \approx 9.0 \text{ Hz} \tag{5.28}$$

For the vertical and rocking modes of vibration, Gazetas recommended that the radiation damping coefficient, $C_Z = C_{\theta x} = C_{\theta y} \approx 0$ at load frequencies $f \prec f_C$, regardless of foundation shape[16]. For lateral modes of vibration, the radiation damping coefficients $C_X = C_y \approx 0$ at $f \prec 0.75 f_S$. Therefore, the radiation damping in the vertical and rocking modes of vibration was nonexistent ($f \approx 6.5$ Hz $\prec f_C \approx 9.0$ Hz). For the lateral modes of vibration, the radiation damping was non-zero but was small ($f \approx 6.5$ Hz $\succ 0.75\, f_S \approx 5.6$ Hz). In addition, the radiation damping in rocking is small even in a halfspace[16]. The results shown in Figs. 5.11 and 5.12 are consistent with these trends. It should be noted that the contribution of the soil hysteretic damping to the overall foundation damping was considerably smaller than the contribution of the radiation damping because the displacement amplitudes during the tests were small.

5.7.3 Effect of Column Stiffness

In bridges subjected to earthquakes, column stiffness can have a significant effect on the response of the bridge[13]. However, no definite trends can be shown. Thus, column stiffness may increase the response in one case and decrease it in

another, depending on the spectral properties of the earthquake. When both the excitation and response measurement are at the footing level, the effect of column may be different. To measure the effect of varying the column stiffness on the response of the footings, 50, 70, and 100 percent of the gross moment of inertia of the three columns were used for the sensitivity study. For the retrofitted part of the column, only the moment of inertia of the reinforced concrete was varied (Eq. B.10 in Appendix B) and the contribution of thee steel jacket was kept the same.

Figures 5.13 and 5.14 are the representative plots showing the effect of varying the gross moment of inertia of the columns on the steady state peak response of footing II. The total foundation damping was included in the results. It can be concluded that the column stiffness did not have a significant effect on the response of the footings. For both directions of loading, the response of the footings decreased slightly as the column stiffness increased. Also, the effect of column stiffness was somewhat more noticeable in the response of the footings in the short direction than that in the long direction (Table 5.4). This was mainly due to the fact that the contribution of the three columns to the transverse response of the footings was more pronounced than that for the longitudinal response.

5.7.4 Effect of Bent Cap Stiffness

To verify the effect of the bent cap stiffness on the response of the footings, a sensitivity analysis was performed at 50, 70, and 100 percent of the gross

moment of inertia of the bent cap. Figures 6.15 and 6.16 show the effect of varying the gross moment of inertia of the bent cap on the steady state peak acceleration response of footing I in the longitudinal and the short direction. It can be noticed that varying the moment of inertia of the bent cap, and therefore, its stiffness, did not significantly affect the response of the footing. This was mainly because of the very little influence of the structure away from the footings (Sec. 5.7.3).

Note that the response in the short direction was slightly more sensitive to the bent cap stiffness than the response in the long direction (Figs. 5.15 and 5.16). This is attributed to the more significant contribution of pier cap to in-plane stiffness than out-of-plane stiffness of the bent. Similar trends were seen for footings II and III.

5.7.5 Effect of Soil Shear Modulus

Soil shear modulus is the most important soil parameter that influences the response of the foundations and the soil-structure interaction. Figures 5.17 through 5.22 show the effect of varying the soil shear modulus on the steady state peak response of the three footings in their longitudinal and short directions. It was noticed from the results of the sensitivity study that the response of the three footings was only sensitive to the soil shear modulus.

For each footing and in each direction, the shear modulus of the soil under

the footing (G) was predicted from the intersection of the predicted and the measured peak acceleration response of the footing (Figs. 5.17 to 5.22). Notice that the measured shear modulus of the soil, G_{max}, was only shown in Figs. 5.18 and 5.20. This was due to the fact that G_{max} was measured between footings I and II and along their short direction (Chapter 4). Due to the great variability of the soil structure at the bridge site, G_{max} was not expected to be similar under the three footings and along each direction. Note that G is the soil shear modulus corresponding to the induced shear strain in the soil. However, G_{max} is the soil shear strain at shear strain less than 10^{-5} percent[16].

In order to predict G_{max} under the three footings in their longitudinal and short directions, the shear strains induced in the soil (γ_c) due to the applied dynamic forces on the footings were calculated at the base of the footings. Then, by using the shear modulus reduction curve for sandy soils (Fig. 5.2), G/G_{max} was identified and G_{max} was determined. Table 5.5 shows the predicted soil shear modulus (G and G_{max}) in addition to the maximum predicted footings displacement (δ) and the corresponding shear strains induced in the soil (γ_c). For each footing, the maximum footing displacement in the longitudinal and the short direction was predicted using the computer program. The induced shear strain was calculated by assuming a representative element in the soil under each footing. This element was assumed at depths of 6.5-ft (1981 mm) and 4.5-ft (1372 mm) for the induced soil shear strain in longitudinal and the short directions of the footing, respectively

(Figs. 5.23 and 5.24). The assumed depths represented half the long and the short dimensions of the footings, respectively. For the determination of the lateral footing stiffness, the depth 2B shown in Figs. 5.23 and 5.24 represents the "depth of influence", along which the soil is stressed due to presence of the footing. Notice the very small-predicted shear strains induced in the soil (Table 5.5). This was mainly because of the small dynamic forces applied to the footings. The small shear strains led to small reductions in the soil shear modulus, G_{max}. According to Fig. 5.2, the ratio G/G_{max} was equal to 0.98 and 0.95 in the longitudinal and the short directions of the footings, respectively

For footings I and II, the predicted soil shear modulus, G_{max}, in the short direction of the footings, agreed well with the measured value (1.5 percent difference). For footing III, the predicted G in the short direction of the footing was approximately 18 percent higher than that for footings I and II. This indicated that the soil was stiffer under footing III. The previous observation complied well with the fact that during the test of the three footings in the short direction, the measured peak acceleration of the soil next to footing III was lower than that of footings I and II (Sec. 3.4.1).

The analytical results shown in Table 5.5 also indicate that the predicted soil shear modulus along the longitudinal direction of footings I, II, and III was approximately 30, 30, and 17 percent higher than that predicted along their short direction. The soil shear modulus, G_{max}, in the longitudinal direction of the

footing was not measured due to difficulties of the field condition and proximity of the railroad track.

Several factors might contribute to the different soil stiffness along the both directions of the footings. The soils near the ground surface and under the footings are randomly mixed with cobbles, which vary in sizes from small to considerably large cobbles. Therefore, different soil stiffness is expected from one location to another. Also, there was a rail road track located along the west side of the footings (Fig. 2.1). Therefore, the soil on the west side of the footings might have been compacted due to the frequent train traffic. Soil compaction can lead to an increase in the soil shear modulus due to the increase in the relative density of the soil and the decrease in the void ratio.

During the dynamic field test, it was noticed that the soil along the east and west sides of the footings was directly exposed to the sunlight. However, the soil between footings I and II was in the shaded area. The sunlight increases the capillary tension in the soil due to the high soil suction. The increase in capillary tension can increase the effective stresses in the soil (due to the negative pore water pressure), and therefore, increase the soil shear modulus. On the south side of footing III, the soil was also exposed to the sunlight.

5.8 Predicted In-Situ Footing Stiffness

Table 5.6 shows the predicted in-situ dynamic footing stiffness for each

mode of vibration of the three footings. The stiffnesses corresponded to the dynamic forces applied to the footings in the longitudinal and short direction. The values are presented according to the global coordinate system shown in Fig. 5.1. For each footing, and in each direction of loading, the stiffness was determined by varying the soil shear modulus (G) in the computation of footing stiffness until the predicted steady state peak acceleration at each of the footing level matched the measured steady state peak acceleration on the corresponding footing. The procedure described in Sec. 5.6 was used in the computation of the footing stiffness. The predicted stiffnesses included the footing embedment effect in addition to the presence of the bedrock at 35-ft (10.67 m) from the grade level.

For footings I, II, and III, the predicted in-situ footing stiffness due to the applied loads in longitudinal direction of the footings, was approximately 33, 29, and 17 percent, respectively, more than that due to the loading in the short direction of the footings. This was mainly due to the variability of the soil structure along the longitudinal and the short direction of the footings.

5.9 Concluding Remarks

From the results of the sensitivity analysis, it was concluded that the structural damping of the bridge, the foundation damping, the column stiffness, and the bent cap stiffness did not have significant effects on the response of the footings when the dynamic load was applied directly to the footing. It was also

concluded that the soil shear modulus was the only parameter that controlled the response. This was mainly because of the fact that those forces were applied at the locations where the accelerations were also measured. Therefore, the structure away from the footings had very small influence on the footing response.

Chapter 6

Development of Design Guideline

6.1 Introduction

Based on the analytical study presented in Chapter 5 and the observations made during the dynamic field test, the following design guideline was formulated. The guideline provides the basis for the computation of the footing stiffness and the implementation of soil-structure interaction in the dynamic analysis of existing and new bridges.

In the guideline, a simple spring-dashpot model is recommended for the representations of soil-structure system. The model includes means of accounting for the strain-dependence of the soil shear modulus and other important factors such as footing embedment and presence of bedrock. For more practical applications, the spring-dashpot model was recommended since it is a quick and inexpensive way to estimate the footing stiffness, without using the more complicated and elaborate finite element models.

The guideline also includes recommendations for the determination of the important soil parameters (soil shear modulus and Poisson's ratio) that affect the footing stiffness. This chapter discusses in details the recommended procedure.

6.2 Determination of Soil Parameters

6.2.1 Soil Shear Modulus, G_{max}

For a better estimation of the footing stiffness, it is very important to determine the soil shear modulus at low strain (G_{max}) with in-situ dynamic tests. Dynamic field tests provide an indirect determination of G_{max} through measurements of the shear wave velocity, $V_{s,\,max}$.

In general, in-situ tests have more advantages over laboratory techniques. In the laboratory, it is very difficult to simulate the effects of aging, capillary stresses, and prehistory stresses on soils found in the field. In addition, sample disturbance may also cause an error in measuring G_{max} in the laboratory. As a result, G_{max} found with in-situ tests may exceed those measured in the laboratory by more than 100 percent[16].

One of the most common in-situ tests for measuring the maximum shear wave velocity ($V_{s,\,max}$) of the soil is the seismic down-hole method. In this method, receivers are placed inside a borehole at various depths. Then, a source located at the surface is used to generate S-wave in the soil. Travel times of shear waves between the source and the receivers are recorded, from which $V_{s,\,max}$ of the soil can be determined (Chapter 4).

It is important that the soil shear modulus (G_{max}) used in the computation of footing stiffness represents the soil condition with the presence of the structure. This is mainly because the presence of structure has the effect

of increasing the mean normal effective stress, $\overline{\sigma}_m$ which significantly influence the measured G_{max}. Therefore, to include effect of soil-structure interaction in the dynamic response of existing bridges, it is recommended that G_{max} be measured at an average depth of about B under the footings (depth of influence $\approx$ 2B), where B is one half the shorter dimension of the rectangular footing (Fig. 5.4). This can be justified as an approximate solution for uniform soil deposit under the footings.

For multi-layered deposit, the soil shear modulus can significantly vary from one layer to another. In this case, the effective shear modulus used in computing the footing stiffness can be approximately averaged over the depth of influence:

$$G_{avg} = \frac{G_1 h_1 + G_2 h_2 + ... + G_n h_n}{h_1 + h_2 + h_n} \tag{6.1}$$

where G_n is the average measured soil shear modulus at the mid-depth of n layer, h_n is the depth of n layer, and $h_1 + h_2 + ... + h_n$ equals the depth of influence mentioned above.

For the design of new bridges, it is not possible to directly measure G_{max} with the presence of the structure. Therefore, it is recommended that G_{max} be measured at the bridge site, at an average depth of about B from the expected footing level (recommended for uniform soil deposit under the footings). Then, the following modifications can be applied to correct for the measured G_{max} without the presence of the structure:

(a) Granular soils:

$$G_{max,\ structure} = G_{max,\ field} * \left(\frac{\overline{\sigma}_{m,\ structure}}{\overline{\sigma}_{m,\ field}} \right)^{1/2} \tag{6.2}$$

where,

$G_{max,\ structure}$ = maximum soil shear modulus with the presence of structure

$G_{max,\ field}$ = measured maximum soil shear modulus without the presence of structure

$\overline{\sigma}_{m,\ structure}$ = total mean normal effective stress with the presence of structure

$\overline{\sigma}_{m,\ field}$ = mean normal effective stress without the presence of structure

The mean normal effective stress for isotropic soil can be calculated as follow:

$$\overline{\sigma}_m = \frac{1}{3}(\overline{\sigma}_v + 2\overline{\sigma}_h) \tag{6.3}$$

where $\overline{\sigma}_v$ and $\overline{\sigma}_h$ are the effective vertical and horizontal stresses, respectively. Therefore, by measuring $G_{max,\ field}$ and calculating $\overline{\sigma}_{m,\ field}$ and $\overline{\sigma}_{m,\ structure}$, the shear modulus of the soils under the footings ($G_{max,\ structure}$) can be predicted.

(b) Saturated clays:

$$G_{max,\ structure} = G_{max,\ field} * \left(\frac{S_{u,\ structure}}{S_{u,\ field}} \right) \tag{6.4}$$

where $S_{u,\ field}$, and $S_{u,\ structure}$ are the undrained shear strength of the clay without and with the presence of the structure, at a depth of about B under the footings, respectively.

6.2.2 Near-Field and Free-Field Soil Shear Strain

The magnitude of the soil shear modulus is significantly affected by the cyclic shear strain induced in the soil. In the dynamic field test conducted on the three footings, only the soil in this near-field region is strained. Therefore, the calculated stiffness of the footings reflects the soil shear modulus at the strain level induced in the near-field region (strain induced by the excitation of the structure or relative shear strain). The FHWA[41] adopts the near-field approach (relative shear strain) in the computation of the dynamic footing stiffness.

In an earthquake, the strains induced in the soil can be divided into strains produced by seismic waves in the free-field, and additional strains caused by the vibrating response of the structure[7, 32]. The former is of a global effect, and therefore, affecting the entire soil region. However, the latter is of a local effect, affecting only the region in the vicinity of the footings.

The Applied Technology Council[1] (ATC) adopts the free-field approach in the computation of the dynamic footing stiffness. For the free-field site response analysis, computer program SHAKE 91[19] can be used to predict the free-field strain associated with a specific magnitude of an earthquake. SHAKE 91 computes the responses in horizontal soil layers subjected to vertically propagating seismic waves. The change of soil shear modulus as a function of shear strain is considered by using a "shear modulus reduction

curve" similar to the one shown in Fig. 5.2. Then, by using iterative procedures, the induced shear strains in different soil layers, which are associated with the design earthquake, can be predicted. Figure 6.1 shows the variation of modulus ratio G/G_{max} versus the relative cyclic shear strain as would be approached by the FHWA and the ATC. Note that because the free-field strain is independent of the relative strain, G/G_{max} remains constant for the ATC approach.

The soil shear modulus used to assess the stiffness of the footings is controlled by the total strain in the near-field (free-field plus relative strain). However, it is not yet known the phase difference between the free-field strain and the relative strain in the near-field.

Norris[32] recommended that the total strain could be taken as a function of the larger of the two components. Therefore, in the case where the relative shear strain is smaller than the free-field strain (left of the intersection of FHWA and ATC in Fig. 6.1), the soil shear modulus used to asses the footing stiffness is governed by the free-field strain[56]. However, to the right of the intersection in Fig. 6.1, the relative shear strain controls the soil shear modulus. By using this approach, it is possible to use the FHWA variation with an ATC cut-off as that shown in Fig 6.2. However, the ATC cut-off should be varied as a function of the computed free-field strain (from SHAKE 91) associated with the design earthquake.

6.2.3 Poisson's Ratio, ν

In addition to shear modulus, a second soil parameter that affect the foundation stiffness, however, to a less extent, is the Poisson's ratio, ν. The effect of ν is less than that of G. As mentioned in Sec. 5.4.2.2, ν shows little sensitivity to soil type, confining pressure, and void ratio[16]. On the other hand, it is significantly affected by the degree of saturation (S_r) and the drainage conditions[16].

For practical cases, the following values of ν can be used in assessing the footing stiffness[16]:

nearly dry sands, stiff clays, and rocks:	$\nu \approx 0.25$
wet silty sands (S_r = 50 to 90 percent):	$\nu \approx 0.35$
nearly saturated clays, above the water table:	$\nu \approx 0.45$
saturated clays and sands, below the water table:	$\nu \approx 0.50$

However, at low strain levels, $\nu \approx 0.10$ can be used[4].

6.3 Computation of Footing Stiffness

The primary goal of this study was to develop a simple and practical procedure that can be used in computing the footing stiffness. In developing the appropriate procedure, several factors that affect the footing stiffness and the soil-structure interaction were considered. Those factors are the shape of the foundation, the presence of bedrock at shallow depths, and the foundation

embedment. The following recommendations will help model soil-structure interaction with sufficient accuracy.

It is recommended that the "substructure method"[6, 7, 41] be used in analysing the soil-structure interaction problem. In this method, the problem of soil-structure interaction is divided into two steps. In the first step, the footings and the supporting soil are analyzed without the structure, and the footing stiffness is computed using a spring-dashpot system. In the second step, the bridge is assumed to be supported on the spring-dashpot system, and the dynamic analysis of the structure can be performed with a loading that depends on the free-field motion.

As a first step in computing the footing stiffness, it is very important to identify, with sufficient accuracy, the depth of embedment of the footings, the depth of the soil to the bedrock, and the properties of soils under the footings. In order to compute the dynamic footing stiffness of rectangular footings embedded in homogeneous stratum over bedrock, the following steps are recommended:

1) The radius of the equivalent circular footing (R) for the various modes of vibration (Eqs. 5.18 to 5.21), can be determined using Eqs. 5.12 to 5.15.
2) Use Eqs. 5.23 to 5.26, presented in Chapter 6, to compute the stiffness of circular footings embedded in a homogeneous stratum over bedrock.
3) For each mode of vibration, the stiffness of the surface circular footings

Chapter 7

Summary and Conclusions

7.1 Summary

This report presents the results of an experimental and analytical study conducted on three footings of an existing bridge. The bridge is located on Interstate 80 south east of Verdi, Nevada. The objectives of this research were twofold: to determine the in-situ stiffness of the three existing footings; and, based on the results of the first part of the study, to recommend a simple integrated procedure to compute the footing stiffness.

Six tests were conducted by shaking each footing once in the long and then in the short direction of the footing. Each footing was subjected to sinusoidal vibration force of amplitude of approximately 20,000 lb (89 KN) at a frequency of about 6.5 Hz. The forces were applied through an eccentric mass shaker. The shaker was anchored to the footing by high strength bolts.

Twenty-three accelerometers were used to measure the response of the soil, bridge footings, and the bent cap of the bridge during shaking. During the test, accelerations recorded on the bent cap were very small and were hence discarded.

Four seismic down-hole tests were conducted in order to measure the shear wave velocity at low-strain, $V_{s,\ max}$, of the soil directly under the footing. In addition, a subsurface exploration of the soil was performed to establish the top

5.5 ft (1.67 m) of the soil profile. Laboratory tests were also conducted on soil samples to measure the properties of the soil at the bridge site.

An analytical study was performed in order to determine the in-situ stiffness of the three existing footings as a function of different variables. A three-dimensional finite element model of the last two spans of the bridge was developed using computer program *COSMOS/M*. Only the last two spans were modeled because it was believed that the effect of foundation shaking was insignificant on the rest of the structure. Due to the small dynamic forces applied to the footings, the columns, the bent cap, the superstructure, and the footings were modeled as linear elastic elements.

A linear response history analysis was performed to determine steady state acceleration response of the three footings. During the analysis, the soil-footing interaction was modeled using a spring-dashpot model. Several refinements were applied to the response history analysis until the predicted steady state peak acceleration at the footing level matched the measured steady state peak acceleration on the corresponding footing during the dynamic field test. In order to improve the prediction of the in-situ stiffness of the three footings, several parameters that influence the response of the footings were identified. A sensitivity analysis was performed in order to measure the effects of varying those parameters on the acceleration response of the footings. The parameters were varied one at time, while the others were kept fixed at their originally computed values.

Design recommendations were also formulated based on the experimental and the analytical results. The recommendations provide the basis for the computation of footing stiffness using spring models and help determining the important soil parameters that affect the footing stiffness. A numerical example was also presented to illustrate the use of the proposed recommendations in calculating the stiffness of footings.

7.2 Conclusions

The following conclusions are based on the study presented in this report:

1. Spring models for the footings provided a convenient and simple means of modeling soil-structure interaction.
2. Although a simple approach was used to compute the footing stiffness, a good agreement between the measured and predicted soil shear modulus was obtained by using soil properties that were independently measured.
3. The Federal Highway Administration's (FHWA) approach[41] for calculating the footing stiffness ignores the presence of bedrock at shallow depths, which significantly affects the footing stiffness.
4. The approach presented in this research for the computation of footing stiffness is more realistic and consistent than that used by FHWA. It includes means of accounting for the strain-dependence of the soil shear modulus and other important factors such as footing embedment and presence of bedrock.
5. For a better estimation of footing stiffness, it is very important to measure the

soil shear modulus at low strain (G_{max}) with in-situ dynamic tests, rather than measuring it in the laboratory. Laboratory data generally do not match the field test data.

6. The great variability of soil matrix and the presence of adjacent structures at the bridge site can lead to soil shear modulus, which is different in both directions. This can affect the computed footing stiffness.

7. In this study, the soil shear modulus was the only parameter that significantly affected the dynamic response.

References

1. Applied Technology Council, ATC 3-06, *"Tentative Provisions for the Development of Seismic Regulations for Buildings,"* ATC Publications, 1978.

2. Beck, J.L. *"Determining Models of Structures from Earthquake Records,"* Report No. EERL 78-01, California Institute of Technology, Earthquake Engineering Research Laboratory, Pasdadena, California, June 1978, 300 pp.

3. Bowles, J.E. *Foundation Analysis and Design,* Fourth Edition, McGraw-Hill, Inc., 1988.

4. Byrne, P.M., Cheung, H., and Yan, L. *"Soil Parameters For Deformation Analysis of Sand Masses,"* Canadian Geotechnical Journal, 24, 1987, pp. 366-376.

5. Chow, Y.K. *"Vertical Vibration of 3-D Rigid Foundation on Layered Media,"* Earthquake Engineering and Structural Dynamics, 15, 1987, pp. 585-594.

6. Clough, R.W. and Penzien, J. *Dynamics of Structures,* 2nd Edition, McGraw-Hill, Inc., 1993.

7. Derecho, A.T. and Huckelbridge, A.A. *"Soil-Structure Interaction-A Brief Overview,"* Earthquake-Resistant Concrete Structures: Inelastic Response and Design, Ghosh, S.K., ed., ACI SP-127, Detroit, Michigan, 1991.

8. Dobry, R. and Gazetas, G. *"Dynamic Response of Arbitrarily Shaped Foundations,"* Journal of Geotechnical Engineering, ASCE, 112, No. 2, February 1986, pp. 109-135.

9. Dobry, R., Gazetas, G., and Stokoe, K.H., II. *"Dynamic Response of Arbitrarily Shaped Foundations: Experimental Verification,"* Journal of Geotechnical Engineering, ASCE, 112, No. 2, February 1986, pp. 136-149.

10. Dobry, R. and Gazetas, G. *"Dynamic Stiffness and Damping of Foundations by Simple Methods,"* Vibration Problems in Geotechnical Engineering, ed. G. Gazetas and E.T. Selig, ASCE, 1985, pp. 77-107.

11. Douglas, B.M., Maragakis, E.M., and Feng, S. *"Stiffness Evaluation of Pile Foundation of Cazenovia Creek Overpass,"* Civil Engineering Department, Report No. CCEER-94-2, University of Nevada, Reno, March 1994.

12. Douglas, B.M., Maragakis, E.A., and Nath, B. *"Static Deformations of Bridges from Quick-Release Accelerograms,"* Journal of Structural Engineering, ASCE, Vol. 116, No. 8, August 1990, pp. 2201-2213.

13. Douglas, B.M. and Reid, W.H. *"Dynamic Tests and System Identification of Bridges,"* Journal of Structural Engineering, ASCE, 108:ST10, October 1982, pp. 2295-2312.

14. Elsabee, F. and Morray, J.P. *"Dynamic Behavior of Embedded Foundations,"* Research Report R77-33, MIT, 1977.

15. Fotopoulou, M. et al. *"Rocking Damping of Arbitrarily Shaped Embedded Foundations,"* Journal of Geotechnical Engineering, ASCE, 115, 1989, pp. 473-490.

16. Gazetas, G. *"Foundation Vibrations,"* Foundation Engineering Handbook, 2nd Edition Fang, H.Y., ed., Van Norstand Reinhold, New York, N.Y., 1991, pp. 553-593.

17. Gazetas, G. *"Simple Physical Models For Foundation Impedances,"* Dynamic Behavior of Foundations and Buried Structures, Elsevier Applied Science, New York, N.Y., Chapter 2, 1987, pp.45-94.

18. Gazetas, G. and Roesset, J.M. "Vertical Vibrations of Machine Foundations," Journal of Geotechnical Engineering, ASCE, 105, 1979, pp. 1435-1454.

19. Idriss, I.M. and Sun, J.I. *"SHAKE 91: A Computer Program for Conducting Equivalent Linear Seismic Response Analyses of Horizontally Layered Soil Deposits,"* Department of Civil & Environmental Engineering, University of California, Davis, November 1992.

20. *Instruction and Maintenance Manual for MK-12.8A-4600 Eccentric Mass Shaker System*", Prepared by Anco Engineers, Inc., Culver City, California.

21. Jakub, M. and Roesset, J.M. *"Dynamic Stiffness of Foundations: 2-D vs 3-D Solutions,"* Research Report R77-36, MIT, 1977.

22. Johnson, G.R., Christiano, P., and Epstein, H.I. *"Stiffness Coefficients For Embedded Footings,"* Journal of Geotechnical Engineering, ASCE, 101, 1975, pp. 789-900.

23. Kausel, E. and Ushijima, R. *"Vertical and Torsional Stiffness of Cylindrical Footings,"* Research Report R76-6, MIT, 1979.

24. Kausel, E., Whitman, R.V., Morray, J.P., and Elsabee, F. *"The Spring Method for Embedded Foundations,"* Nuclear Engineering and Design, Vol. 48, 1978, pp. 377-392.

25. Kausel, E. *"Forced Vibrations of Circular Foundations on Layered Media,"* Research Report R74-11, MIT, 1974.

26. Knox, D.P., Stokoe, K.H., and Kopperman, S.E. *"Effect of State of Stress on Velocity of Low-Amplitude Shear Waves Along Principal Stress Directions in Dry Sand,"* Research Report GR82-23, University of Texas, Austin, 1982.

27. Levine, M.B. and Scott, R. *"Dynamic Response Verification of Simplified Bridge-Foundation Model,"* Journal of Geotechnical Engineering, ASCE, 115, No. 2, February 1989, pp. 246-260.

28. Lysmer, J., Tabatabaie-Raissi, M., Vahdani, S., and Ostadan, F. *"SASSI - A System for Analysis of Soil-Structure Interaction,"* Report UCB/GT/81-02, University of California, Berkeley, 1981, 54pp.

29. Lysmer, J. and Kuhlemeyer, R.L. *"Finite Dynamic Model for Infinite Media,"* Journal of the Engineering Mechanics Division, ASCE, Vol. 95, No. EM4, August 1969, pp. 859-877.

30. *"Manuals of COSMOS/M Version 1.75: Finite Element Analysis Computer Program,"* Structural Research and Analysis Corporation, Los Angeles, California.

31. Newmark, N.M. and Rosenblueth, E. *Fundamentals of Earthquake Engineering,* Prentice-Hall, Inc., Englewood Cliffs, N.J., 1971.

32. Norris, G.M. *"Pile Foundation Stiffness as a Function of Free-Field or Near-Field Soil Strain,"* ASCE Geotechnical Special Publication No. 51, John P. Turner, ed., 1995, pp. 32-44.

33. Priestley, M.J.N., Seible, F., and Calvi, G.M. *Seismic Design and Retrofit of Bridges,* John Wiley & Sons, Inc., 1996.

34. Saiidi, M., Hart, J., and Douglas, B. *"A Nonlinear Model for Static and Dynamic Transverse Load Analysis of Reinforced Concrete Highway Bridges,"* Journal of Computers and Structures, Vol. 26, No. 5, pp. 831-840.

35. Seed, H.B., Wong, R.T., Idriss, I.M., and Tokimatsu, K. *"Moduli and Damping Factors For Dynamic Analyses of Cohesionless Soils,"* University of California, Berkeley, Earthquake Engineering Research Center, Report No. UCB/EERC-84/14, 1984, pp. 37.

36. Seed, H.B. and Lysmer, J. *"Soil-Structure Interaction Analysis by Finite Element Methods, State-of-the-Art,"* Trans., 4th Int'l. Conf. On Structural Mechanics in Reactor Technology, SmiRT4, Vol. K (a), Paper K2/1, San Francisco, California, August 1977, pp. 1-11.

37. Seed, H.B. and Idriss, I.M. *"Soil Moduli and Damping Factors for Dynamic Response Analysis,"* Research Report EERC70-10, University of California, Berkeley, 1970.

38. Siddharthan, R. and Maragakis, E.M. *"Performance of Flexible Retaining Walls Supporting Dry Cohesionless Soils Under Cyclic Loads,"* International Journal For Numerical and Analytical Methods in Geomechanics, Vol. 13, 309-326, 1989.

39. Siddharthan, R. and Norris, G.M. *"Seismic Displacement Response of Surface Footings in Sand,"* Fifth Canadian Conference on Earthquake Engineering, Ottawa, Canada, July 1987, pp. 407-416.

40. The Federal Highway Administration. *"Seismic Design and Retrofit Manual For Highway Bridges,"* Report No. FHWA-IP-87-6, Washington, D.C., 1987.

41. The Federal Highway Administration. *"Highway Bridge Foundation Design to Resist Earthquake Motion,"* Report No. FHWA/RD/86-102, Washington, D.C, 1986.

42. Veletsos, A.S. and Prasad, A.M. *"Seismic Interaction of Structures and Soil: Stochastic Approash,"* Journal of Structural Engineering, ASCE, Vol. 115, No. 4, April 1989, pp. 935-956.

43. Velestos, A.S. and Vebric, B. *"Vibrations of Viscoelastic Foundations,"* Earthquake Engineering and Structural Dynamics, 2, 1973, pp. 87-102.

44. Veletsos, A.S. and Wei, Y.T. *"Lateral and Rocking Vibrations of Footings,"* Journal of Soil Mechanics and Foundations Division, ASCE, 97, No. SM-9, 1971, pp. 1227-1248.

45. Vrontinos, S. *"Analytical and Experimental Studies on the Seismic Response of Short Span Reinforced Concrete Bridges,"* PhD Dissertation, Civil Engineering Department, University of Nevada, Reno, May 1994, 377 pp.

46. Wolf, J.P. *"Spring-Dashpot-Mass Models for Foundation Vibrations,"* Earthquake Engineering and Structural Dynamics, Vol. 26, 931-949 (1997).

47. AASHTO, *Standard Specifications for Highway Bridges, 15th Edition.* Washington, D.C.: American Association of State Highway and Transportation Officials, 1992.

Table 3.1. Measured Soil and Footing Steady State Accelerations During the Test of Footing I in the Longitudinal Direction

Footing No.	Shaking Direction	Force Kips (KN)	Frequency Hz	Accelerometer No.	Acceleration g
I	L	19.16 (85.23)	6.39	DIL4	0.0023
I	L	19.16 (85.23)	6.39	EIL5	0.00088
I	L	19.16 (85.23)	6.39	IL9	0.0033
I	L	19.16 (85.23)	6.39	IL11	0.0033

Table 3.2. Measured Soil and Footing Steady State Accelerations During the Test of Footing I in the Short Direction

Footing No.	Shaking Direction	Force Kips (KN)	Frequency Hz	Accelerometer No.	Acceleration g
I	S	18.9 (84)	6.36	BIS2	0.00089
I	S	18.9 (84)	6.36	CIS3	0.0026
I	S	18.9 (84)	6.36	FIS6	0.0026
I	S	18.9 (84)	6.36	GIS7	0.00134
I	S	18.9 (84)	6.36	IS9	0.00133
I	S	18.9 (84)	6.36	IS10	0.00134
I	S	18.9 (84)	6.36	IS11	0.0012
I	S	18.9 (84)	6.36	IS12	0.0059

Table 3.3. Measured Soil and Footing Steady State Accelerations During the Test of Footing II in the Longitudinal Direction

Footing No.	Shaking Direction	Force Kips (KN)	Frequency Hz	Accelerometer No.	Acceleration g
II	L	19.7 (87.6)	6.49	IIIL4	0.0029
II	L	19.7 (87.6)	6.49	JIIL5	0.0012
II	L	19.7 (87.6)	6.49	IIL13	0.00355
II	L	19.7 (87.6)	6.49	IIL14	0.00355

Table 3.4. Measured Soil and Footing Steady State Accelerations During the Test of Footing II in the Short Direction

Footing No.	Shaking Direction	Force Kips (KN)	Frequency Hz	Accelerometer No.	Acceleration g
II	S	19.5 (86.7)	6.45	GIIS2	0.00133
II	S	19.5 (86.7)	6.45	HIIS3	0.0027
II	S	19.5 (86.7)	6.45	KIIS6	0.0029
II	S	19.5 (86.7)	6.45	LIIS7	0.00138
II	S	19.5 (86.7)	6.45	IIS13	0.0013
II	S	19.5 (86.7)	6.45	IIS14	0.0016
II	S	19.5 (86.7)	6.45	IIS15	0.001
II	S	19.5 (86.7)	6.45	IIS16	0.0057

Table 3.5. Measured Soil and Footing Steady State Accelerations During the Test of Footing III in the Longitudinal Direction

Footing No.	Shaking Direction	Force Kips (KN)	Frequency Hz	Accelerometer No.	Acceleration g
III	L	20 (89)	6.52	NIIIL4	0.0024
III	L	20 (89)	6.52	OIIIL5	0.001
III	L	20 (89)	6.52	IIIL17	0.0033
III	L	20 (89)	6.52	IIIL19	0.0033

Table 3.6. Measured Soil and Footing Steady State Accelerations During the Test of Footing III in the Short Direction

Footing No.	Shaking Direction	Force Kips (KN)	Frequency Hz	Accelerometer No.	Acceleration g
III	S	19.5 (86.7)	6.45	LIIIS2	0.00096
III	S	19.5 (86.7)	6.45	MIIIS3	0.0023
III	S	19.5 (86.7)	6.45	PIIIS6	0.0023
III	S	19.5 (86.7)	6.45	QIIIS7	0.001
III	S	19.5 (86.7)	6.45	IIIS17	0.0012
III	S	19.5 (86.7)	6.45	IIIS18	0.0015
III	S	19.5 (86.7)	6.45	IIIS19	0.00084
III	S	19.5 (86.7)	6.45	IIIS20	0.005

Table 5.1. Superstructure Gross Section Properties

Element No.	Nodes		A	I_{x-x}	I_{y-y}	J	$\gamma_{equiv.}$
	From	To	ft^2 (m^2)	ft^4 (m^4)	ft^4 (m^4)	ft^4 (m^4)	lb/ft^3 (KN/m^3)
1	1	2	6.47 (0.60)	9.79 (0.084)	1039.10 (8.970)	0.435 (0.00375)	807 (126.76)
2	2	3	7.20 (0.121)	13.97 (0.121)	1127.53 (9.732)	0.450 (0.00388)	777 (122.15)
3	3	4	7.20 (0.121)	13.97 (0.121)	1127.53 (9.732)	0.450 (0.00388)	777 (122.15)
4	4	5	6.47 (0.60)	9.79 (0.084)	1039.10 (8.970)	0.435 (0.00375)	807 (126.76)
5	5	6	6.47 (0.60)	9.79 (0.084)	1039.10 (8.970)	0.435 (0.00375)	807 (126.76)
6	6	7	7.20 (0.67)	13.97 (0.121)	1127.53 (9.732)	0.450 (0.00388)	777 (122.15)
7	7	8	7.20 (0.67)	13.97 (0.121)	1127.53 (9.732)	0.450 (0.00388)	777 (122.15)
8	8	9	6.47 (0.60)	9.79 (0.084)	1039.10 (8.970)	0.435 (0.00375)	807 (126.76)

Table 5.4. Effect of Column Stiffness on the Steady State Response of the Footing

Footing No.	Loading Direction	Steady State Acceleration (g)			[1-(0.5 I_g)/I_g] (%)
		0.5 $I_{g\,(CoL)}$	0.7 $I_{g\,(CoL)}$	$I_{g\,(CoL)}$	
I	Long	0.00412	0.0041	0.00406	1.33
I	Short	0.00357	0.00347	0.00335	6.16
II	Long	0.00441	0.00439	0.00435	1.36
II	Short	0.00379	0.00368	0.00354	6.6
III	Long	0.00451	0.00449	0.00445	1.4
III	Short	0.00382	0.00371	0.00359	5.9

Table 5.5. Predicted and Measured Soil Shear Modulus for the Three Footings in the Longitudinal and Short Direction

Footing No.	Loading Direction	$G_{predicted}$ Ksi (MPa)	$\delta_{Predicted}$ in. (mm)	$\gamma_{c\ predicted}$ %	G/G_{max} "Pred."	$G_{max\ predicted}$ Ksi (MPa)	$G_{max\ measured}$ Ksi (MPa)
I	Long	39.5 (272.3)	7.8×10^{-4} (0.020)	5×10^{-4}	0.98	40.3 (277.8)	N/A
I	Short	29.8 (205.4)	8.9×10^{-4} (0.023)	8×10^{-4}	0.95	31.5 (217.2)	32 (220.6)
II	Long	39.5 (272.3)	8.0×10^{-4} (0.021)	5×10^{-4}	0.98	40.3 (277.8)	N/A
II	Short	31.0 (213.7)	8.7×10^{-4} (0.022)	8×10^{-4}	0.95	32.5 (224.0)	32 (220.6)
III	Long	42.0 (289.5)	7.8×10^{-4} (0.020)	5×10^{-4}	0.98	42.8 (295.0)	N/A
III	Short	36.0 (248.2)	7.8×10^{-4} (0.020)	7×10^{-4}	0.96	37.5 (258.5)	N/A

Table 5.6. Predicted In-Situ Footing Stiffness Due to the Applied Dynamic Forces to the Footings in the Longitudinal and Short Direction

G Ksi (MPa)	K_Y K/ft (KN/m)	K_X K/ft (KN/m)	K_Z K/ft (KN/m)	K_t K-ft (KN-m)	$K_{\theta X}$ K-ft (KN-m)	$K_{\theta Z}$ K-ft (KN-m)
39.5 (272.3)	2.8×10^5 (4.1×10^6)	3.0×10^5 (4.4×10^6)	2.9×10^5 (4.2×10^6)	18.5×10^6 (27.0×10^6)	11.9×10^6 (17.4×10^6)	7.4×10^6 (10.7×10^6)
29.8 (206.8)	2.1×10^5 (3.0×10^6)	2.3×10^5 (3.3×10^6)	2.2×10^5 (3.2×10^6)	13.9×10^6 (20.2×10^6)	9.0×10^6 (13.0×10^6)	5.6×10^6 (8.0×10^6)
39.5 (272.3)	2.8×10^5 (4.1×10^6)	3.0×10^5 (4.4×10^6)	2.9×10^5 (4.2×10^6)	18.5×10^6 (27.0×10^6)	11.9×10^6 (17.4×10^6)	7.4×10^6 (10.7×10^6)
31.0 (213.7)	2.2×10^5 (3.2×10^6)	$2.4x\ 10^5$ (3.4×10^6)	2.3×10^5 (3.3×10^6)	14.8×10^6 (21.6×10^6)	9.3×10^6 (13.5×10^6)	5.8×10^6 (8.4×10^6)
42.0 (289.5)	3.0×10^5 (4.3×10^6)	3.2×10^5 (4.7×10^6)	3.0×10^5 (4.4×10^6)	19.4×10^6 (28.3×10^6)	12.6×10^6 (18.3×10^6)	7.9×10^6 (11.3×10^6)
36 (248.2)	2.5×10^5 (3.7×10^6)	2.7×10^5 (4.0×10^6)	2.6×10^5 (3.8×10^6)	16.7×10^6 (24.3×10^6)	10.8×10^6 (15.7×10^6)	6.8×10^6 (9.7×10^6)

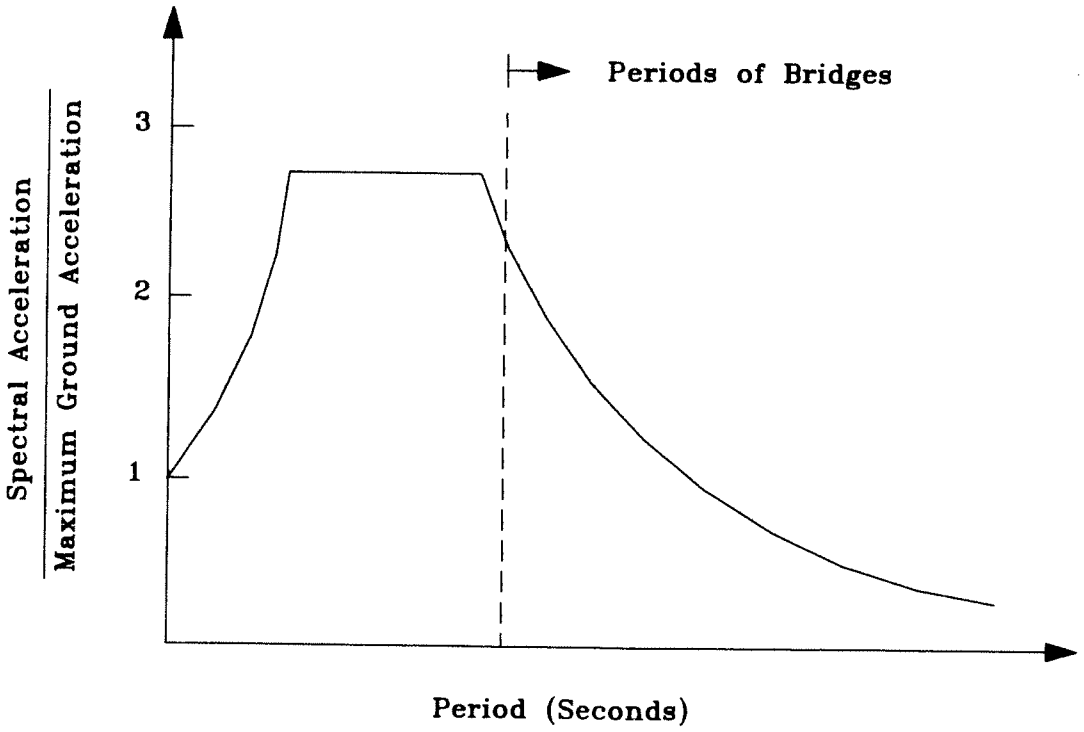

Figure 1.1. Normalized Acceleration Response Spectra for Elastic Systems

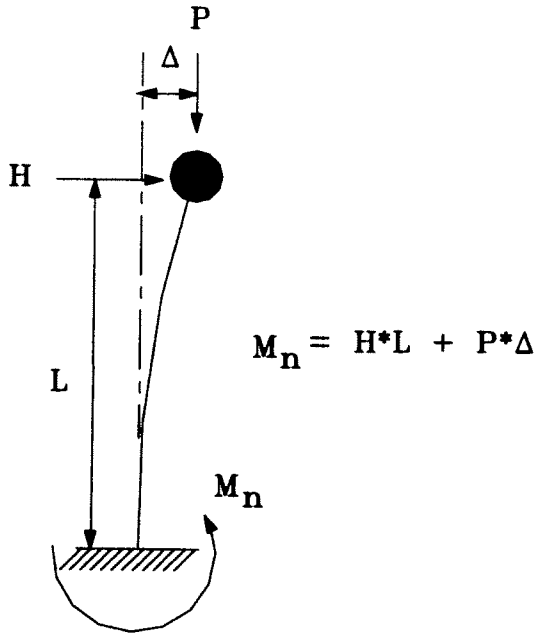

Figure 1.2. Effect of P-Δ on the Lateral Load Capacity of Bridge Columns

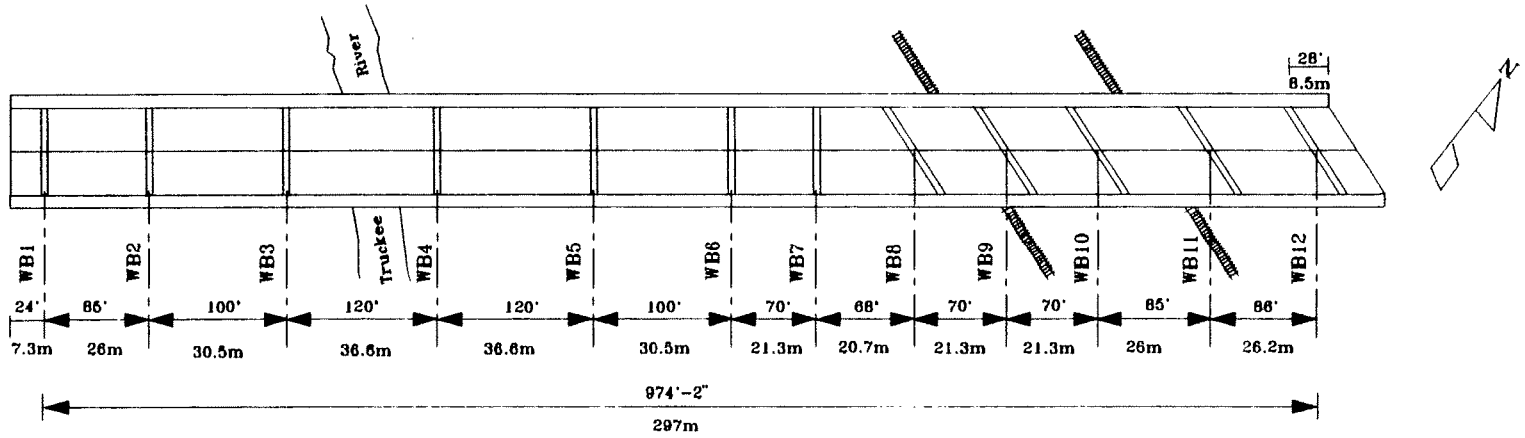

PLAN

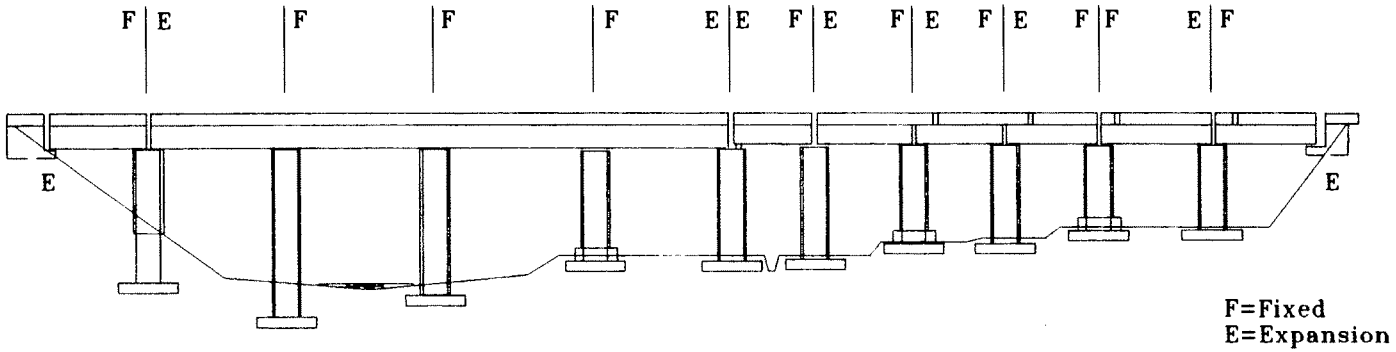

WEST BOUND ELEVATION

Figure 2.1. "G-772 W" Bridge Plan And Elevation

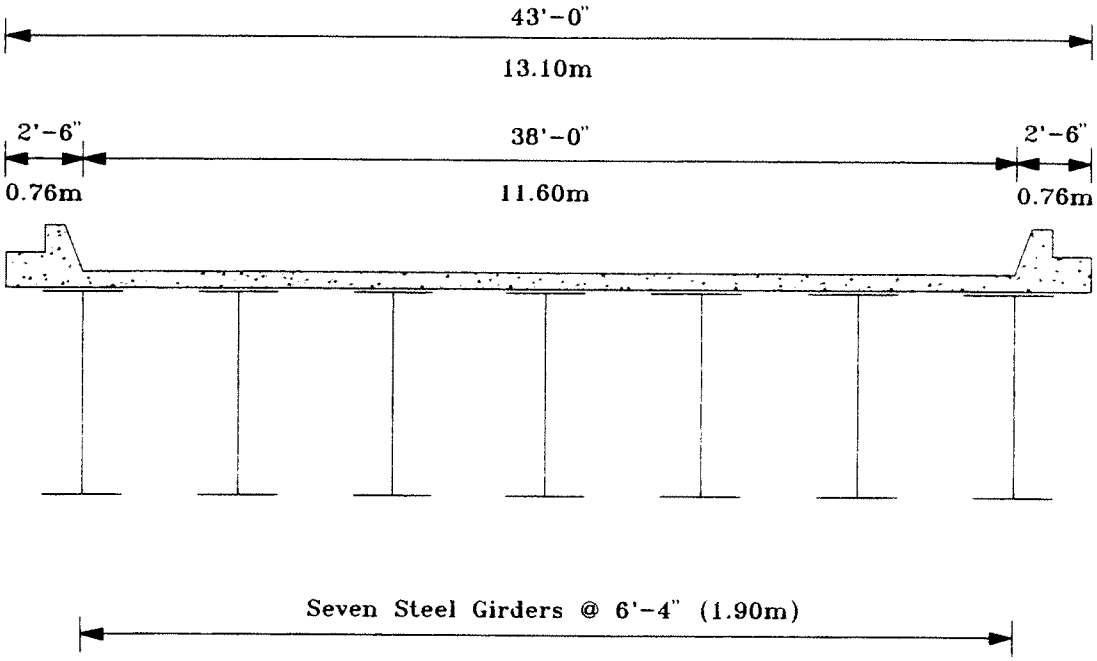

Figure 2.2. Cross Section of "G-772 W" Bridge

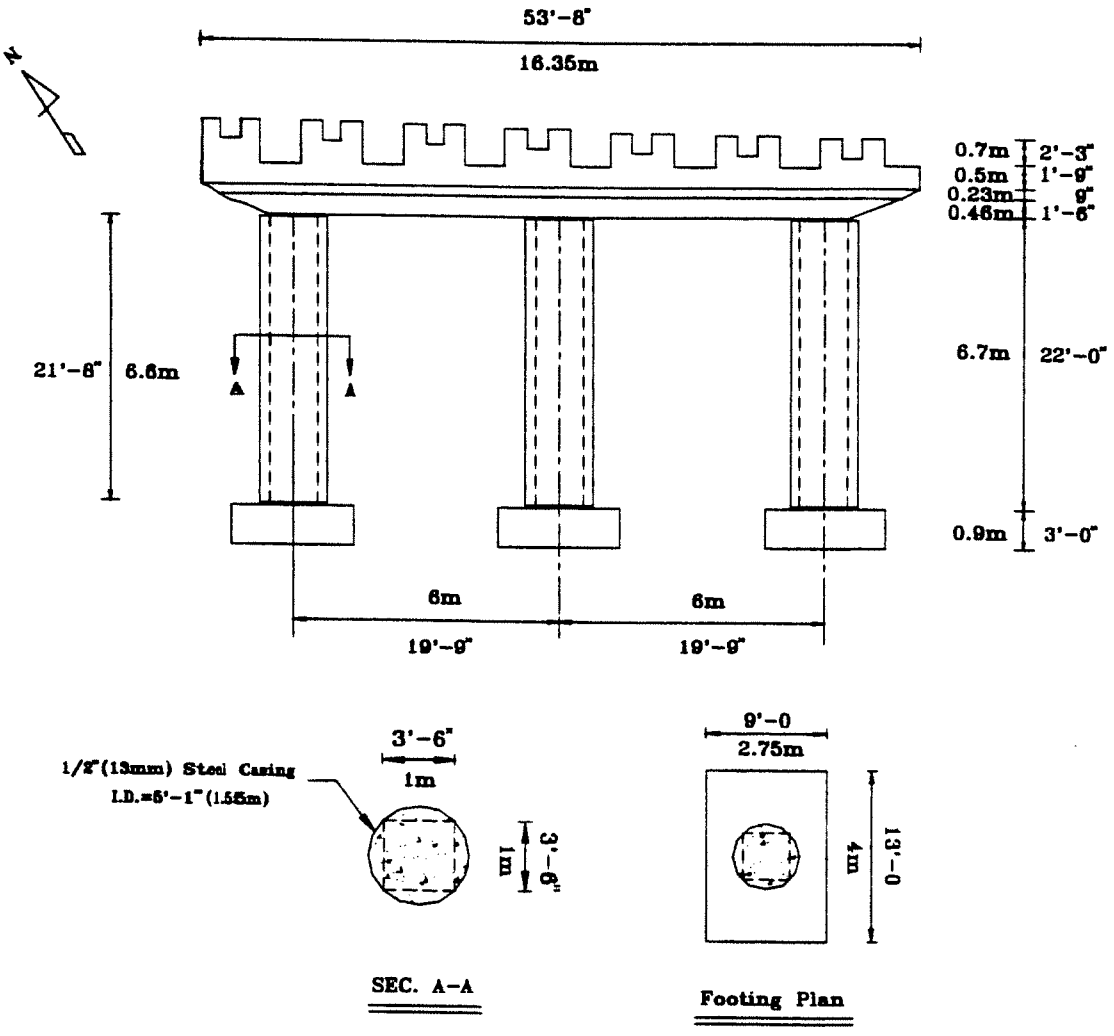

Figure 2.3. Column and Footing Details of Bent WB11

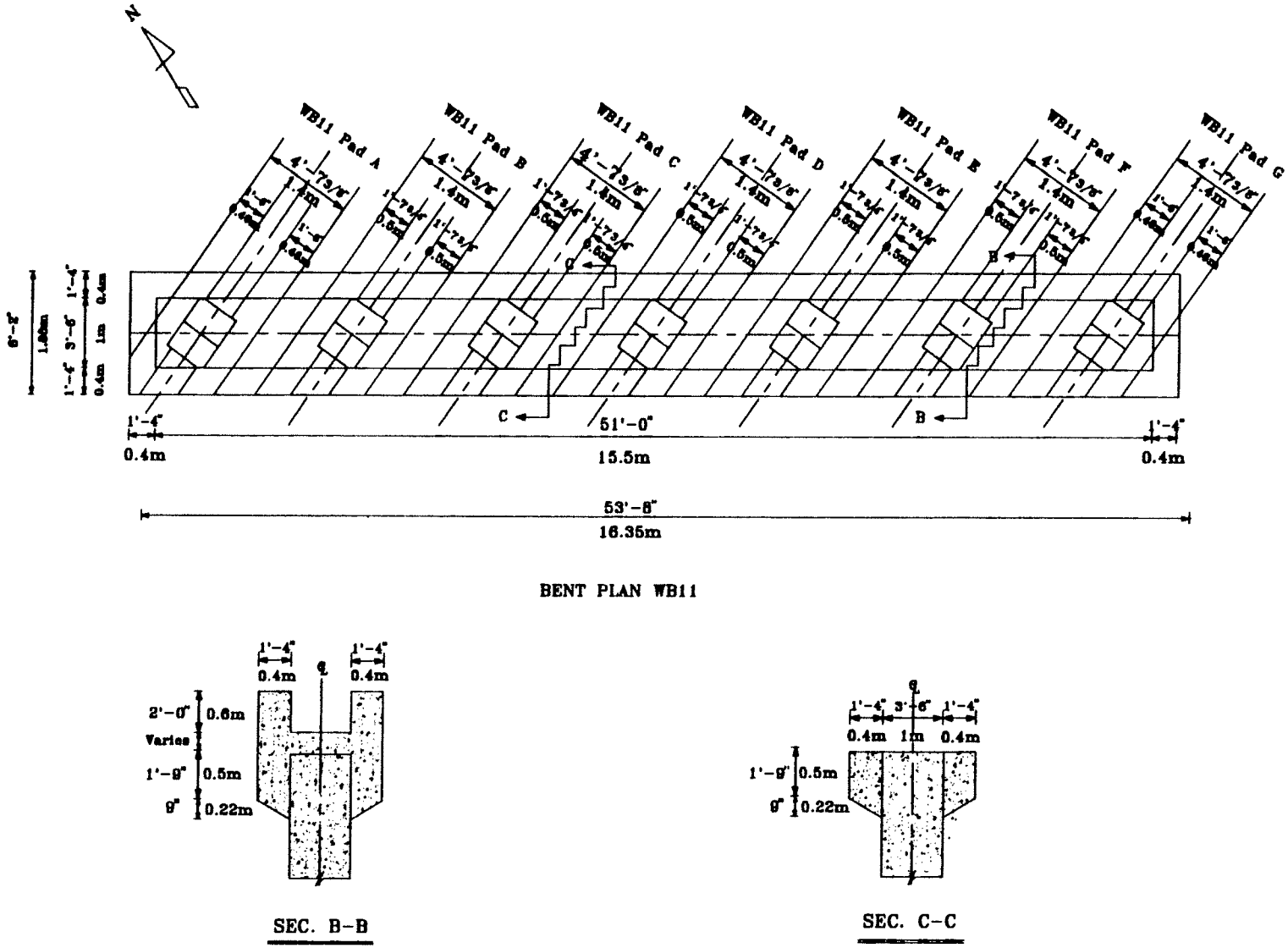

Figure 2.4. Plan View of Bent WB11

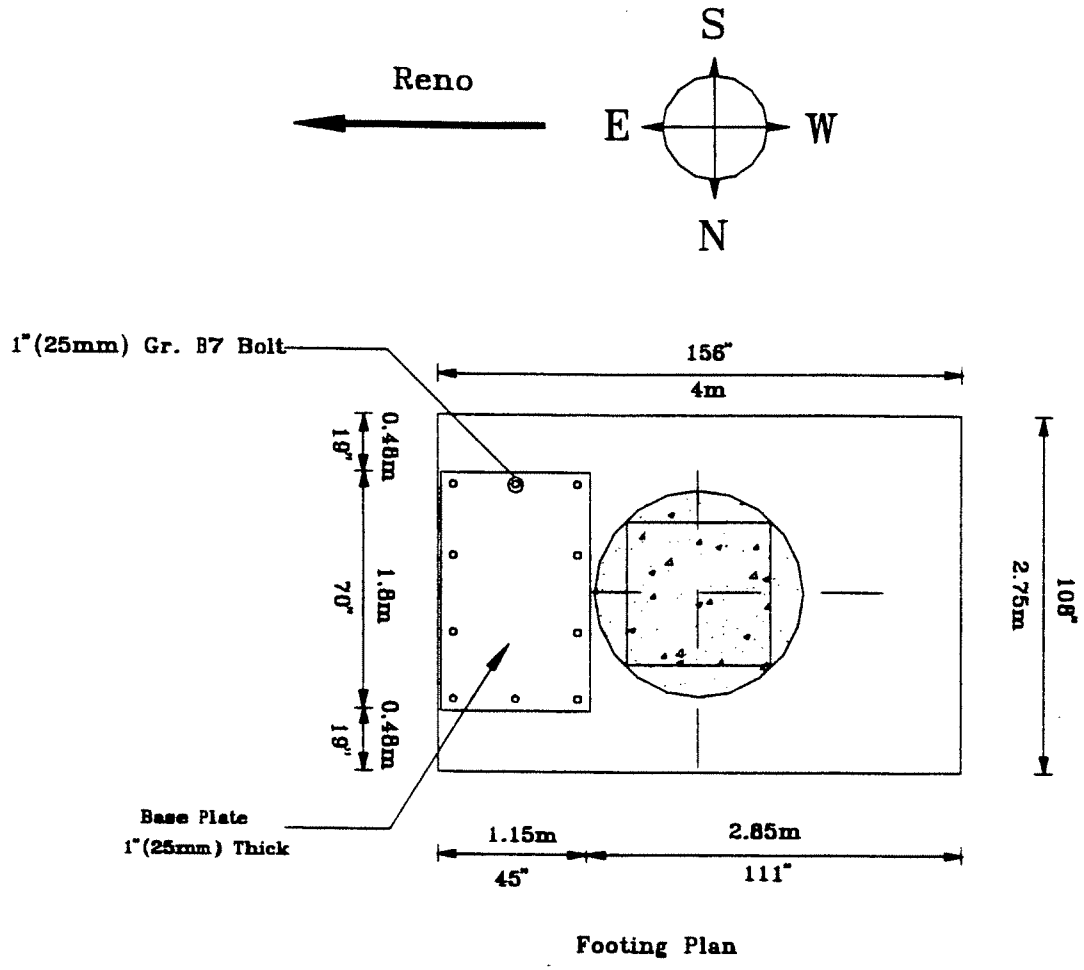

Figure 2.5. Steel Base Plate Attachment to the Bridge Footing

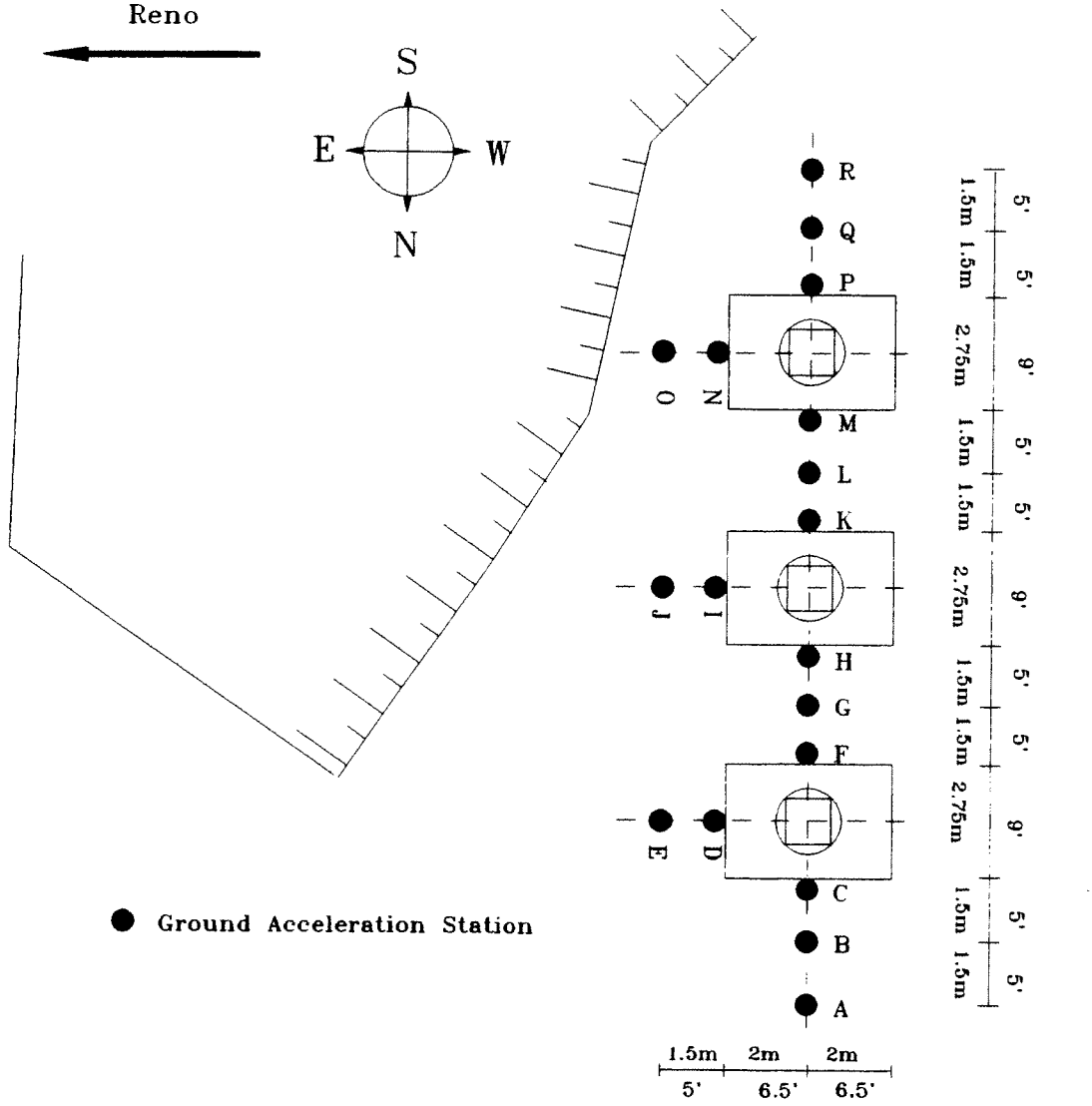

Figure 2.6. Layout of Ground Acceleration Stations

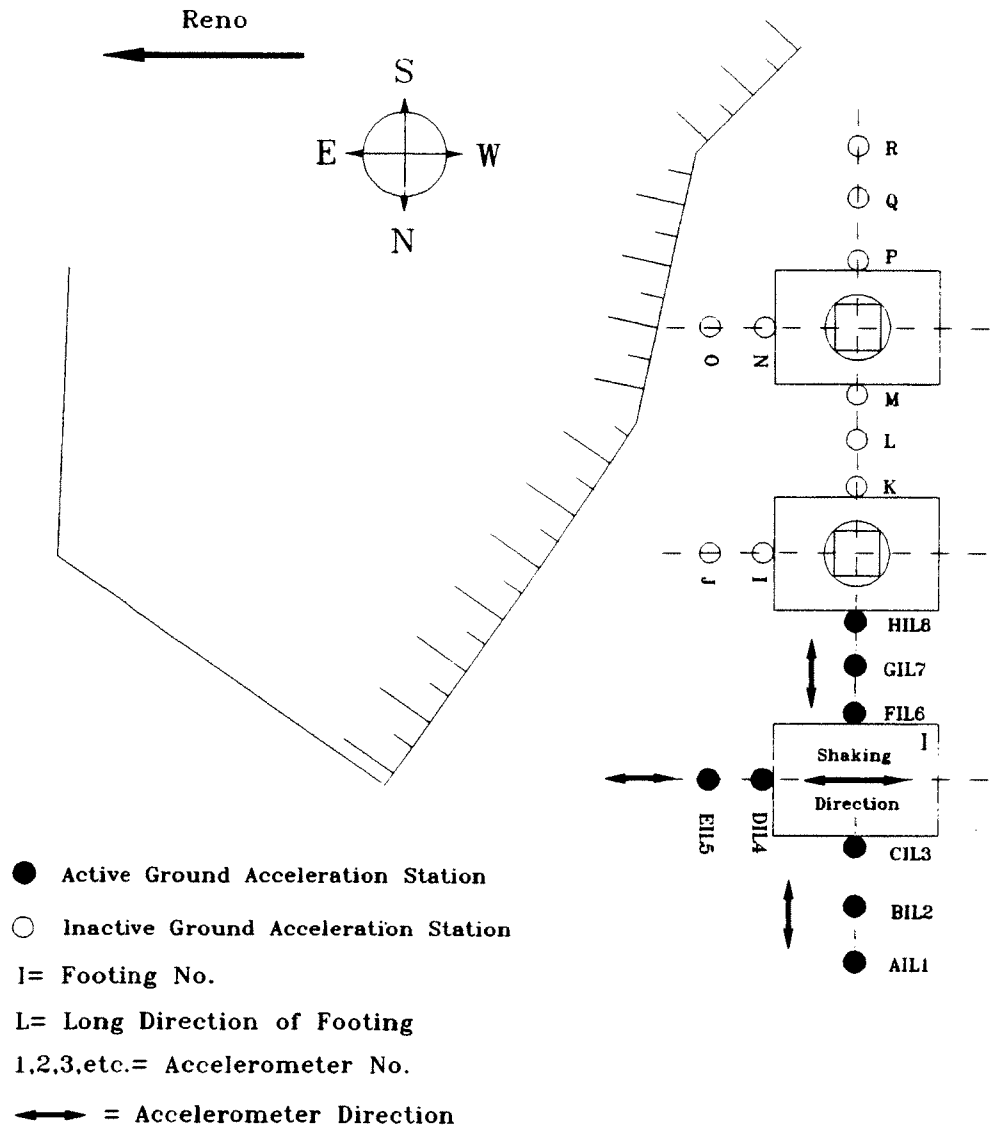

Figure 2.7. Numbering and Location of Ground Accelerometers During the Test of Footing I in the Longitudinal Direction

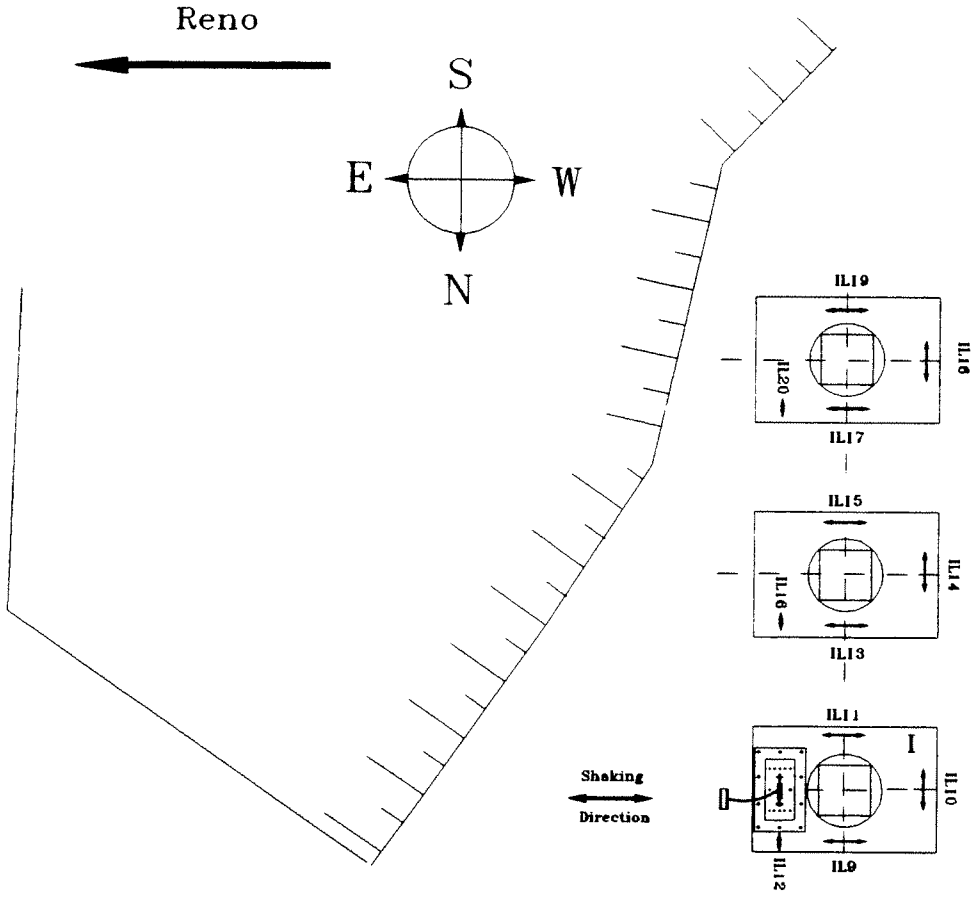

I= Footing No.
L= Long Direction of Footing
8.9.10. etc.= Accelerometer No.

Figure 2.8. Numbering and Location of Footing Accelerometers During the Test of Footing I in the Longitudinal Direction

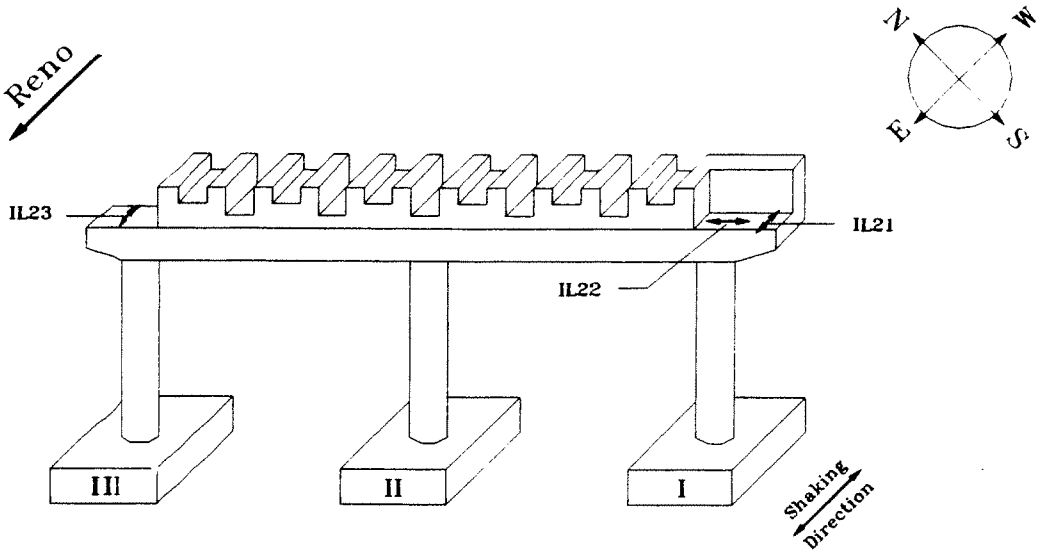

Figure 2.9. Numbering and Location of Bent Cap Accelerometers During the Test of Footing I in the Longitudinal Direction

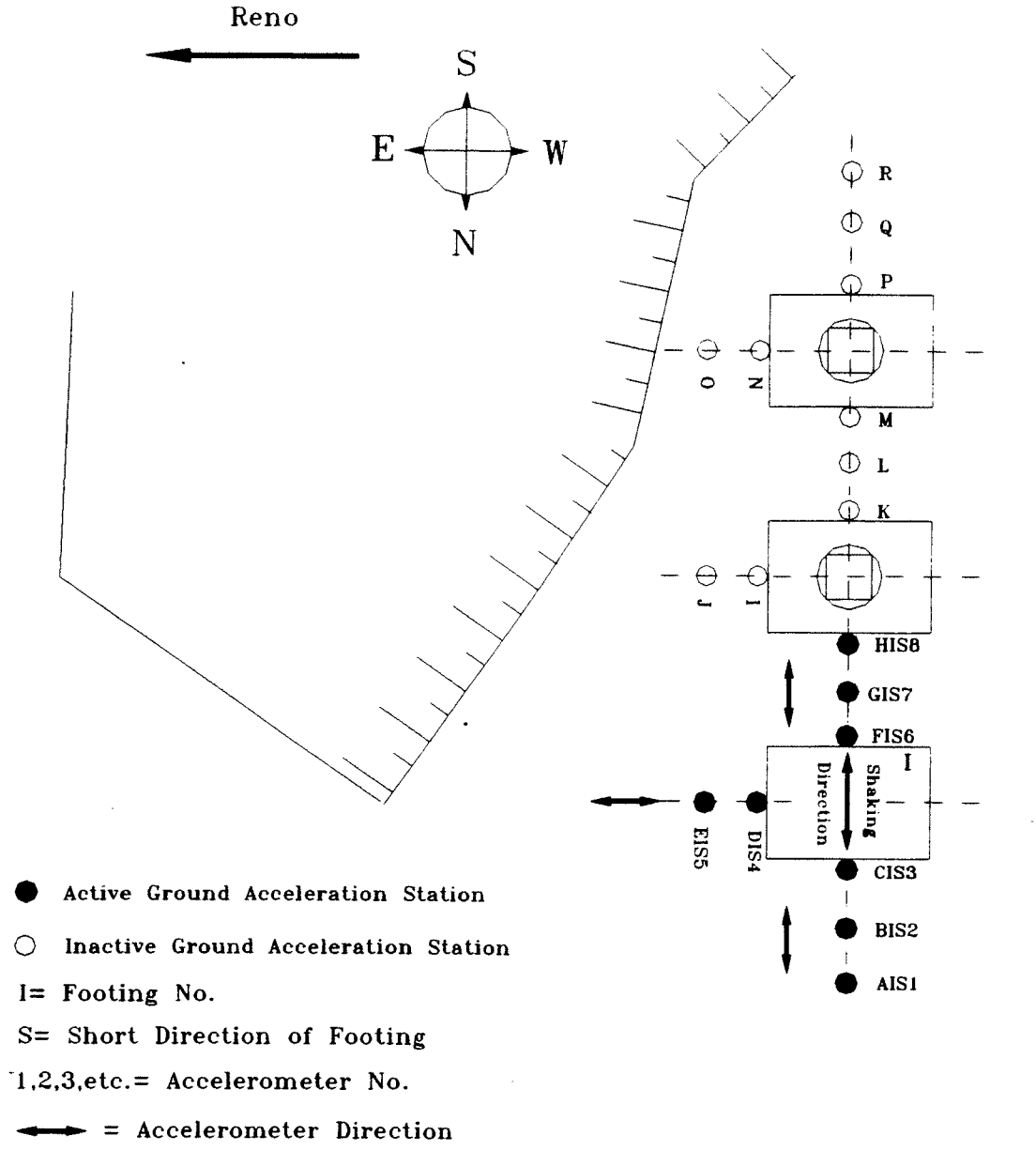

Figure 2.10. Numbering and Location of Ground Accelerometers During the Test of Footing I in the Short Direction

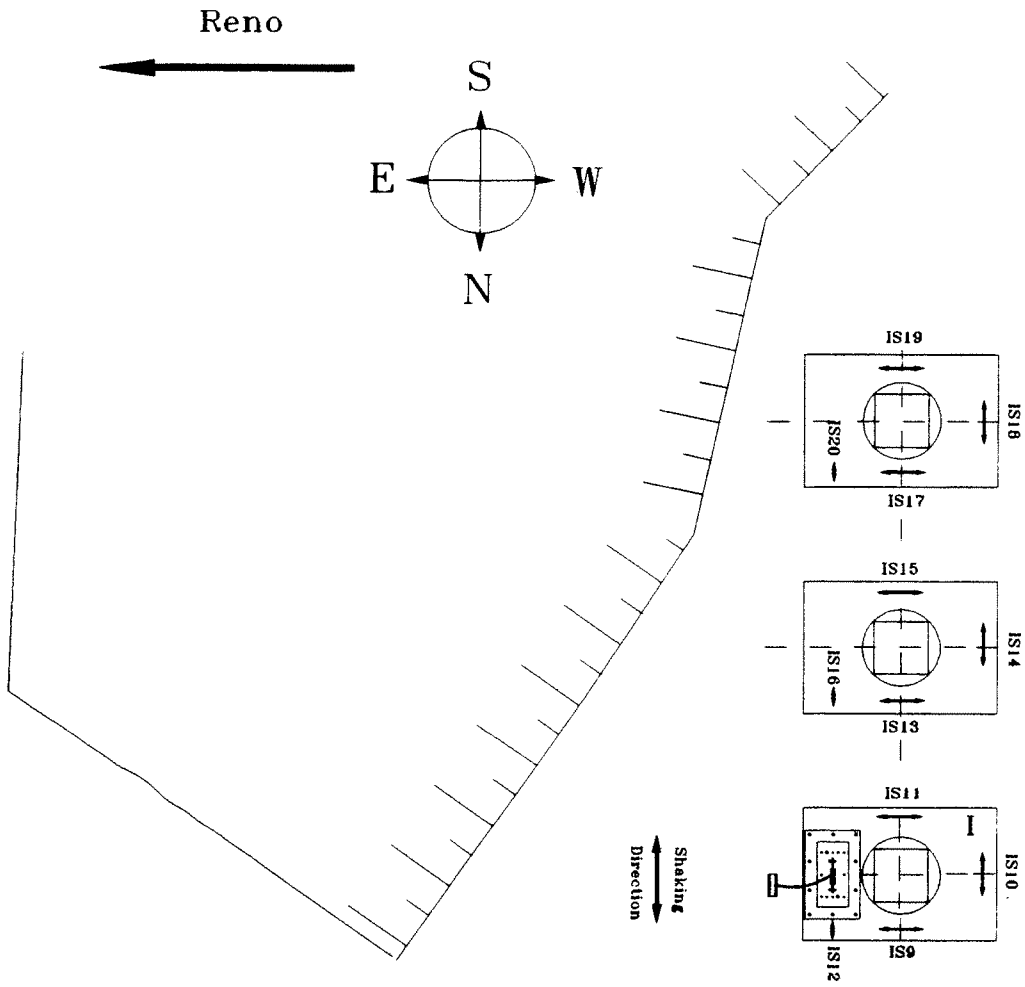

Figure 2.11. Numbering and Location of Footing Accelerometers During the Test of Footing I in the Short Direction

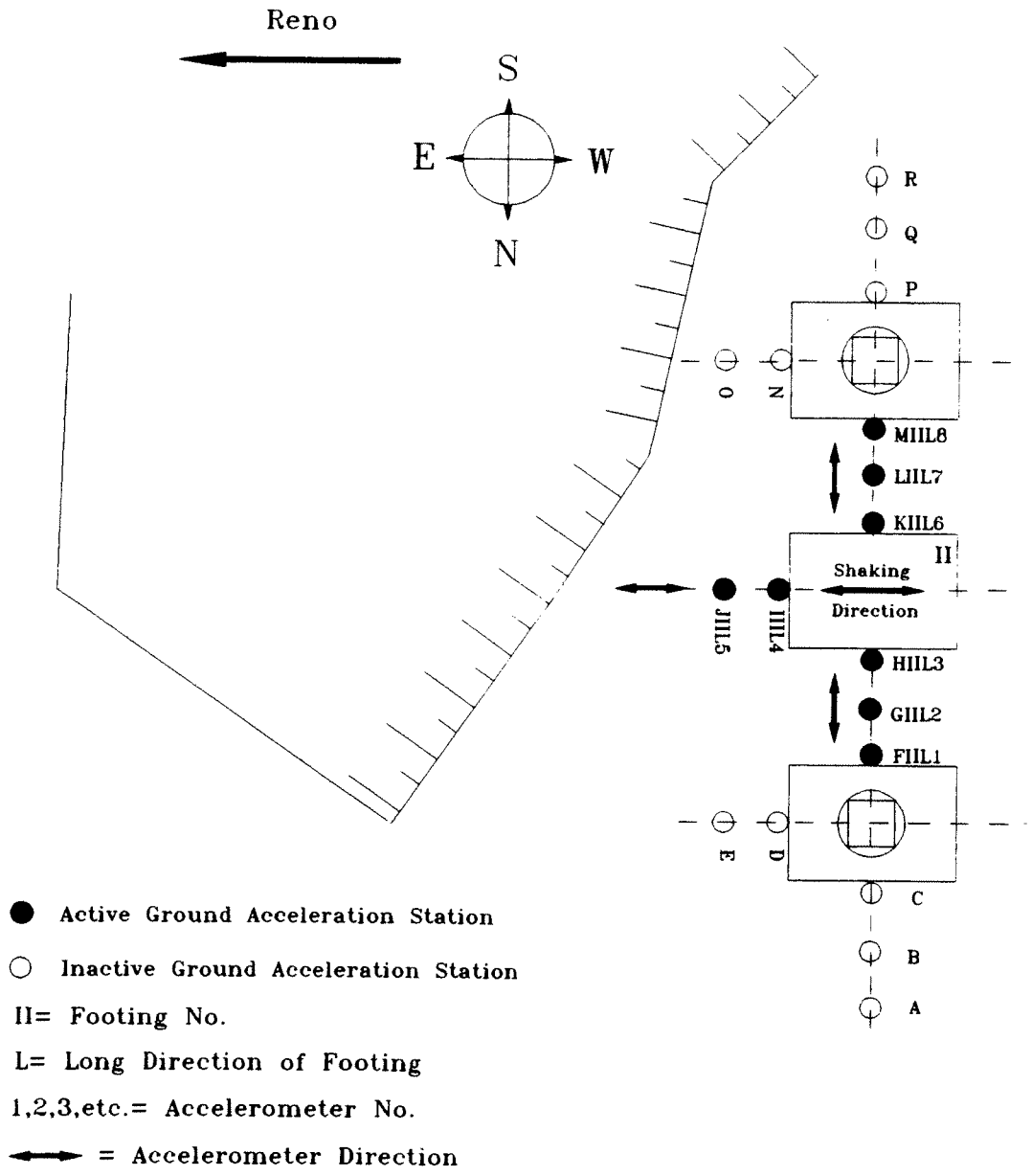

Figure 2.12. Numbering and Location of Ground Accelerometers During the Test of Footing II in the Longitudinal Direction

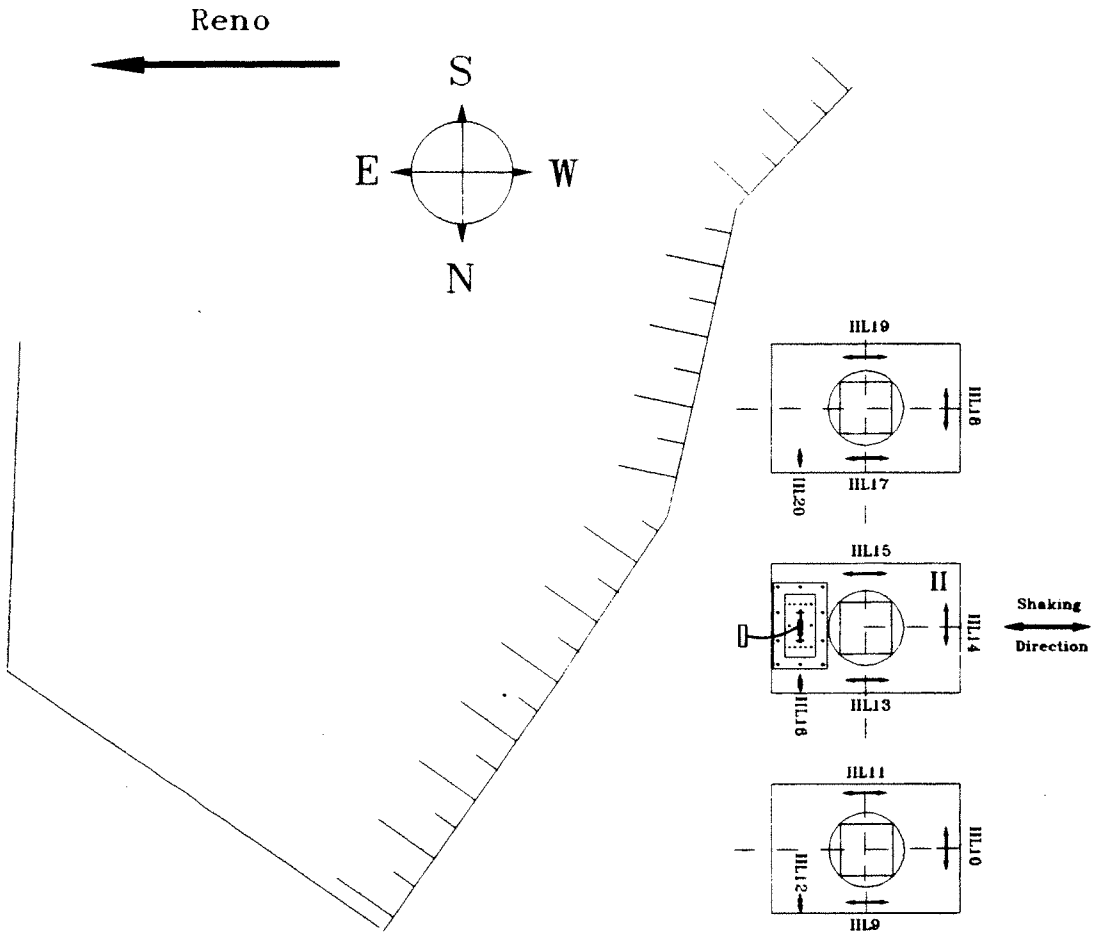

II= Footing No.
L= Long Direction of Footing
8,9,10, etc.= Accelerometer No.

Figure 2.13. Numbering and Location of Footing Accelerometers During the Test of Footing II in the Longitudinal Direction

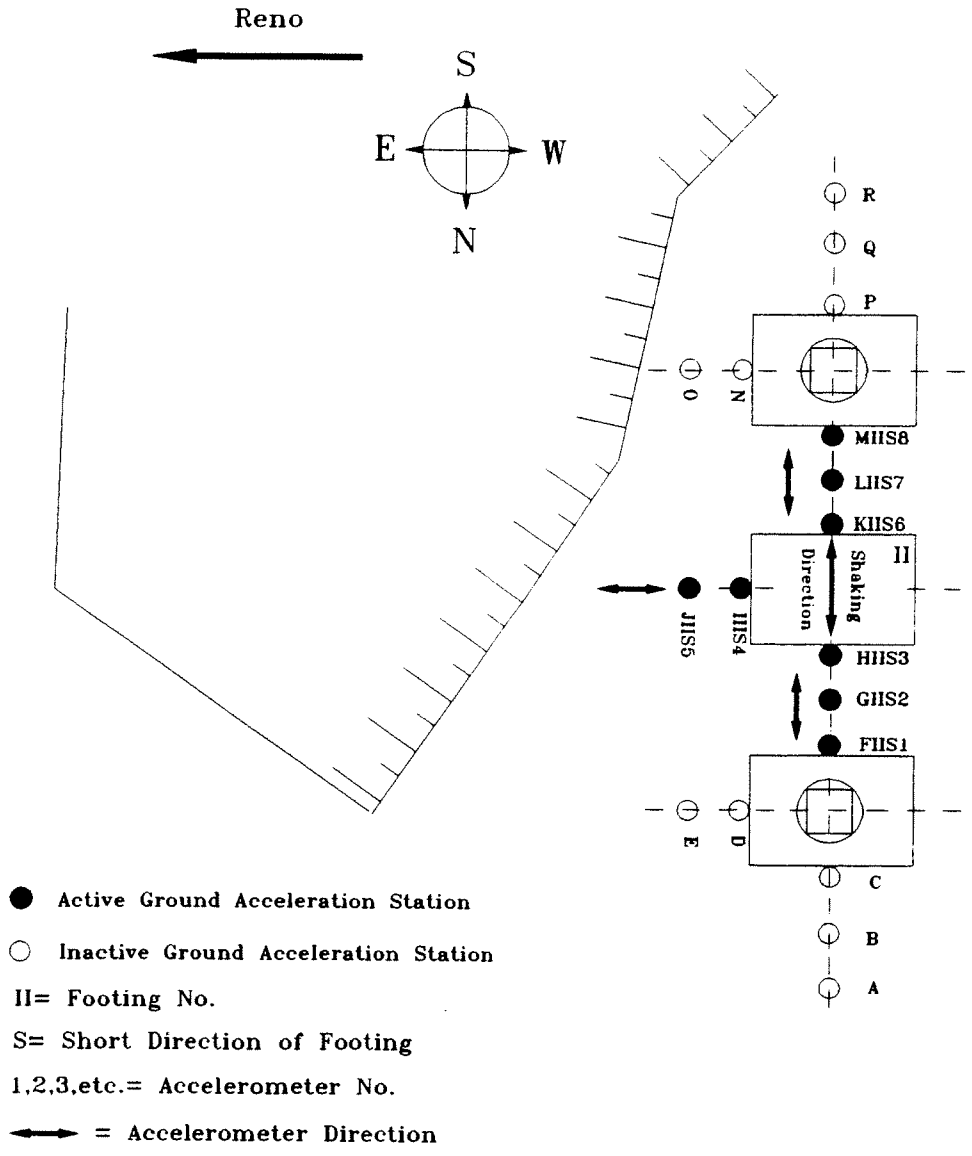

Figure 2.14. Numbering and Location of Ground Accelerometers During the Test of Footing II in the Short Direction

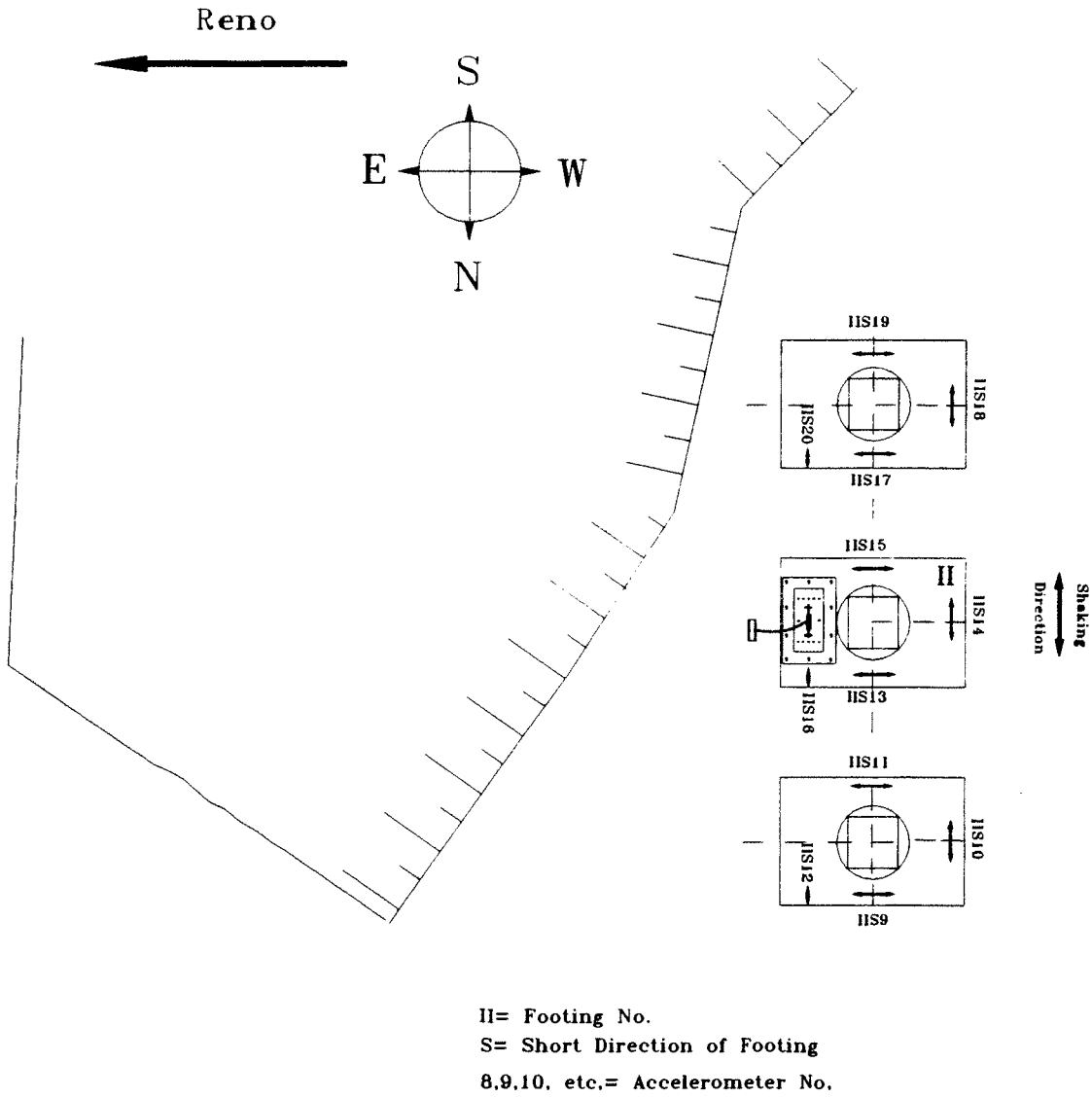

II= Footing No.
S= Short Direction of Footing
8,9,10, etc.= Accelerometer No.

Figure 2.15. Numbering and Location of Footing Accelerometers During the Test of Footing II in the Short Direction

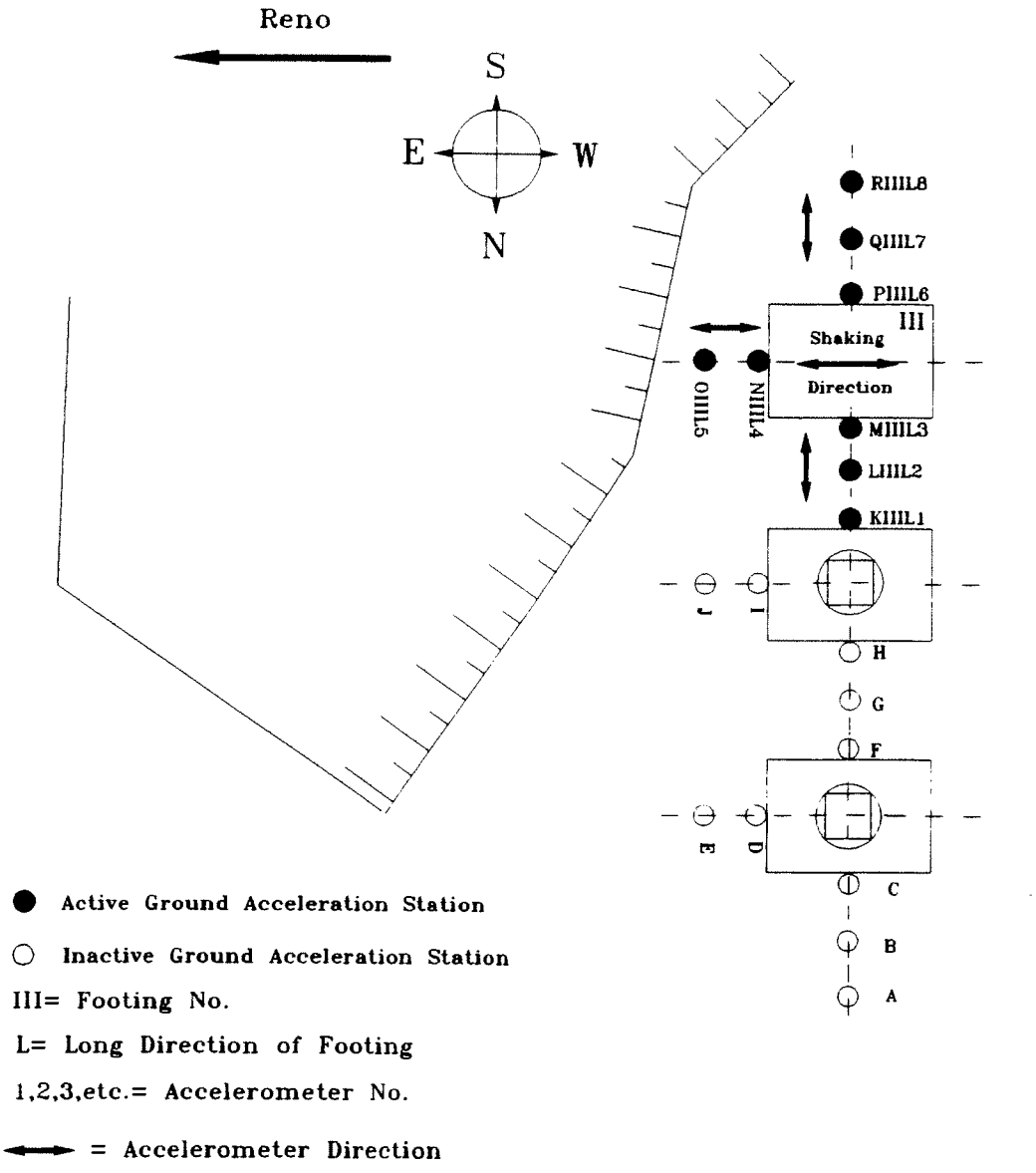

Figure 2.16. Numbering and Location of Ground Accelerometers During the Test of Footing III in the Longitudinal Direction

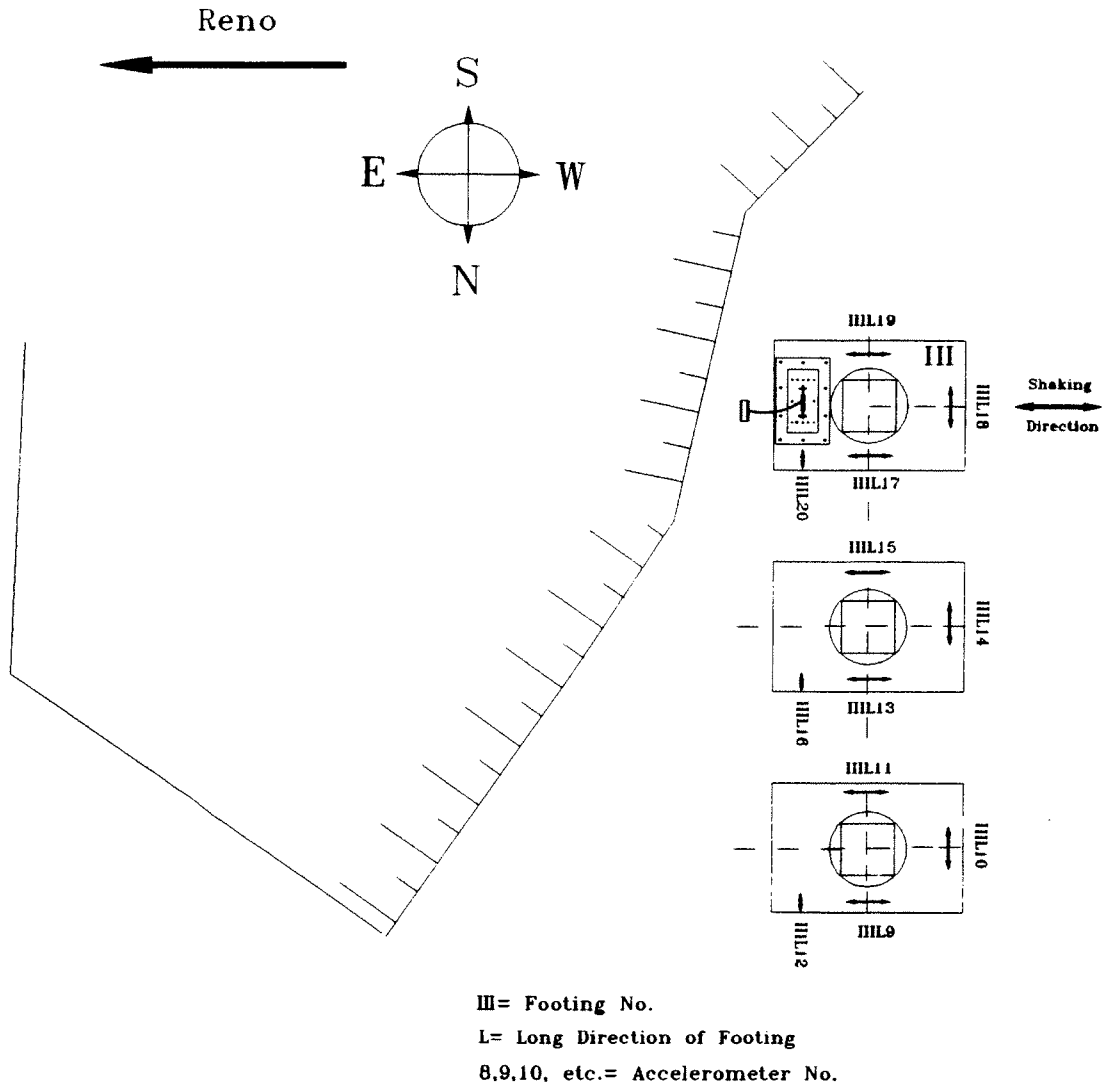

Figure 2.17. Numbering and Location of Footing Accelerometers During the Test of Footing III in the Longitudinal Direction

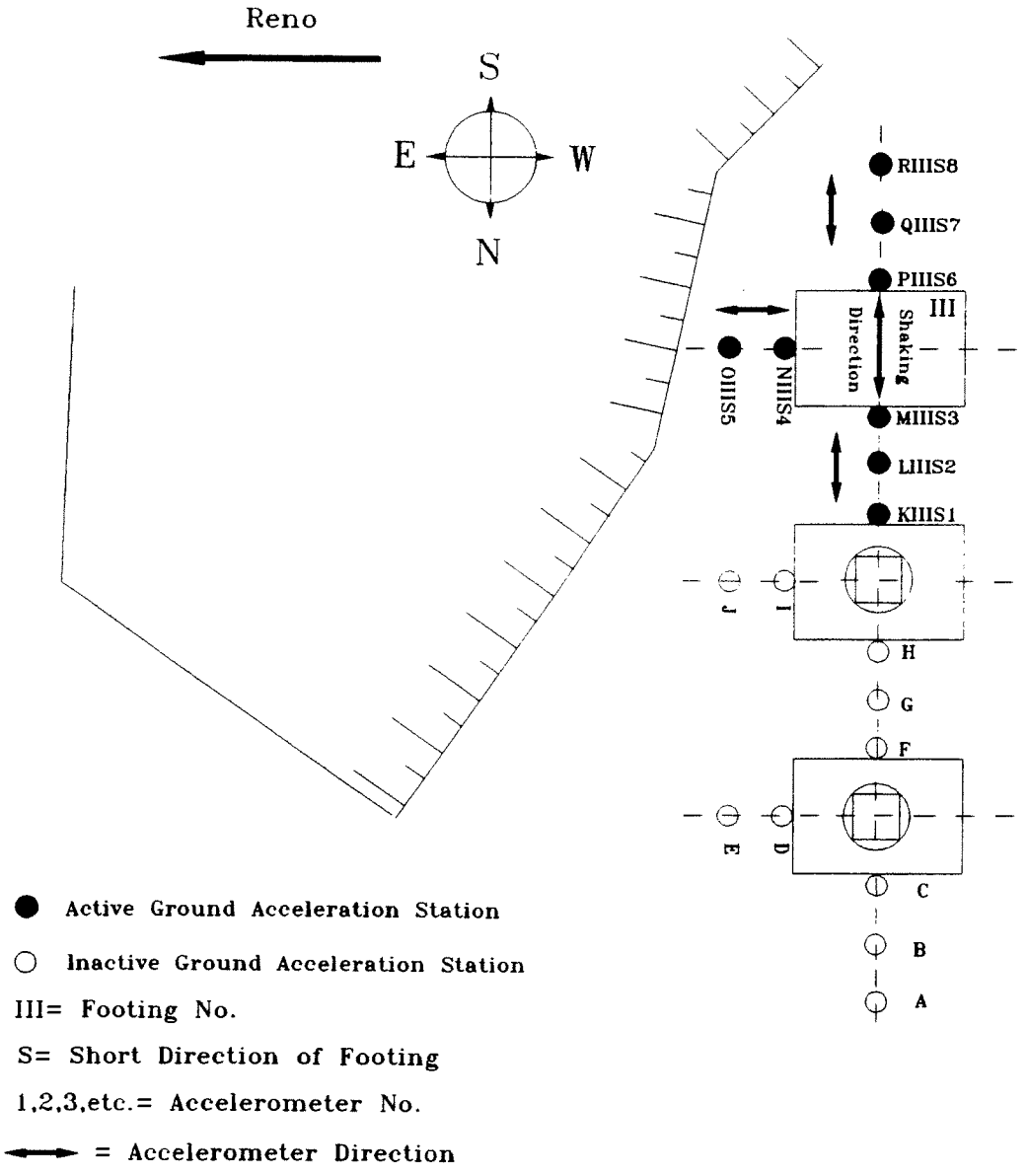

Figure 2.18. Numbering and Location of Ground Accelerometers During the Test of Footing III in the Short Direction

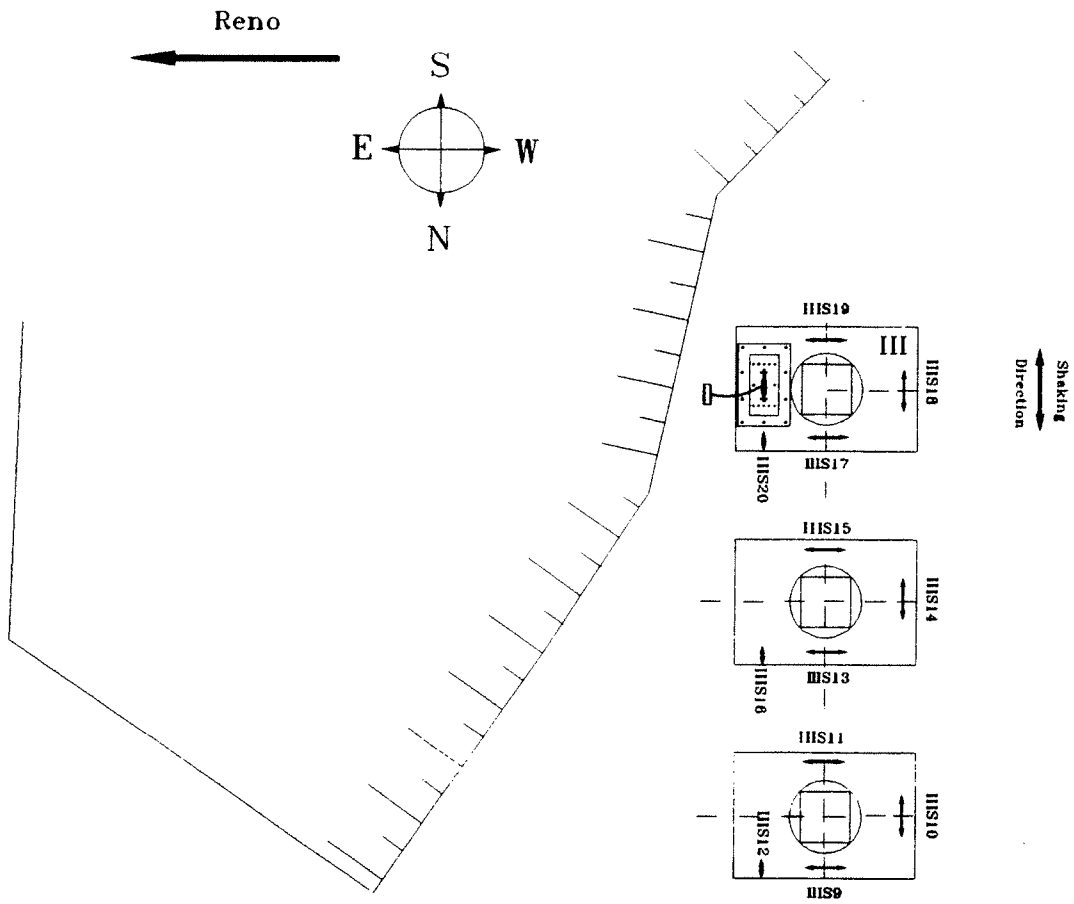

III= Footing No.
S= Short Direction of Footing
8.9.10. etc.= Accelerometer No.

Figure 2.19. Numbering and Location of Footing Accelerometers During the Test of Footing III in the Short Direction

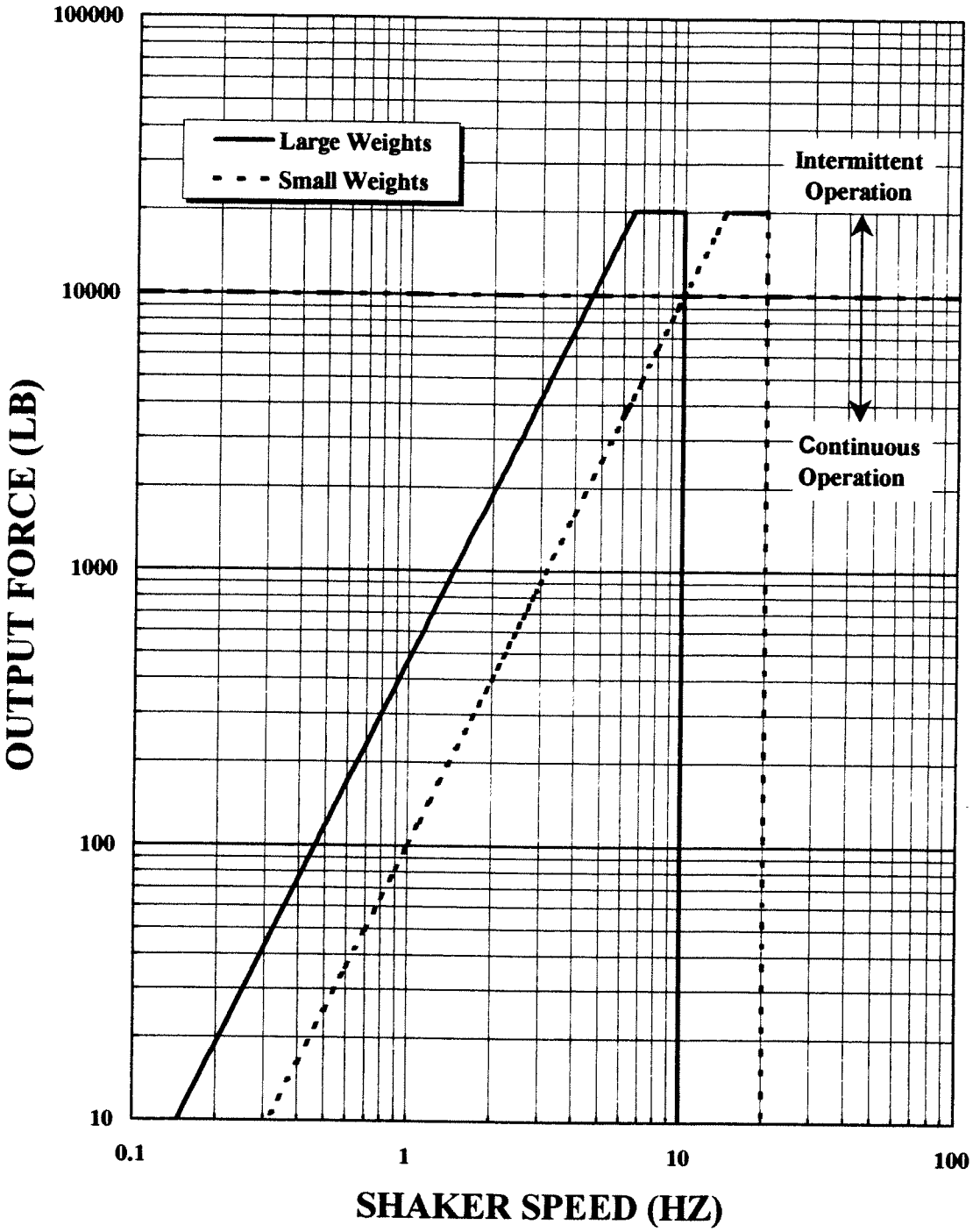

Figure 2.20. Maximum Safe Operating Limits for MK-12.8A-4600 Shaker

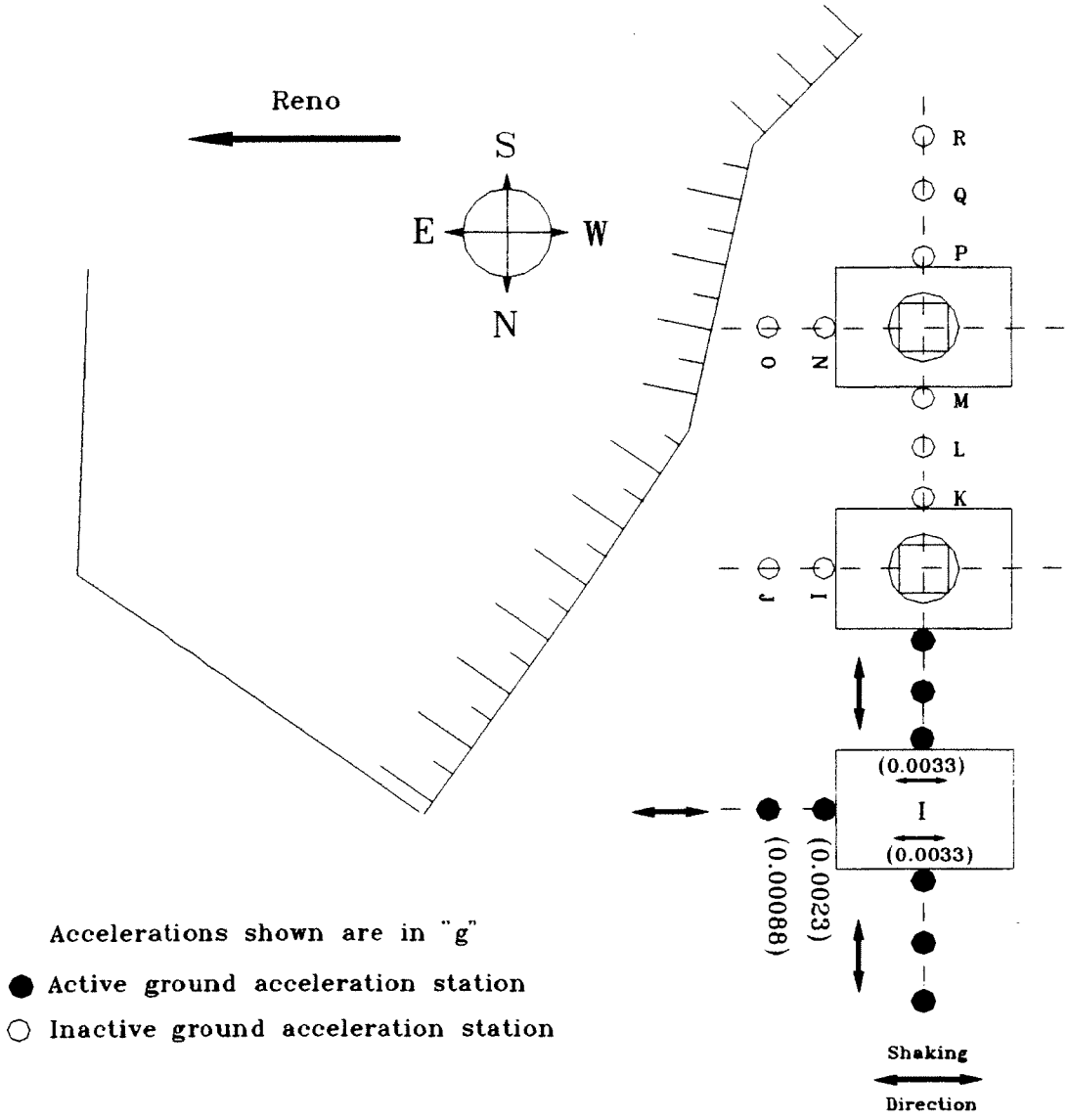

Figure 3.1. Measured Soil and Footing Steady State Accelerations During the Test of Footing I in the Longitudinal Direction.

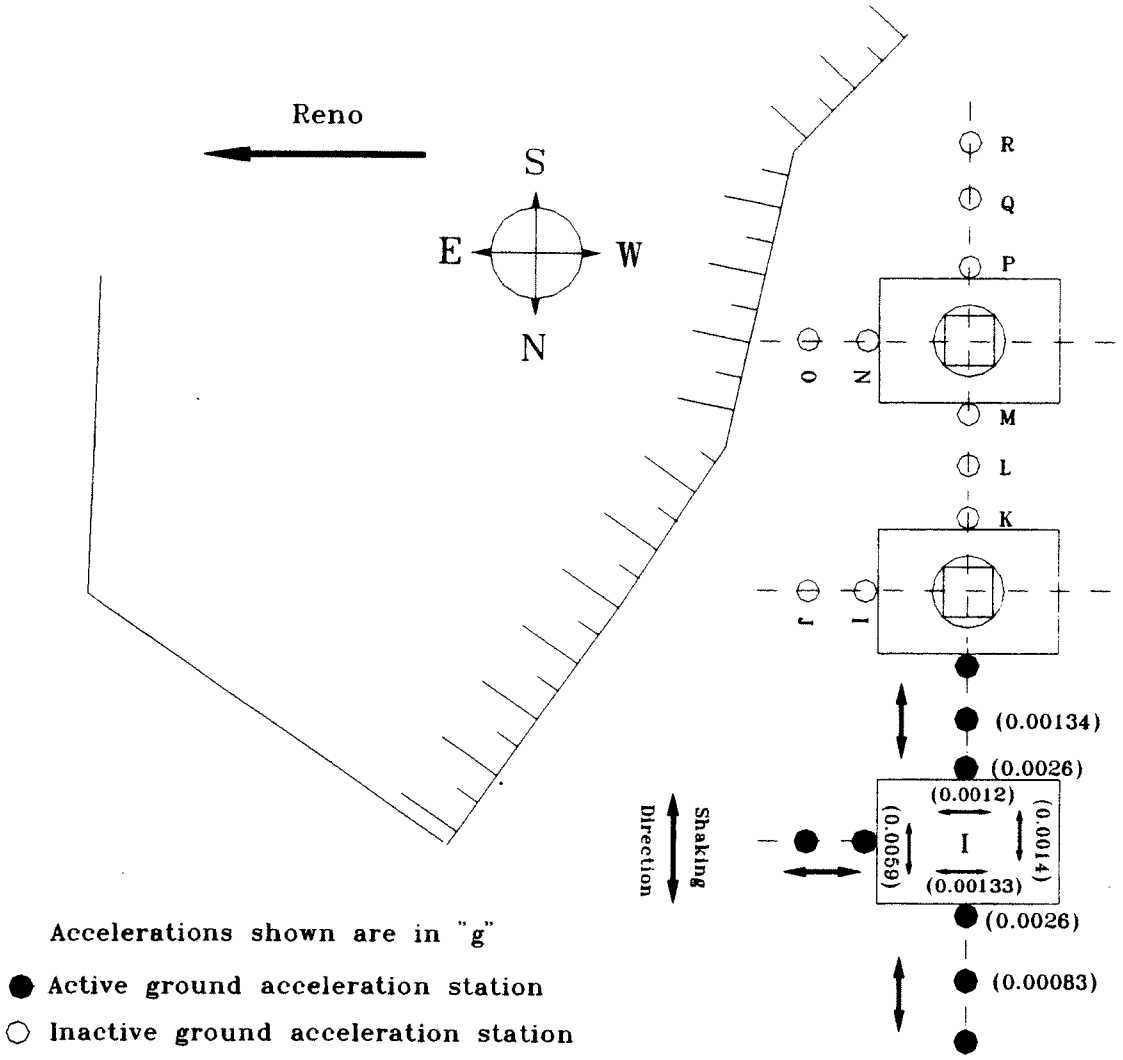

Figure 3.2. Measured Soil and Footing Steady State Accelerations During the Test of Footing I in the Short Direction.

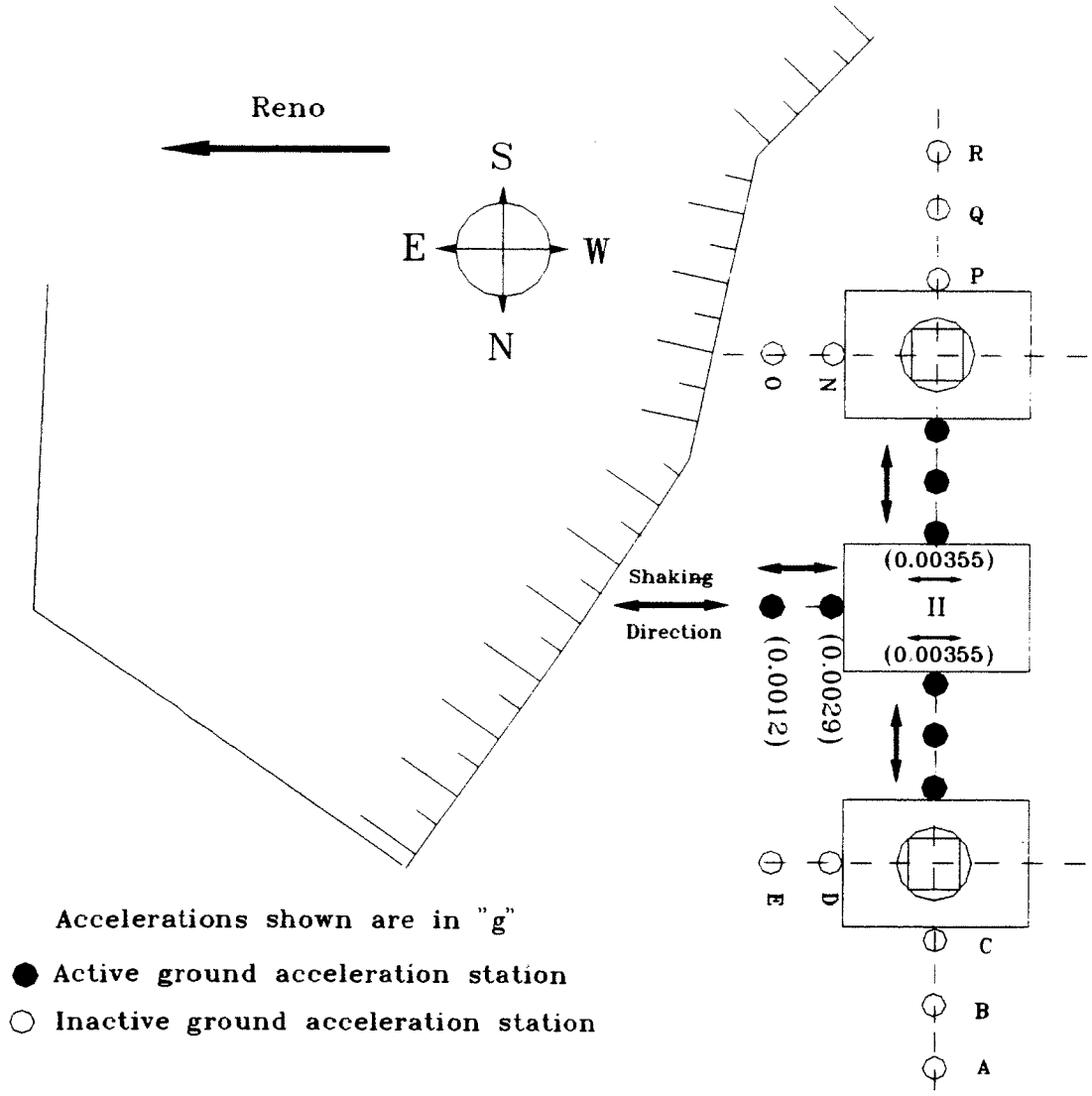

Figure 3.3. Measured Soil and Footing Steady State Accelerations During the Test of Footing II in the Longitudinal Direction.

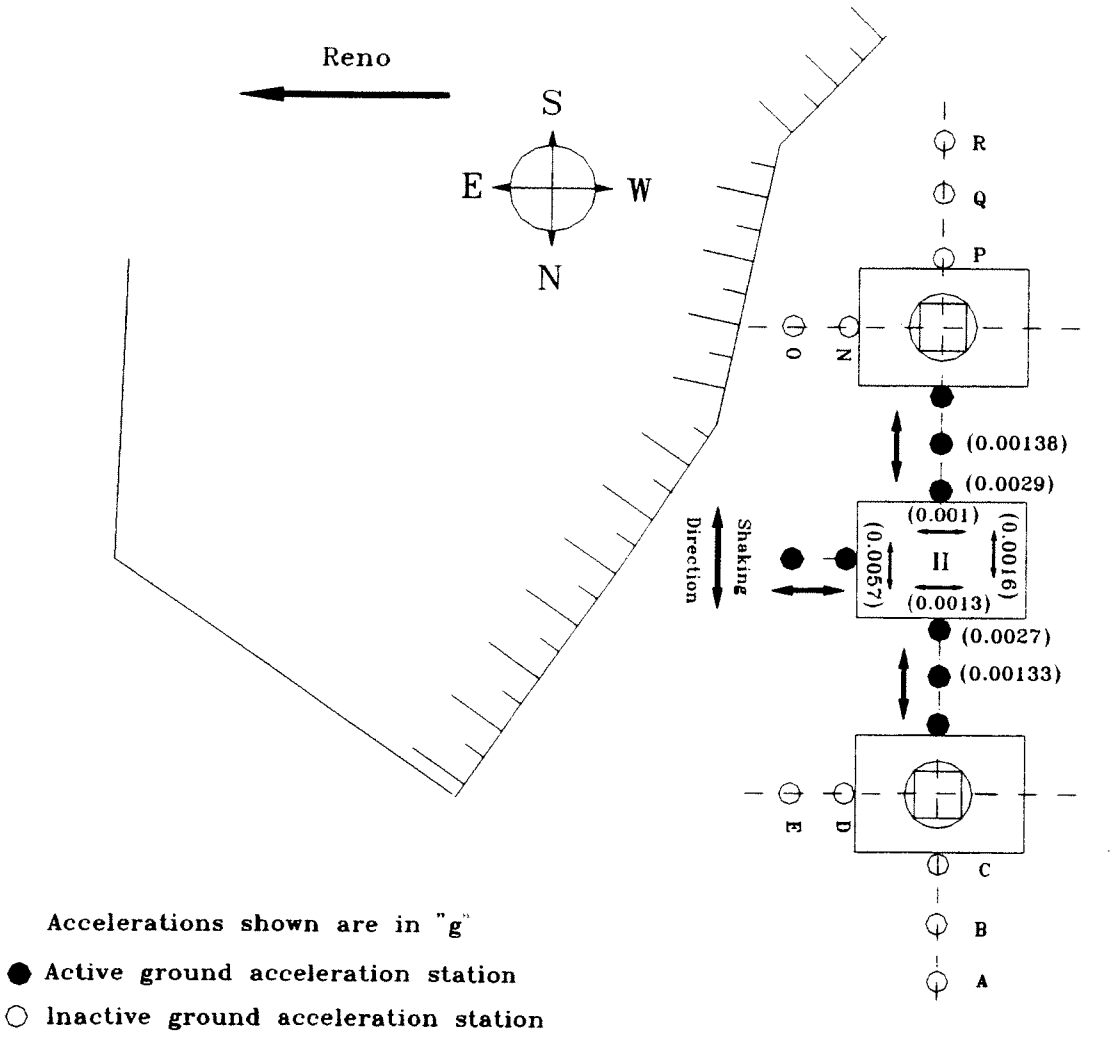

Figure 3.4. Measured Soil and Footing Steady State Accelerations During the Test of Footing II in the Short Direction.

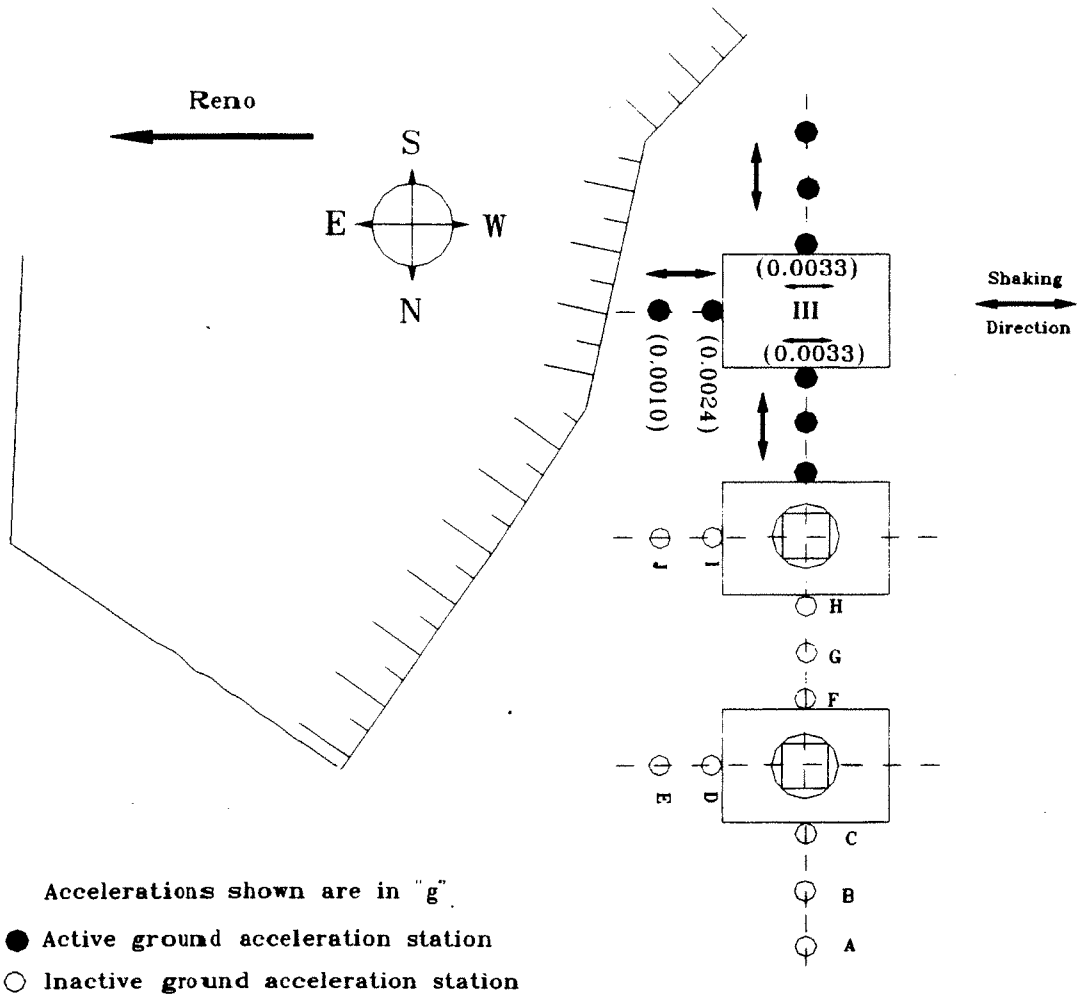

Figure 3.5. Measured Soil and Footing Steady State Accelerations During the Test of Footing III in the Longitudinal Direction.

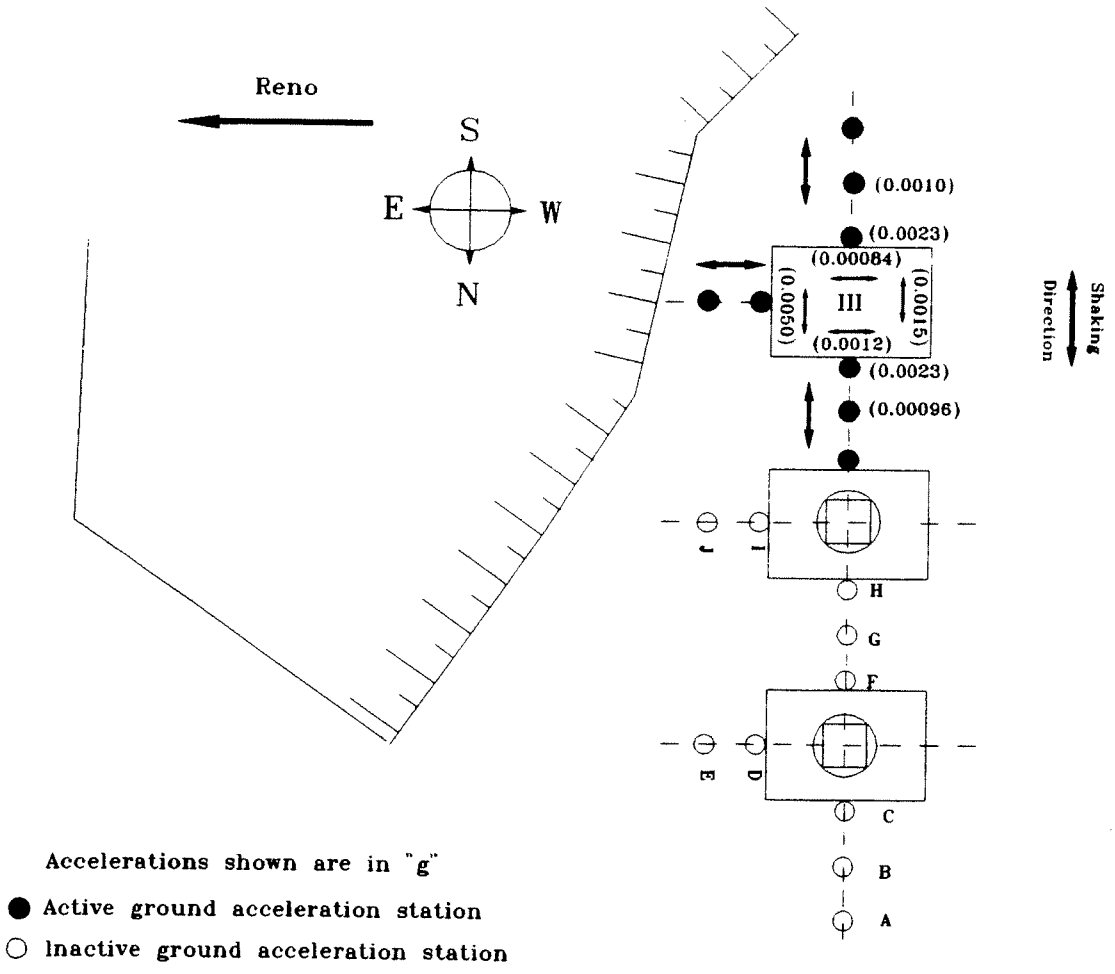

Figure 3.6. Measured Soil and Footing Steady State Accelerations During the Test of Footing III in the Short Direction.

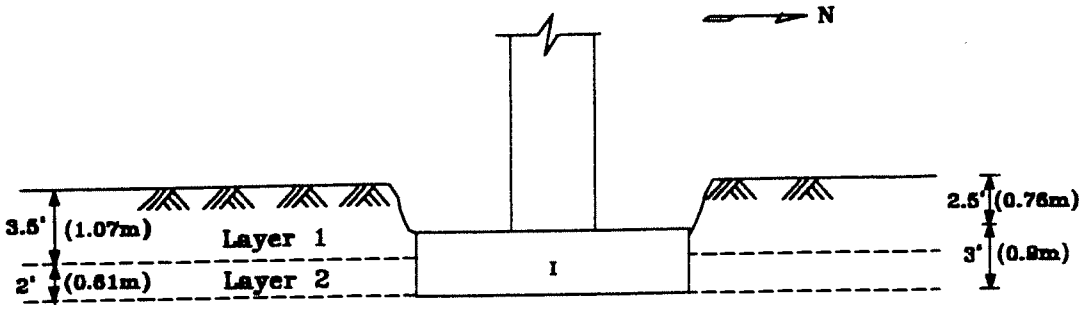

Layer	Classification	PI	γ_{moist} pcf (KN/m^3)	γ_{dry} pcf (KN/m^3)	Water Content
1	Sandy Clay with Cobbles	11	135 (20.8)	120 (18.5)	13.3%
2	Fine Gravely Sand with Cobbles	–	112 (17.25)	105 (62.4)	9.4%

Figure 4.1. Profile and Measured Properties of Soil at the Bridge Site

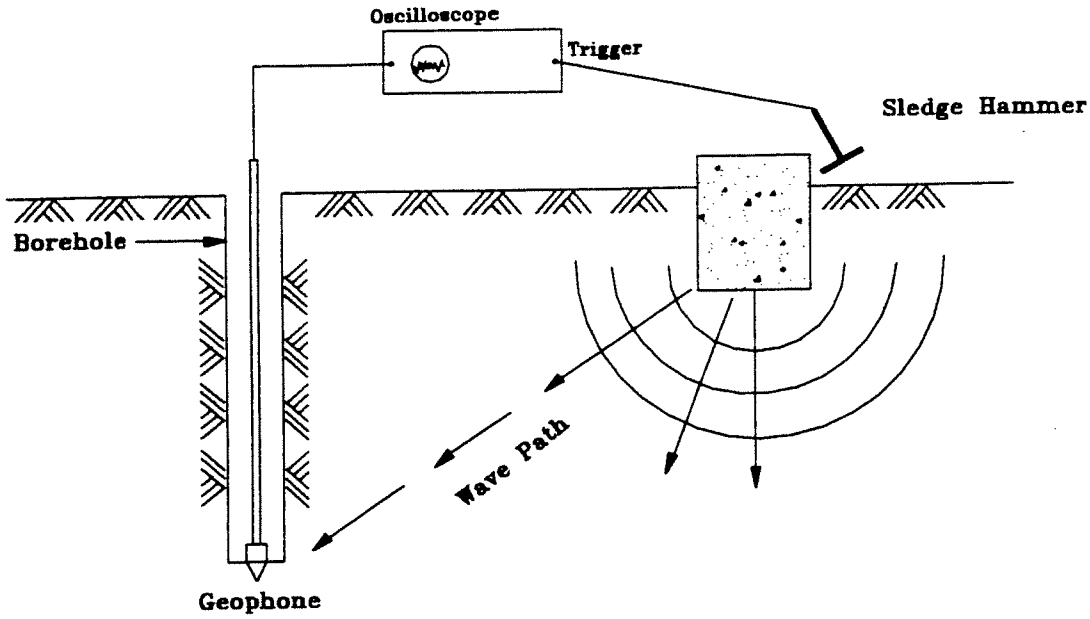

Figure 4.2. The Seismic Down-hole Method for Measurement of Velocity of Wave Propagation

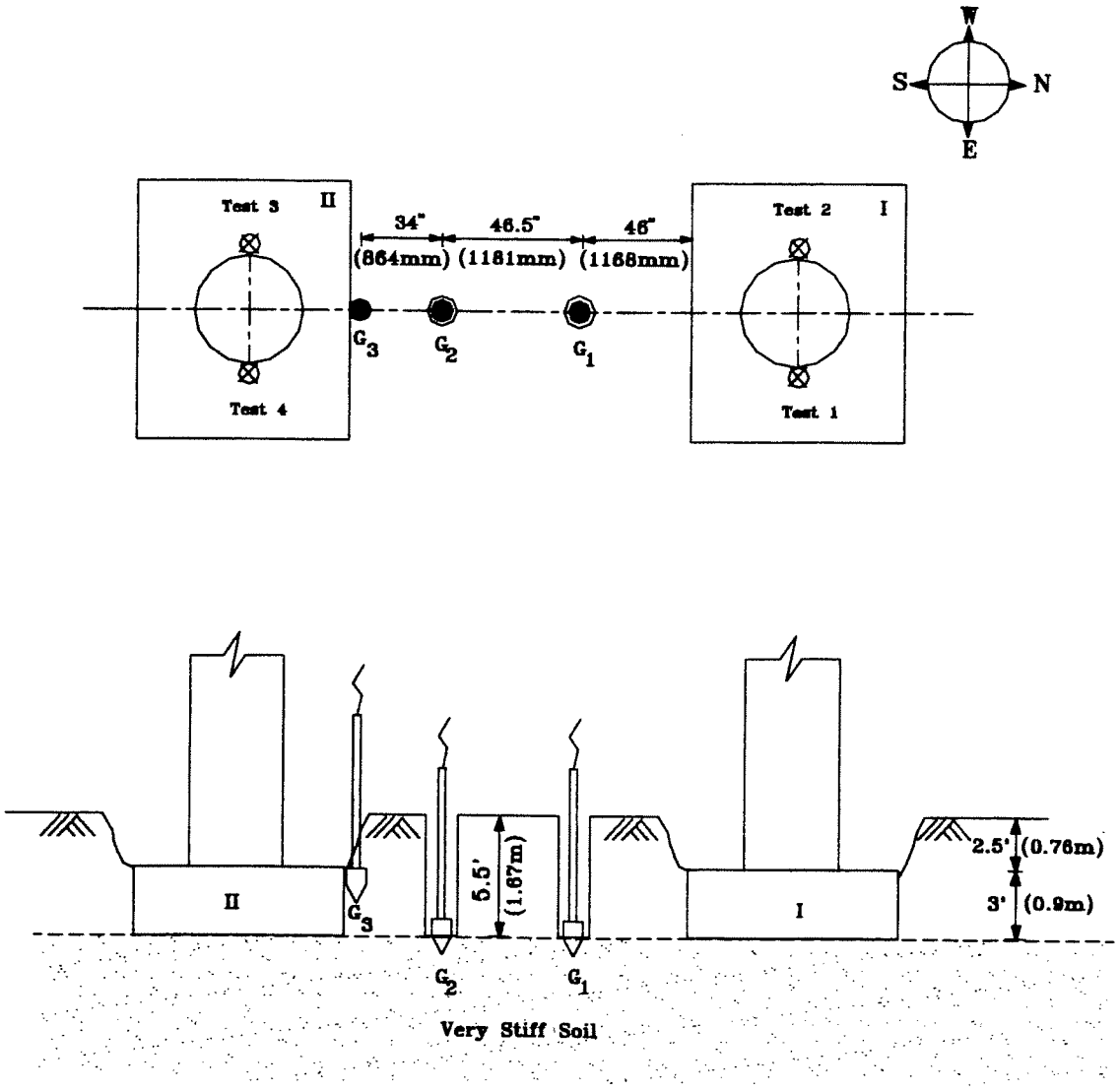

Figure 4.3. Test Setup for the Modified Seismic Down-hole Test

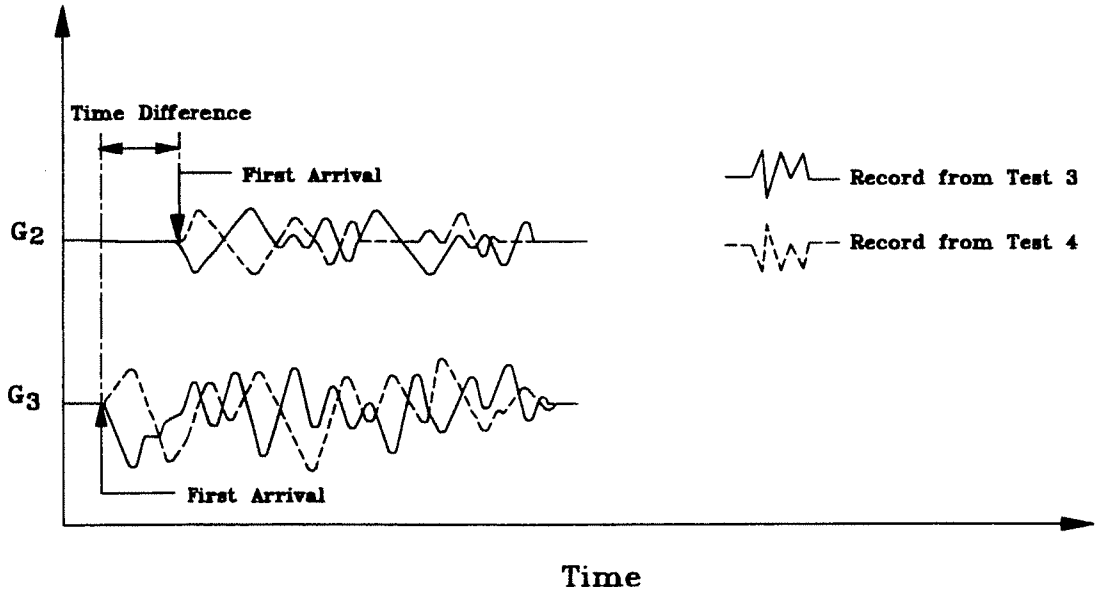

Figure 4.4. Determination of Shear Wave Velocities from the Geophone Records at Footing II

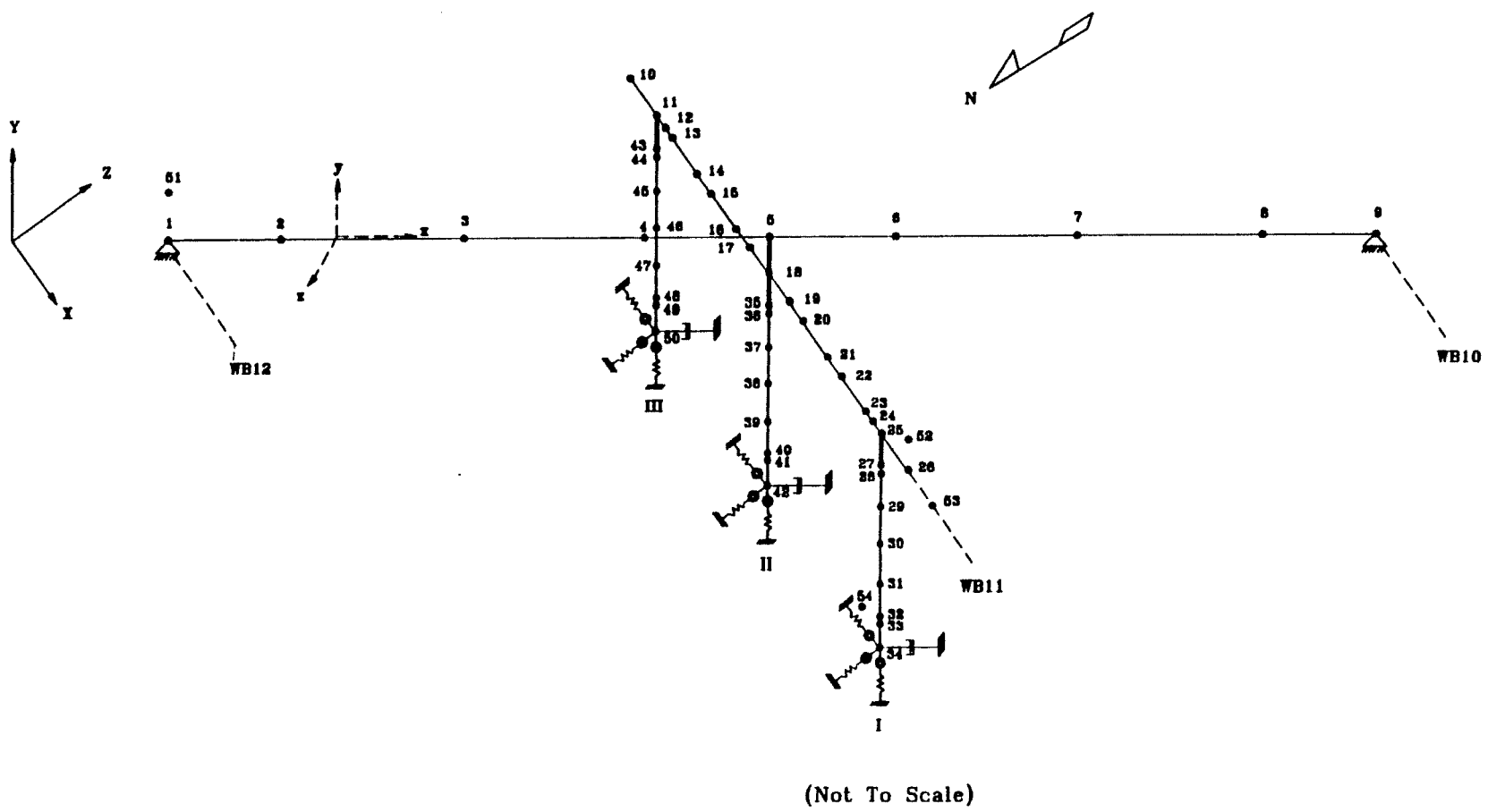

Figure 5.1. Finite Element Model of the Last Two Spans of G-772 W Bridge

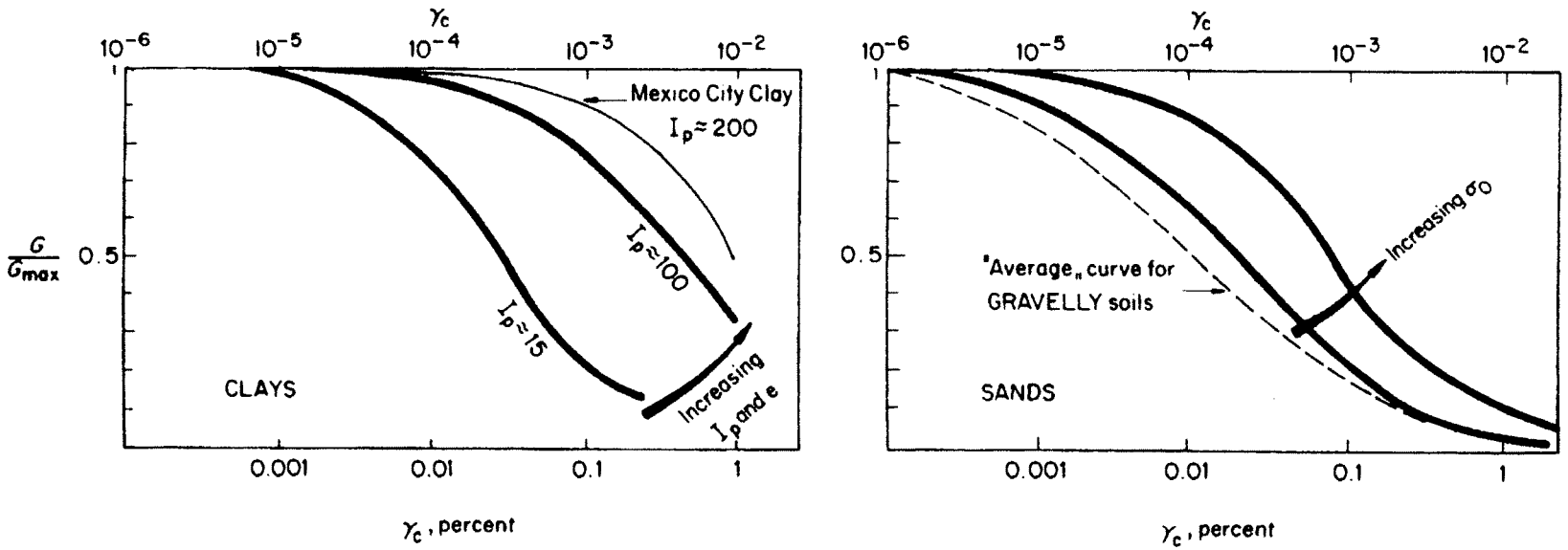

Figure 5.2. Variation of Shear Modulus with Shear Strain for Clay, Sand, and Gravels (Adopted from Ref. 16)

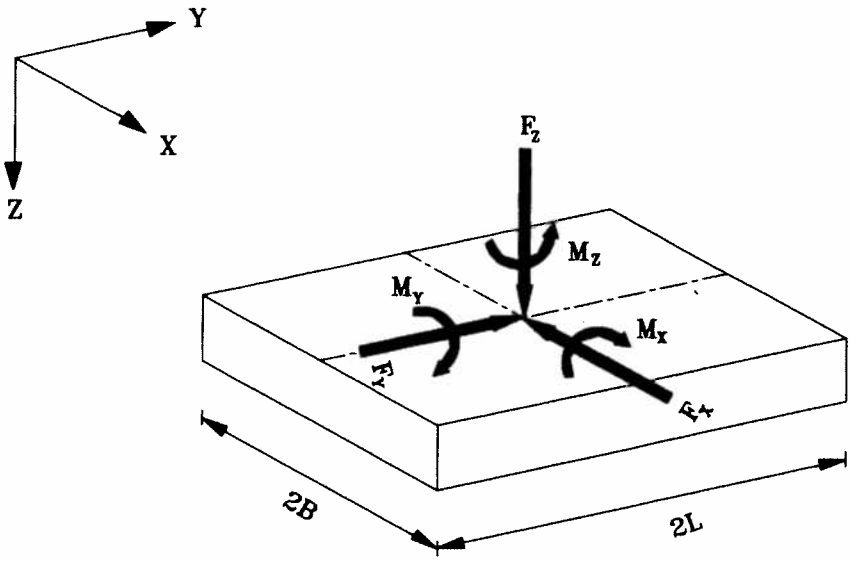

Figure 5.3. Rigid Footing with Six Degrees of Freedom

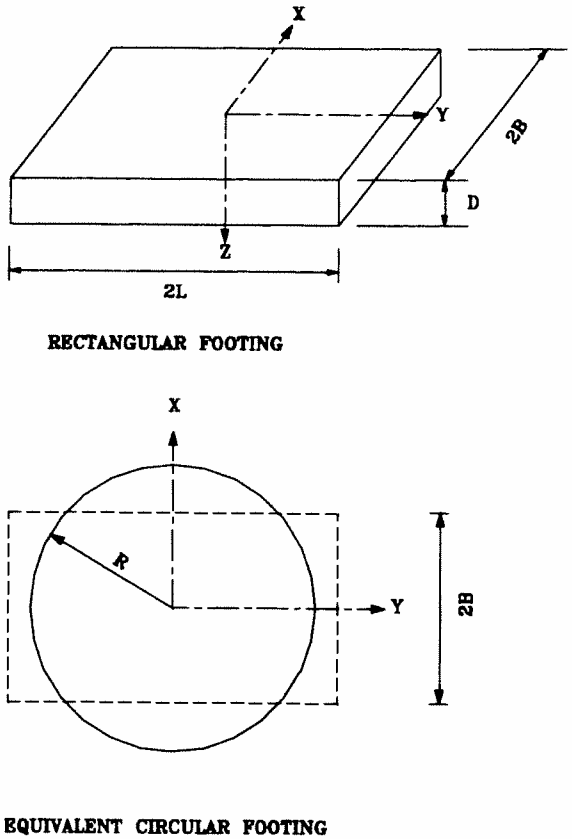

Figure 5.4. Equivalent Radius for a Rectangular Footing

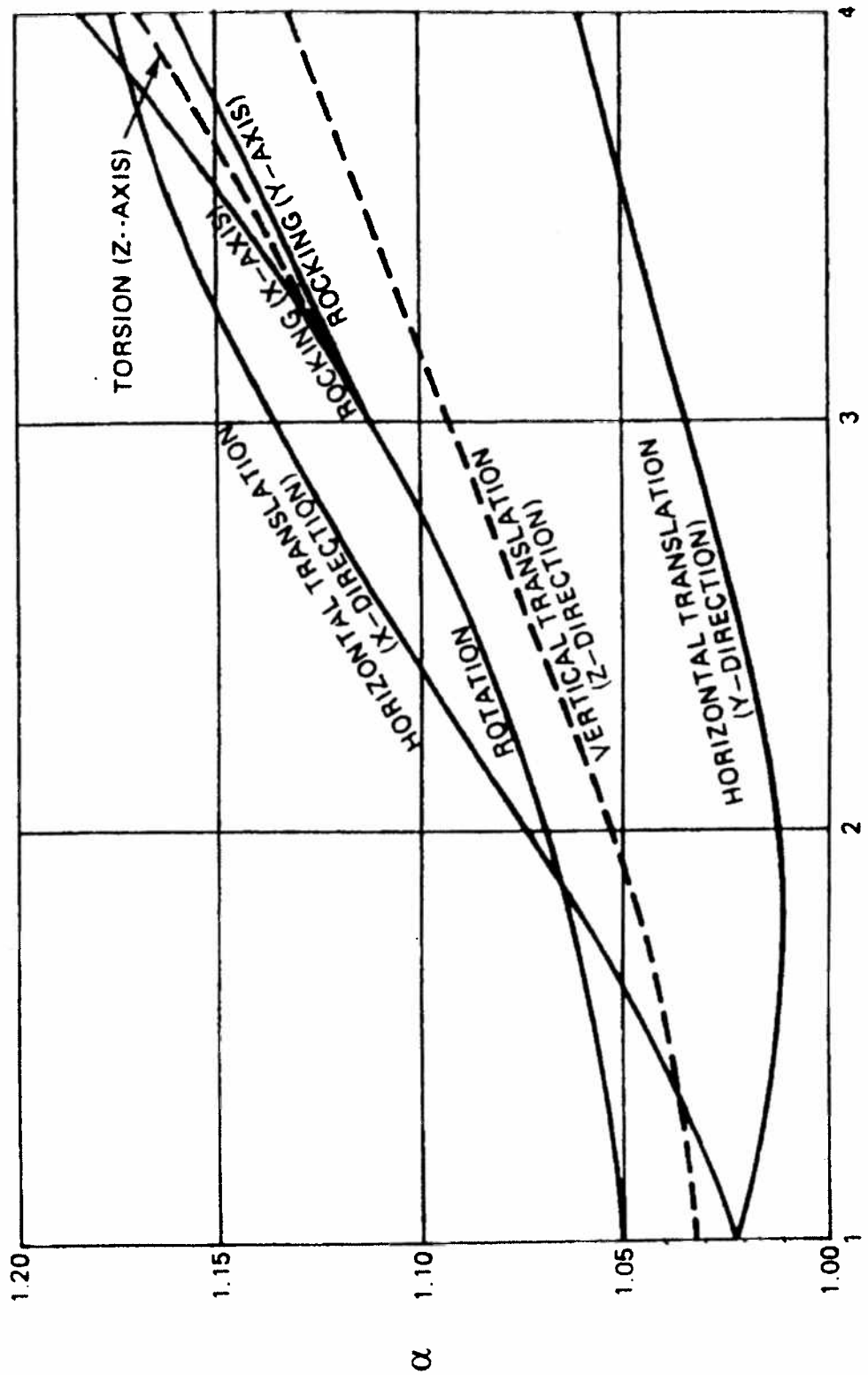

Figure 5.5. Shape Factor for Rectangular Footings (Adopted from Ref. 41)

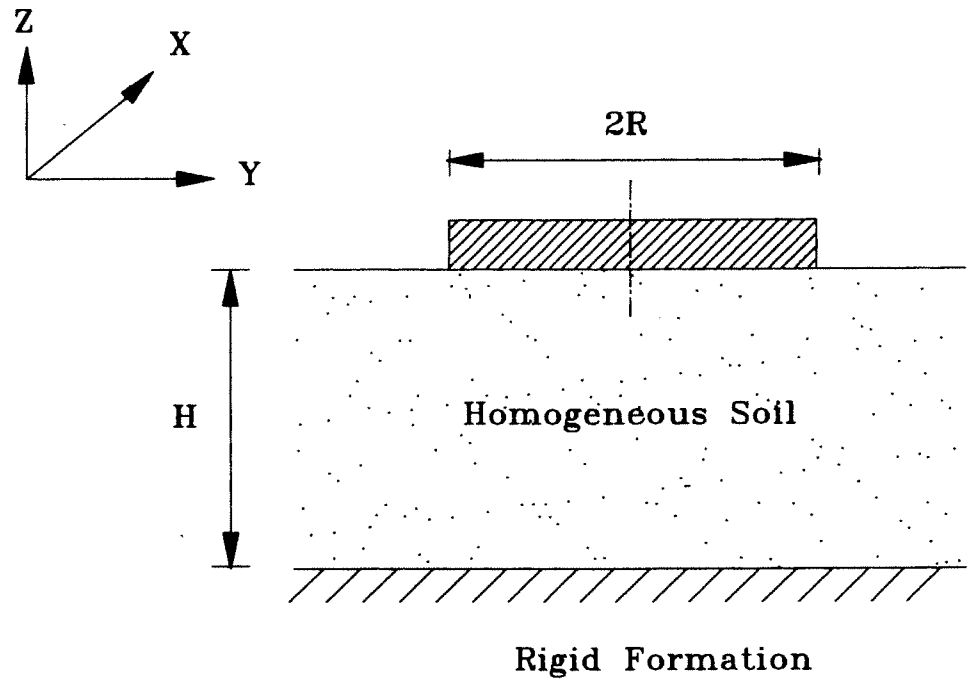

Figure 5.6. Surface Circular Footing on Homogeneous Stratum Over Bedrock

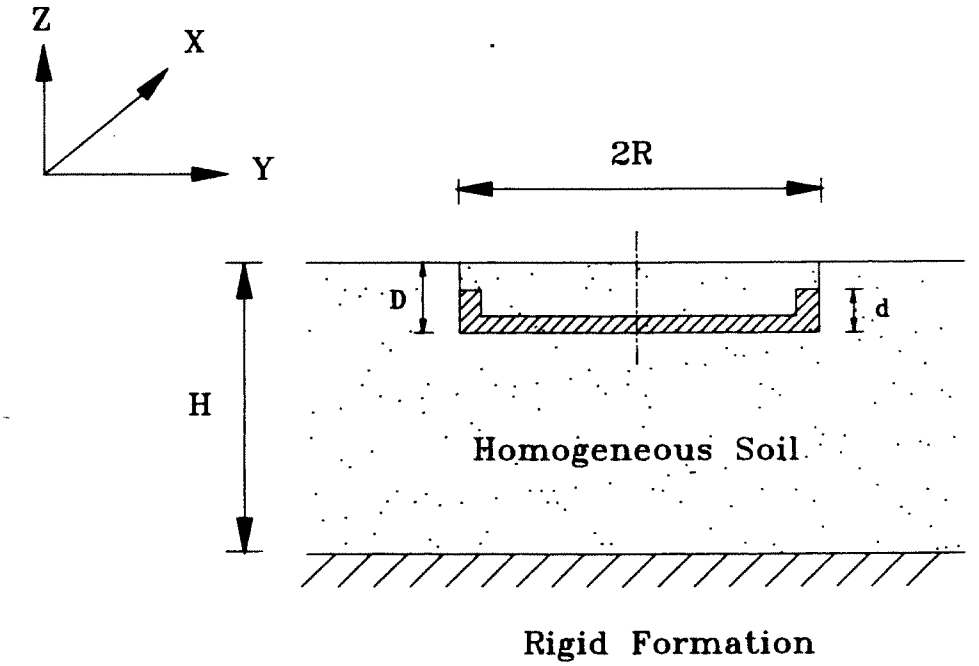

Figure 5.7. Embedded Circular Footing on Homogeneous Stratum Over Bedrock

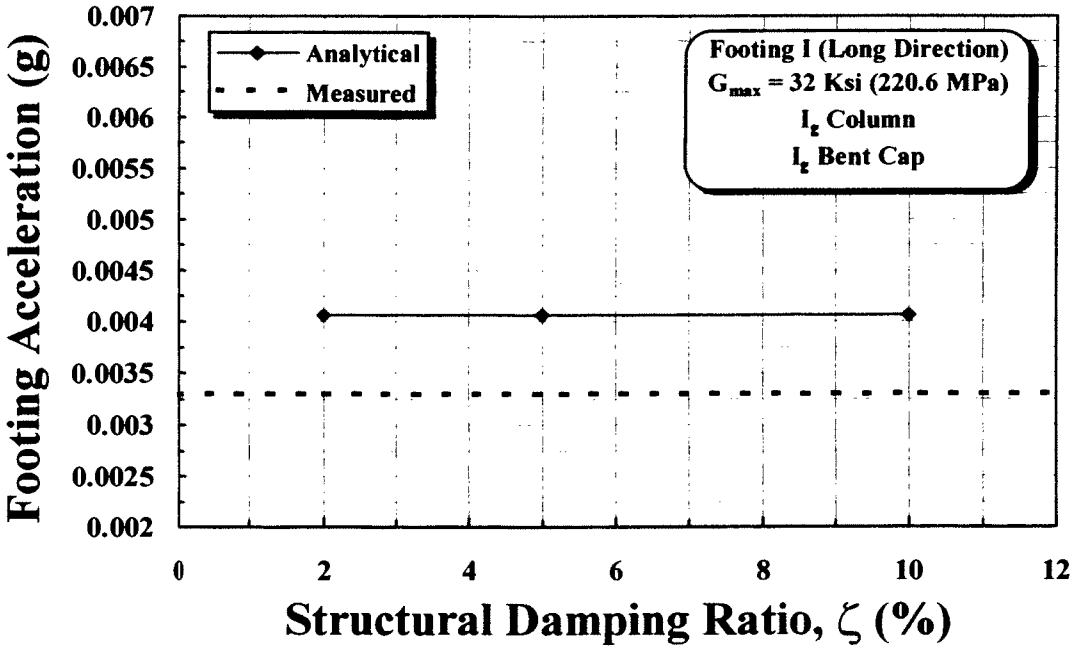

Figure 5.8. Effect of Structural Damping on the Steady State Acceleration of Footing I in the Longitudinal Direction

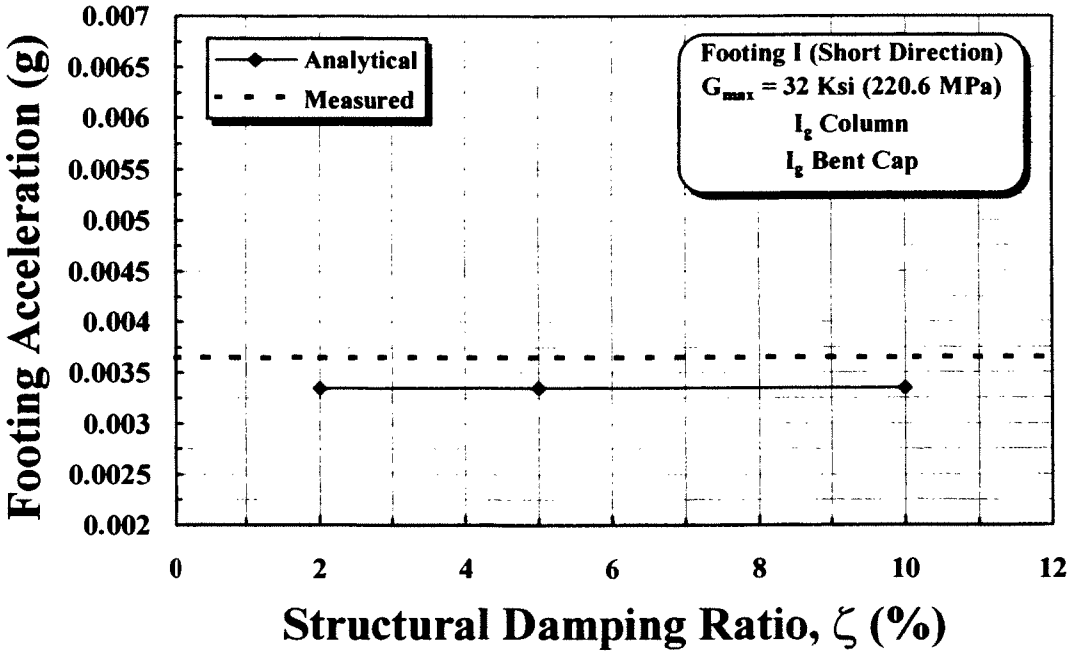

Figure 5.9. Effect of Structural Damping on the Steady State Acceleration of Footing I in the Short Direction

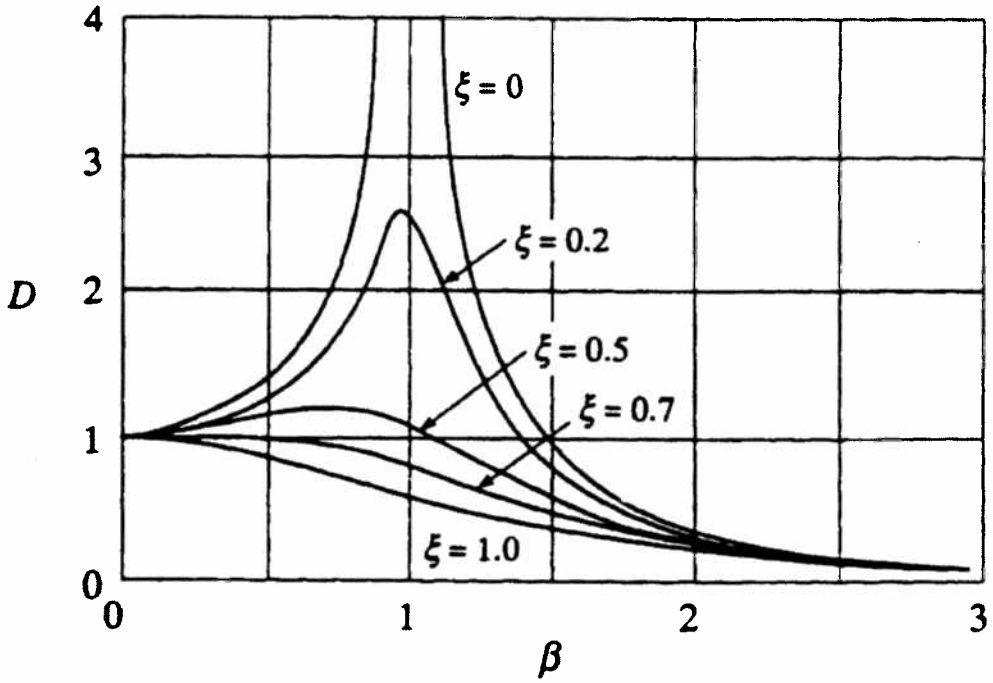

Figure 5.10. Variation of Dynamic Magnification Factor with Structural Damping and Frequency (Adopted from Ref. 6)

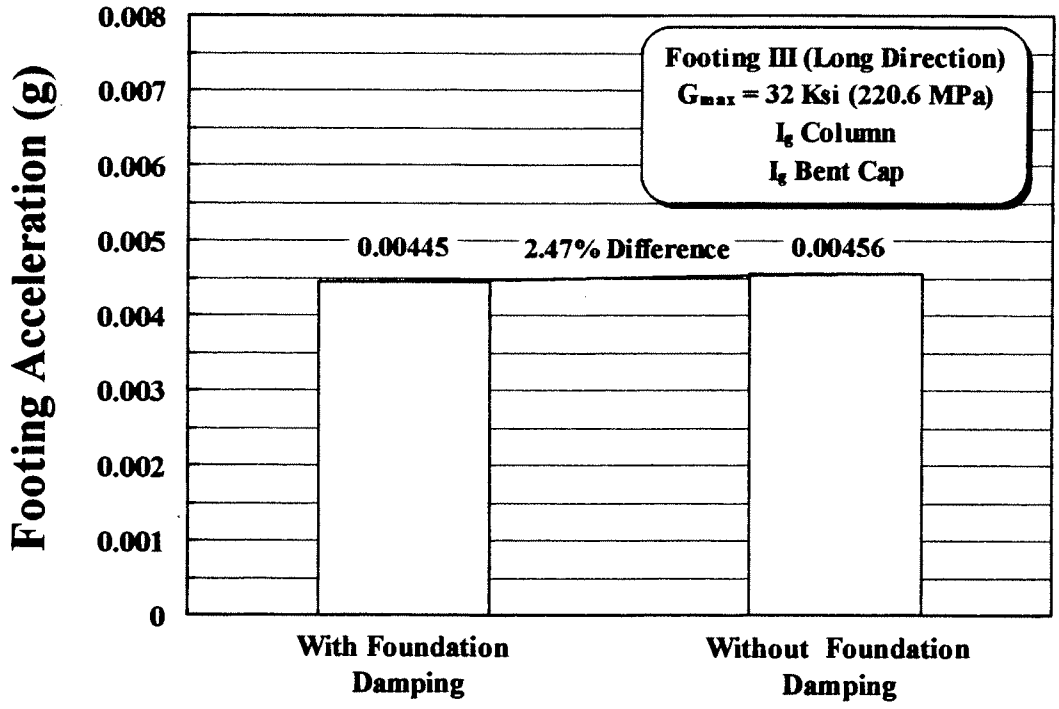

Figure 5.11. Effect of Foundation Damping on the Steady State Acceleration of Footing III in the Longitudinal Direction

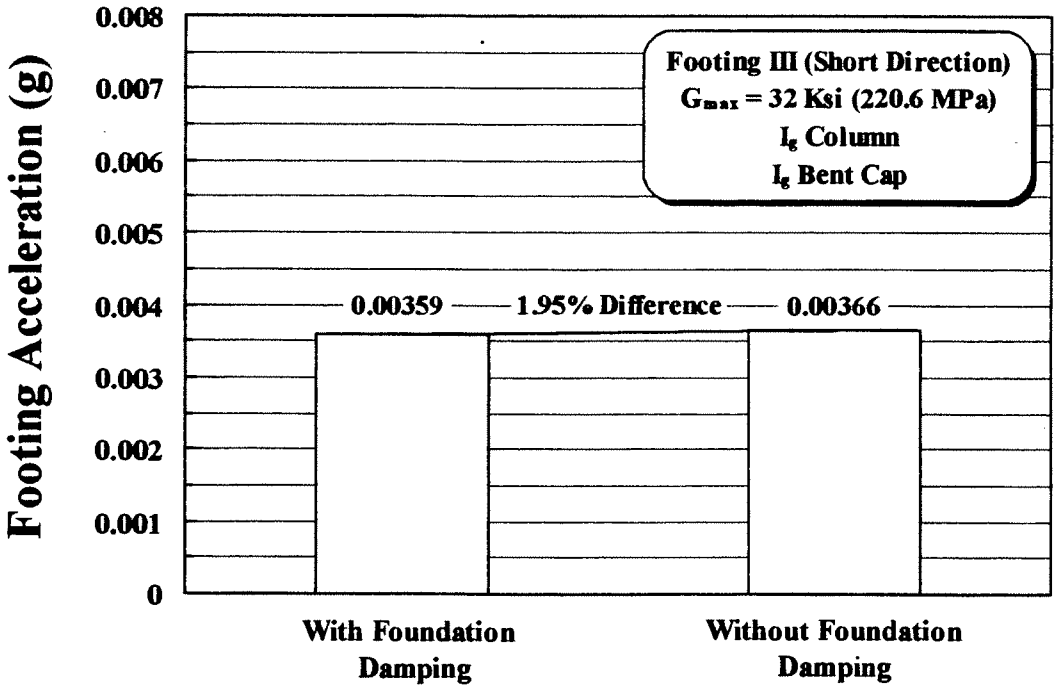

Figure 5.12. Effect of Foundation Damping on the Steady State Acceleration of Footing III in the Short Direction

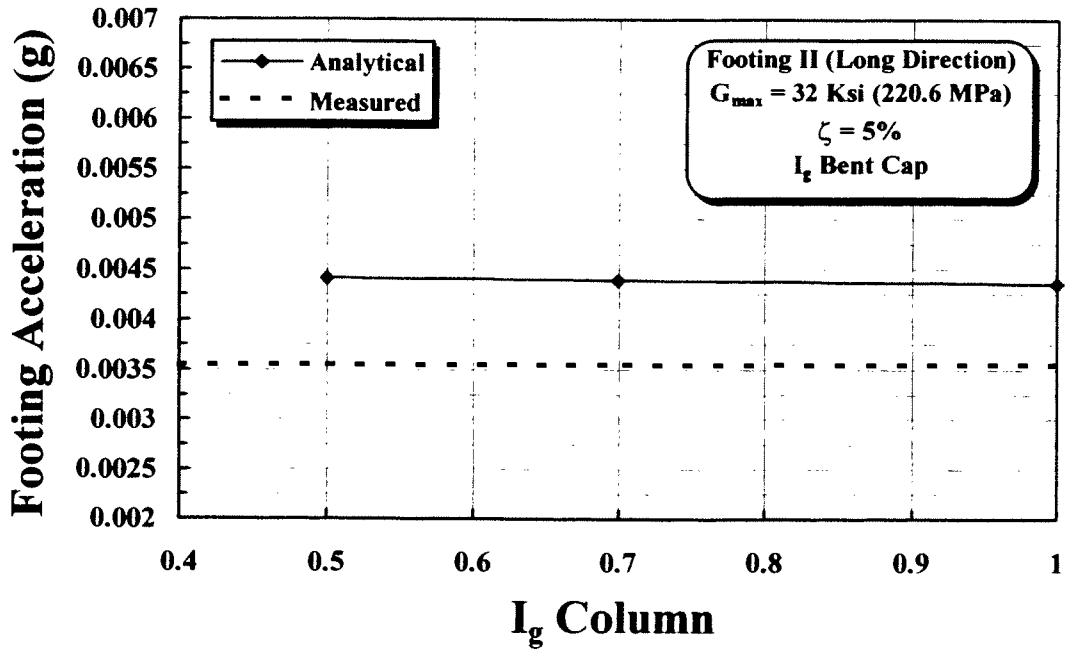

Figure 5.13. Effect of Column Moment of Inertia on the Steady State Acceleration of Footing II in the Longitudinal Direction

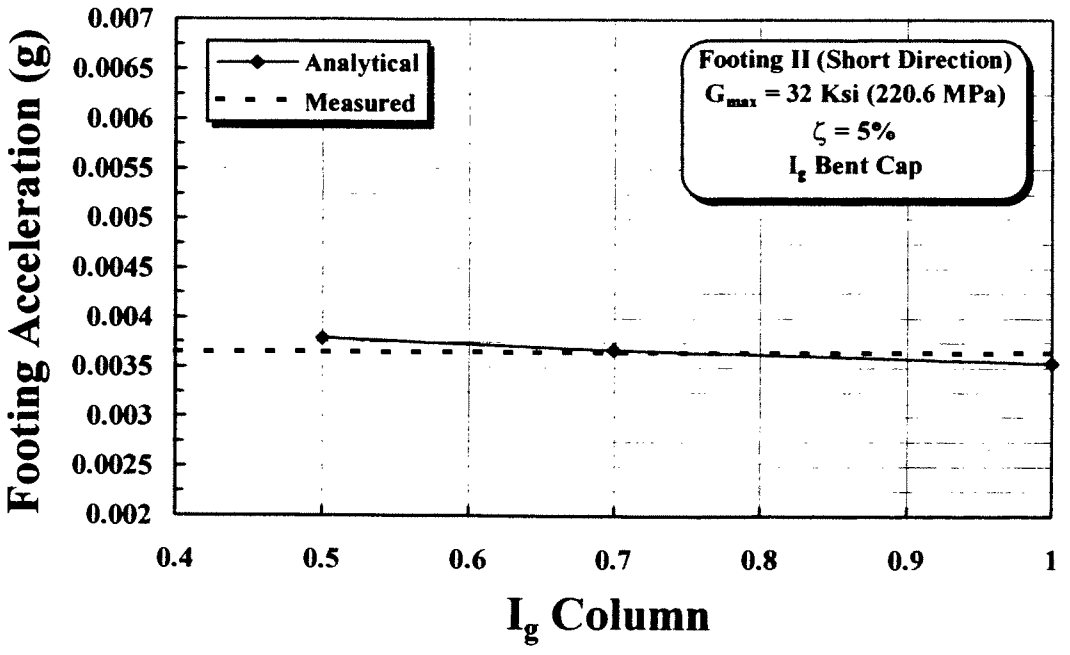

Figure 5.14. Effect of Column Moment of Inertia on the Steady State Acceleration of Footing II in the Short Direction

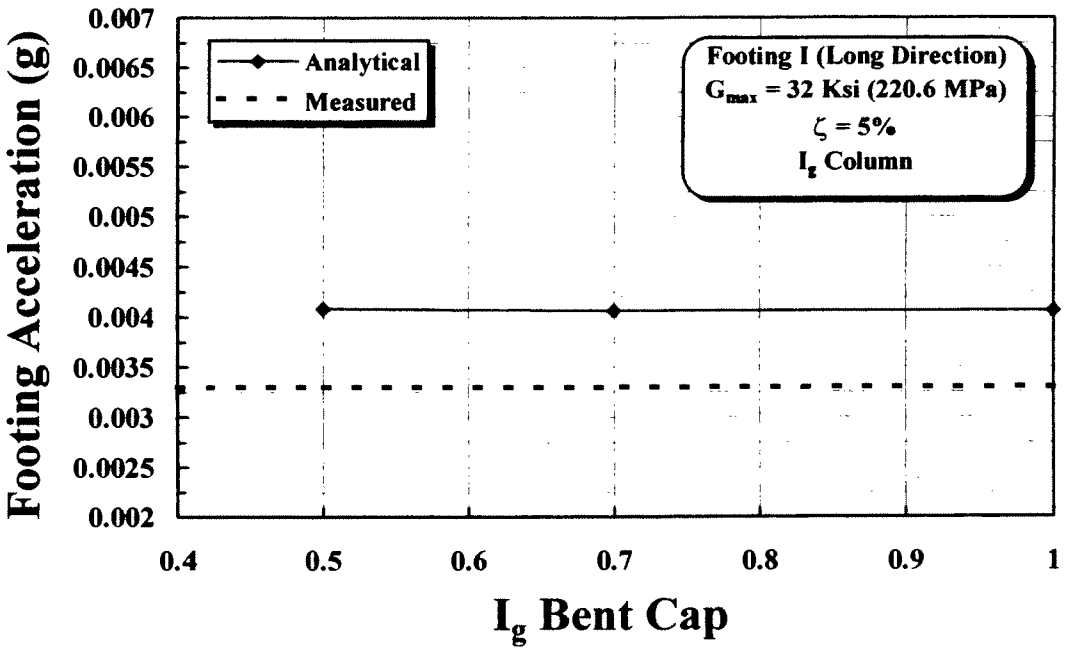

Figure 5.15. Effect of Bent Cap Moment of Inertia on the Steady State Acceleration of Footing I in the Longitudinal Direction

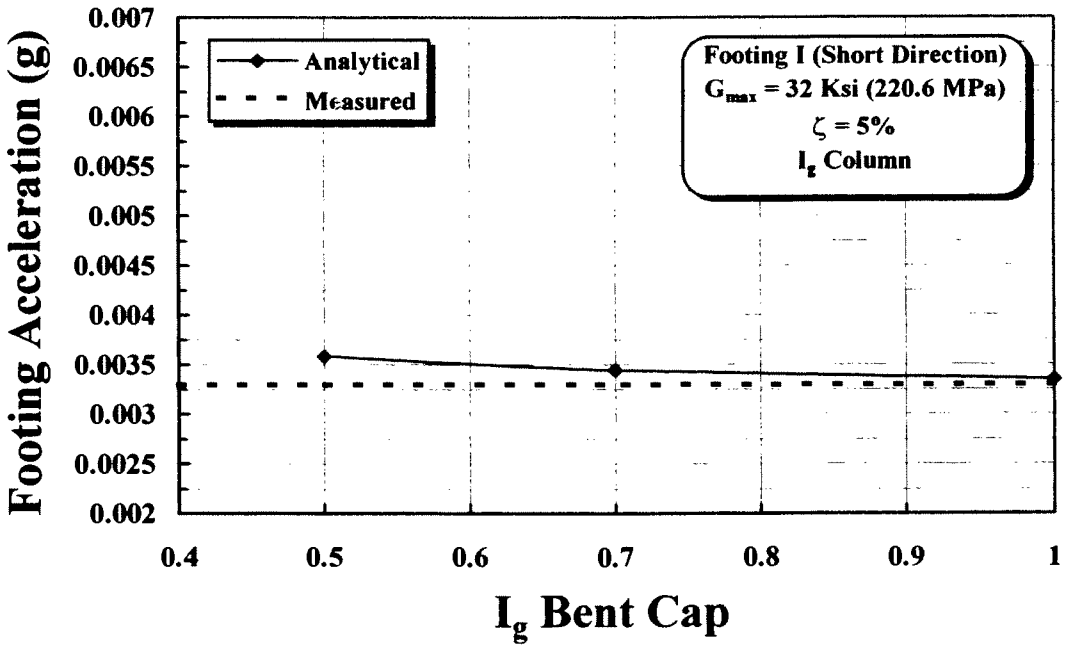

Figure 5.16. Effect of Bent Cap Moment of Inertia on the Steady State Acceleration of Footing I in the Short Direction

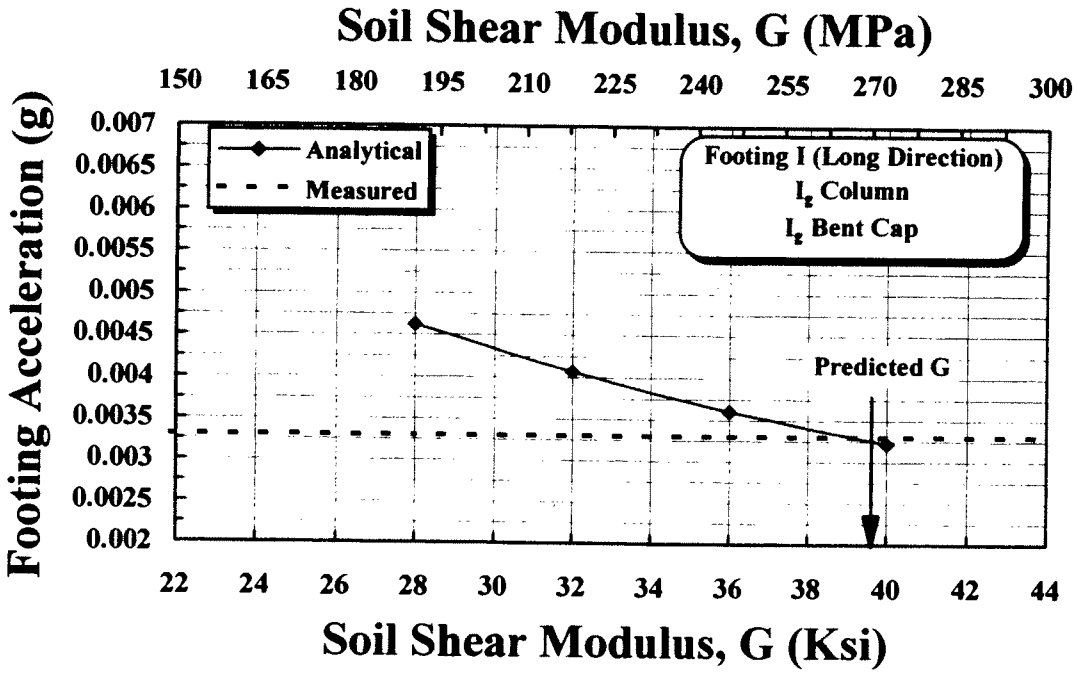

Figure 5.17. Effect of Soil Shear Modulus on the Steady State Acceleration of Footing I in the Longitudinal Direction

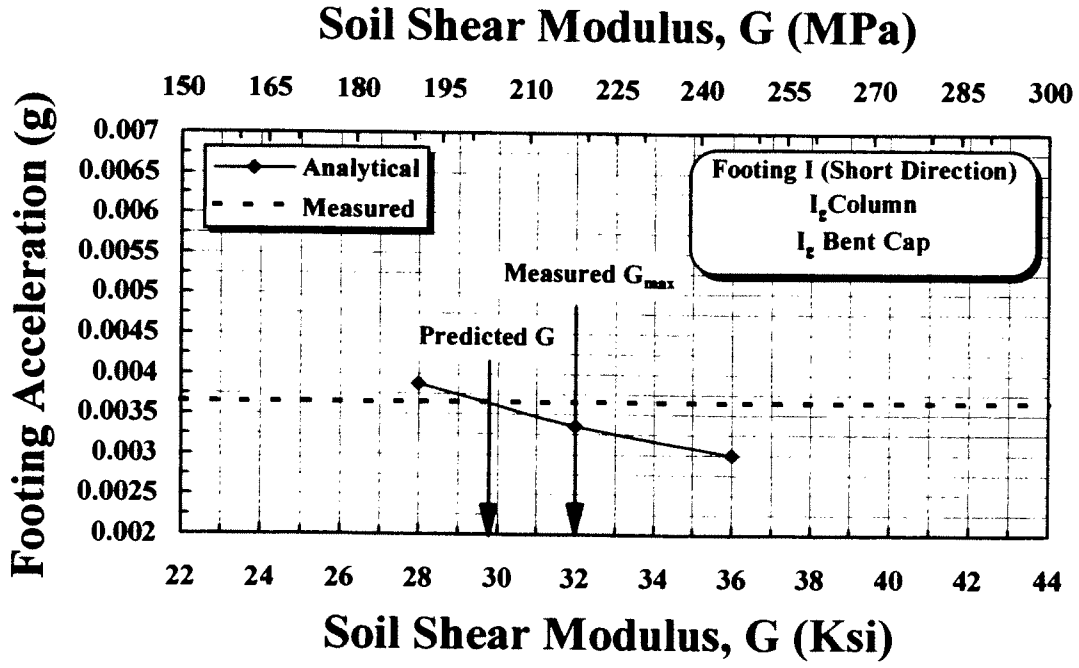

Figure 5.18. Effect of Soil Shear Modulus on the Steady State Acceleration of Footing I in the Short Direction

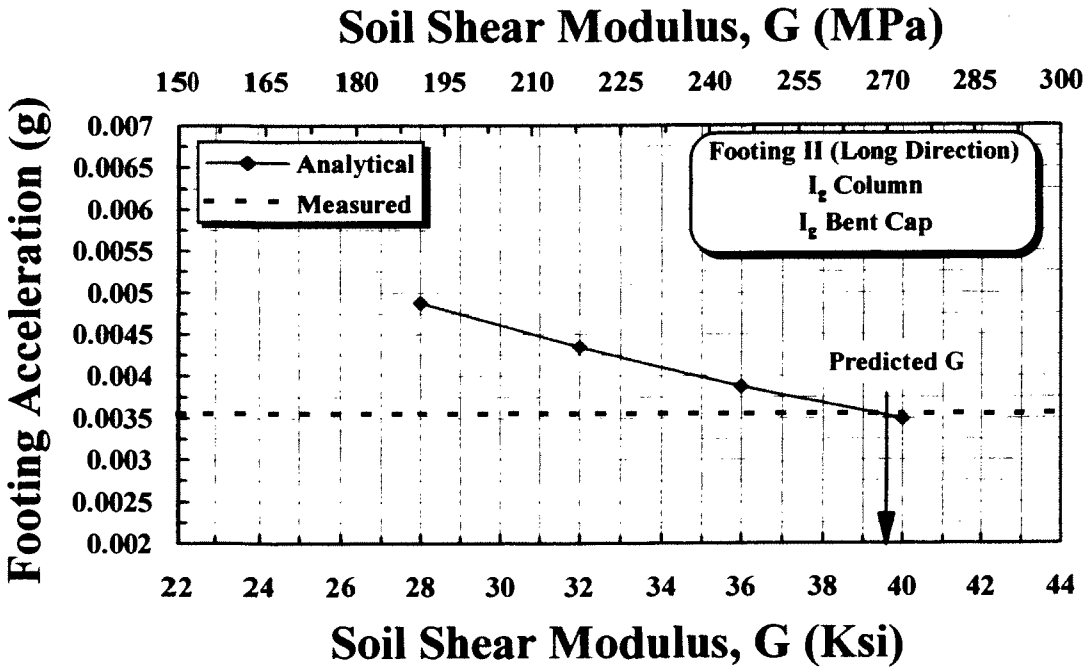

Figure 5.19. Effect of Soil Shear Modulus on the Steady State Acceleration of Footing II in the Longitudinal Direction

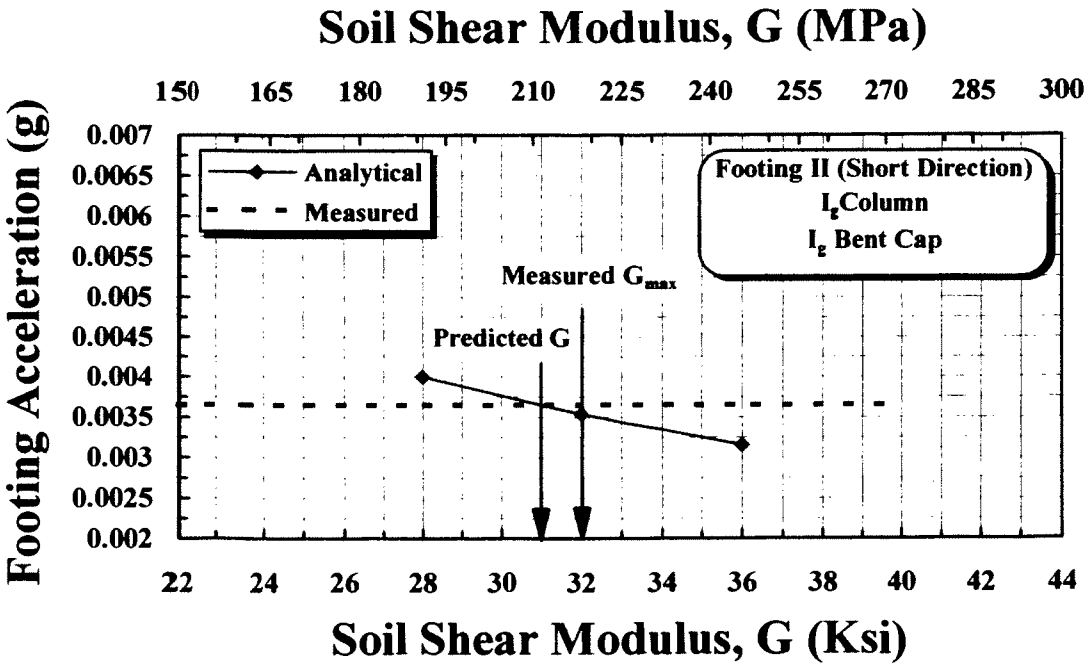

Figure 5.20. Effect of Soil Shear Modulus on the Steady State Acceleration of Footing II in the Short Direction

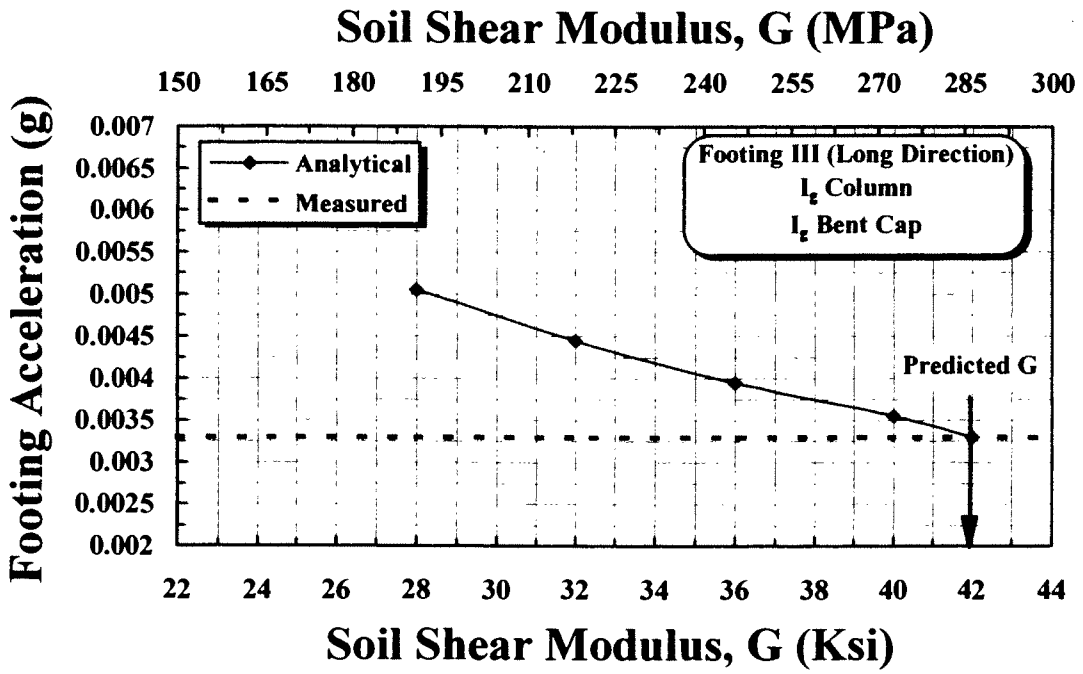

Figure 5.21. Effect of Soil Shear Modulus on the Steady State Acceleration of Footing III in the Longitudinal Direction

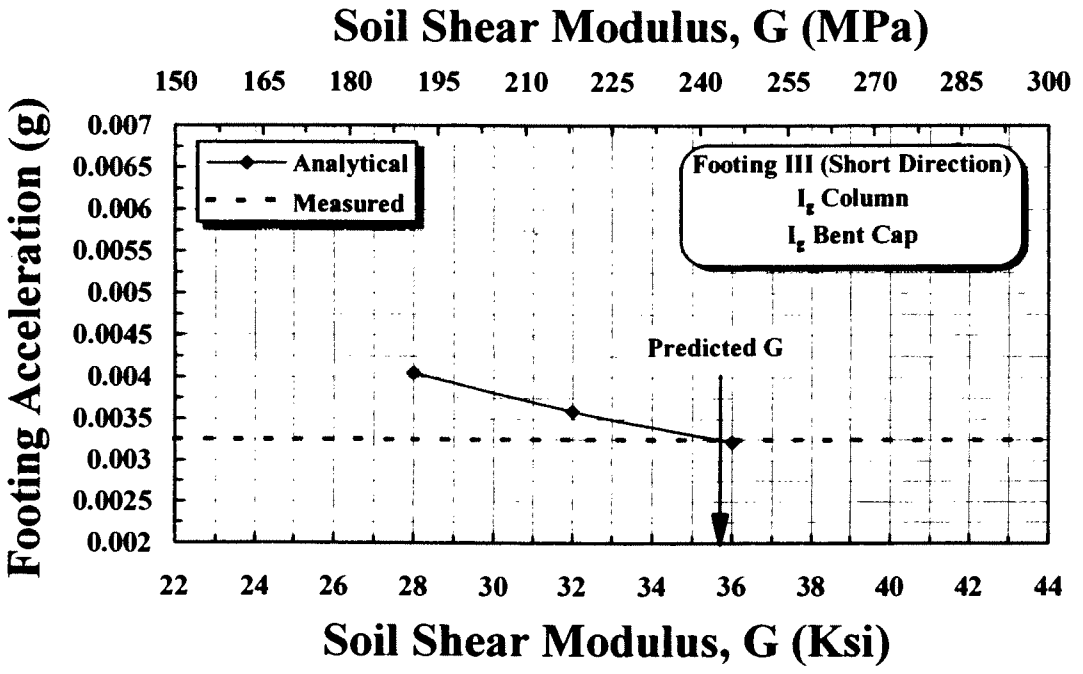

Figure 5.22. Effect of Soil Shear Modulus on the Steady State Acceleration of Footing III in the Short Direction

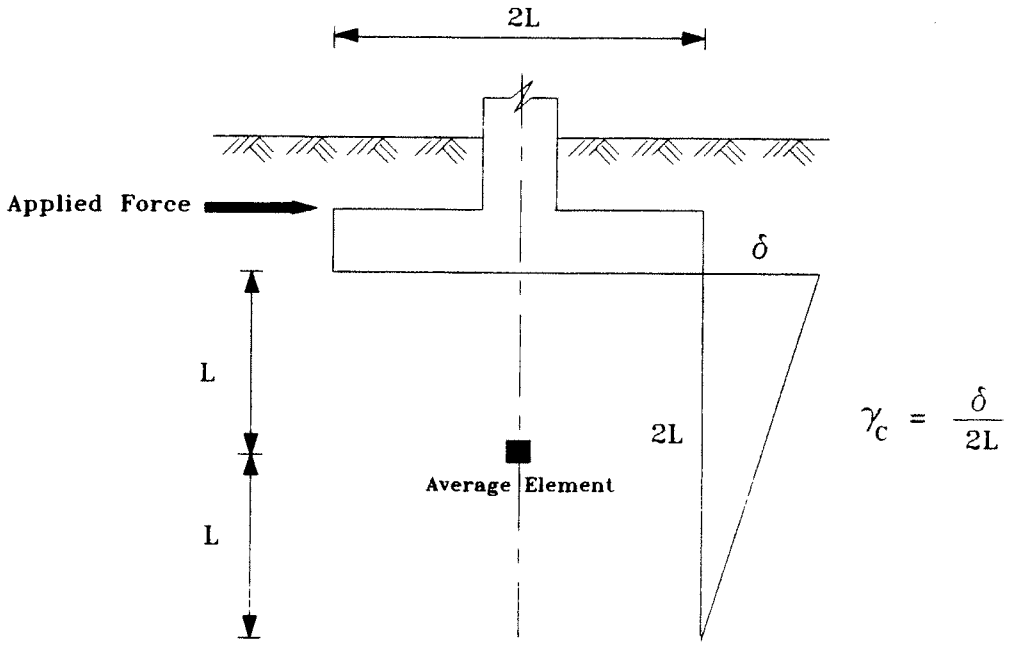

Figure 5.23. Prediction of Shear Strain in the Soil due to Forces Applied to the Footings in the Longitudinal Direction

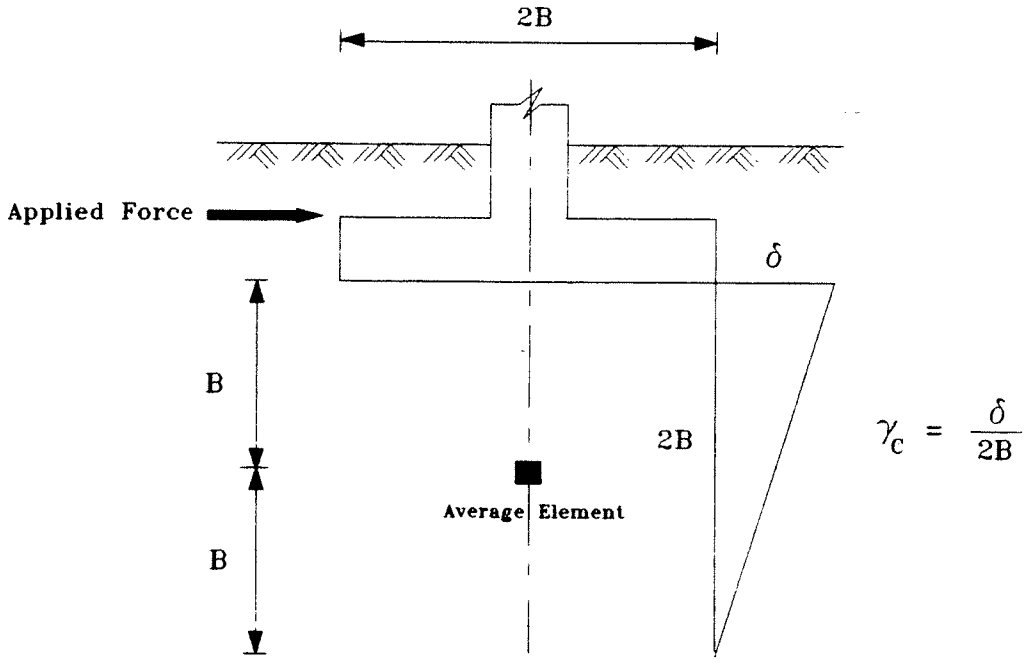

Figure 5.24. Prediction of Shear Strain in the Soil due to Forces Applied to the Footings in the Short Direction

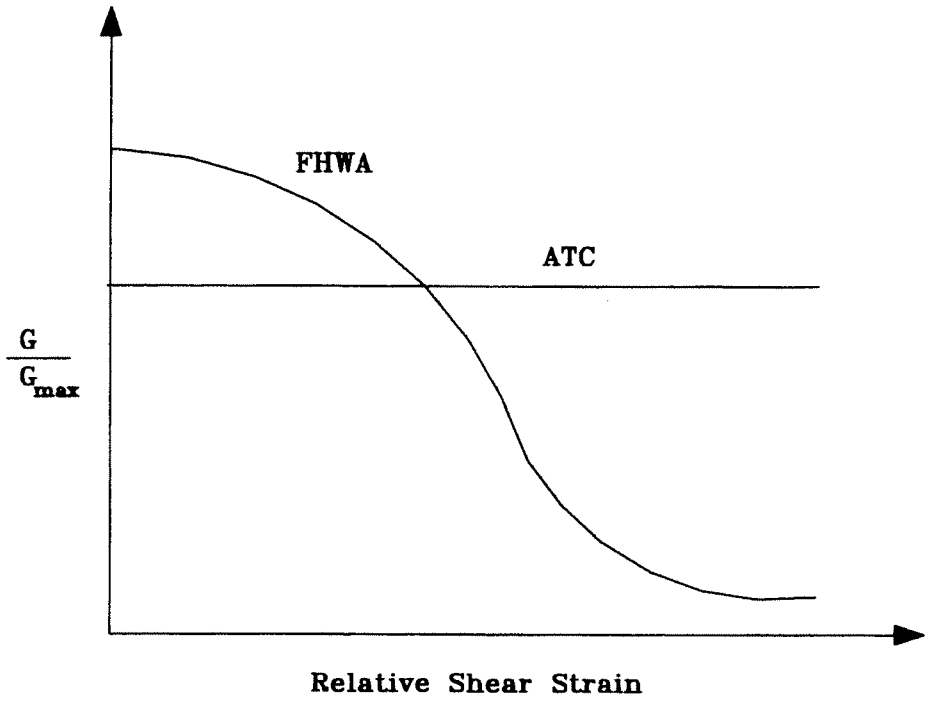

Figure 6.1. Shear Modulus Variations with the Near-Field Strain (FHWA) and the Far-Field Strain (ATC) (Adopted from Ref. 32)

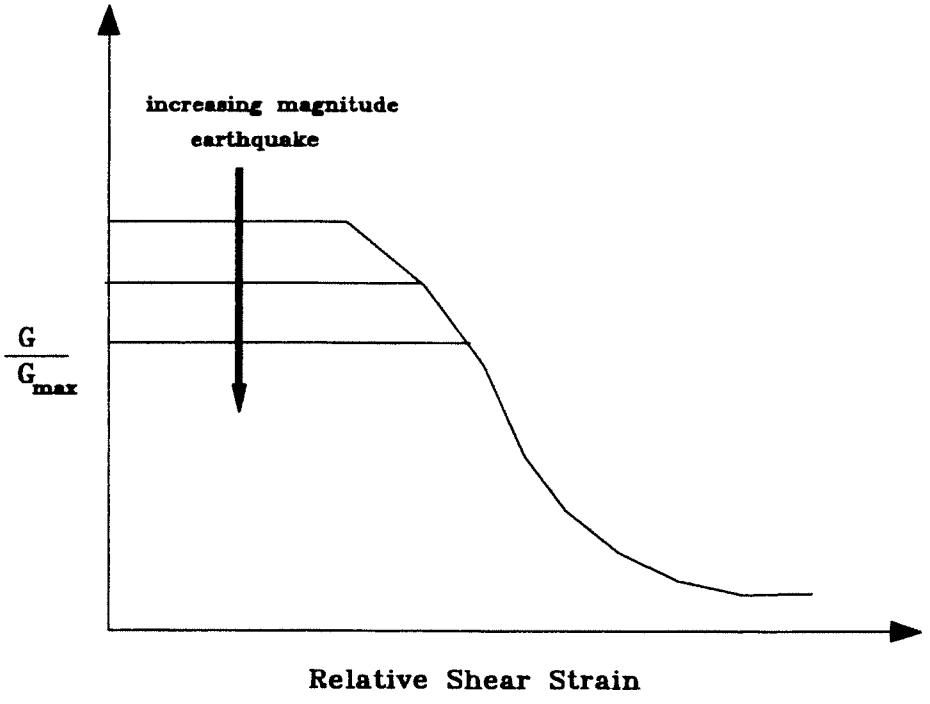

Figure 6.2. Shear Modulus Variations as a Function of Earthquake Magnitude (Adopted from Ref. 32)

Analog Se[redacted]tivity o[redacted]

n	Attenua[redacted] Setting[redacted]
1	66 db
2	60 db
3	54 db
4	48 db
5	42 db
6	36 db
7	30 db
8	24 db
9	18 db
10	12 db
11	6 db
12	0 db

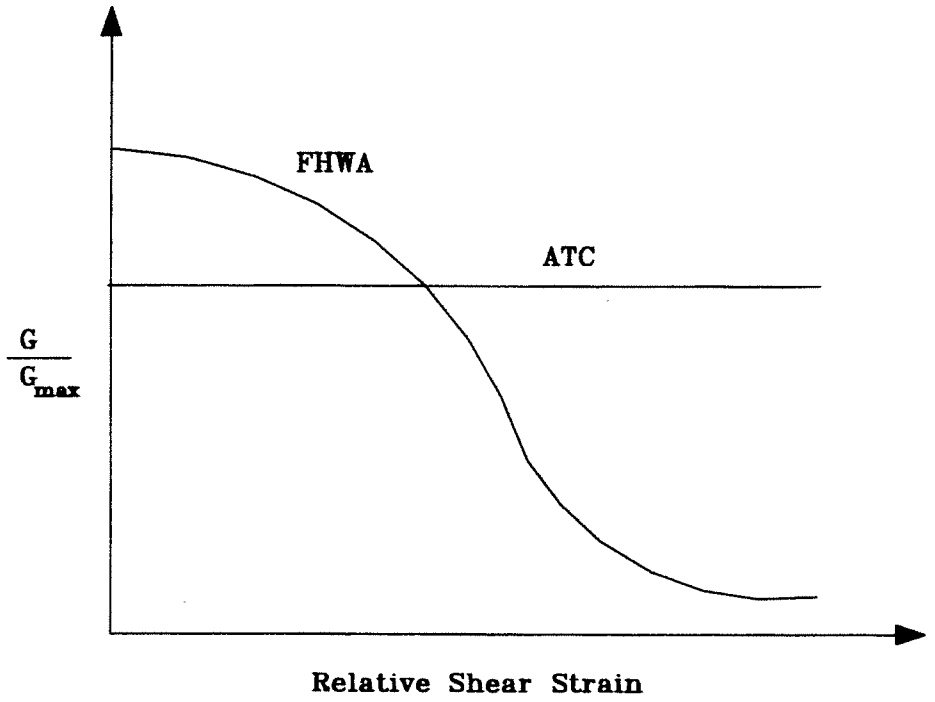

Figure 6.1. Shear Modulus Variations with the Near-Field Strain (FHWA) and the Far-Field Strain (ATC) (Adopted from Ref. 32)

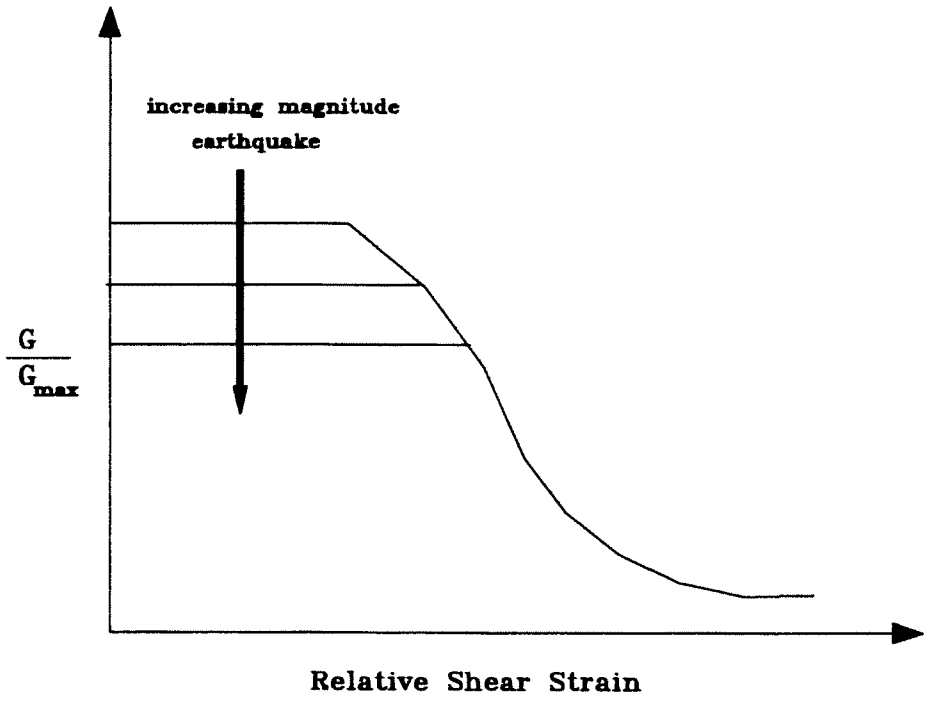

Figure 6.2. Shear Modulus Variations as a Function of Earthquake Magnitude (Adopted from Ref. 32)

Appendix A

Analog Sensitivity of Accelerometers Used in the Field Testing

n	Attenuator Setting	Full Scale (0 to Peak)	
		Volts	*g's*
1	66 db	2.5	4
2	60 db	1.25	2
3	54 db	0.625	1
4	48 db	0.3125	0.5
5	42 db	0.15625	0.25
6	36 db	0.078125	0.125
7	30 db	0.03906	0.0625
8	24 db	0.01953	0.03125
9	18 db	0.00965	0.015625
10	12 db	0.004883	0.007812
11	6 db	0.00244	0.003906
12	0 db	0.001221	0.001952

Appendix B

Equivalent Moment of Inertia of the Retrofitted Column

To calculate the equivalent moment of inertia of the retrofitted part of the column, the following procedure is adopted:

Assume that: $$n = \frac{E_s}{E_c} \tag{B.1}$$

where, E_s and E_c are the modulus of elasticity of steel and concrete, respectively. For the steel jacket and concrete column, the stresses are related to strains as follow:

$$\sigma_{xs} = E_s . \varepsilon_x \tag{B.2}$$

$$\sigma_{xc} = E_c . \varepsilon_x \tag{B.3}$$

where σ_{xs} and σ_{xc} are stresses in steel and concrete, respectively, and ε_x is the corresponding strain. The moment acting on the concrete column with the circular steel jacket is given by:

$$M = \int \sigma_x \, y \, dA = \int_s \sigma_{xs} \, y \, dA + \int_c \sigma_{xc} \, y \, dA \tag{B.4}$$

or:

$$M = \int_s E_s \, \varepsilon_x \, y \, dA + \int_c E_c \, \varepsilon_x \, y \, dA \tag{B.5}$$

where, dA is a differential area parallel to the x-axis, and y is its distance from the x-axis.

Therefore, the angle of twist, θ, becomes:

$$\theta = \frac{T L}{G_s J_s + G_c J_c} \tag{C.6}$$

Assume that: $n_t = \frac{G_s}{G_c}$ (C.7)

Finally, the angle of twist, θ, (converting the steel into transferred concrete) is given by:

$$\theta = \frac{T L}{G_c (J_c + n_t J_s)} \tag{C.8}$$

Then, the equivalent polar moment of inertia of the retrofitted part of the column can be expressed as:

$$J_{equiv} = J_c + n_t J_s \tag{C.9}$$

Appendix D

Numerical Example for the Computation of Footing Stiffness

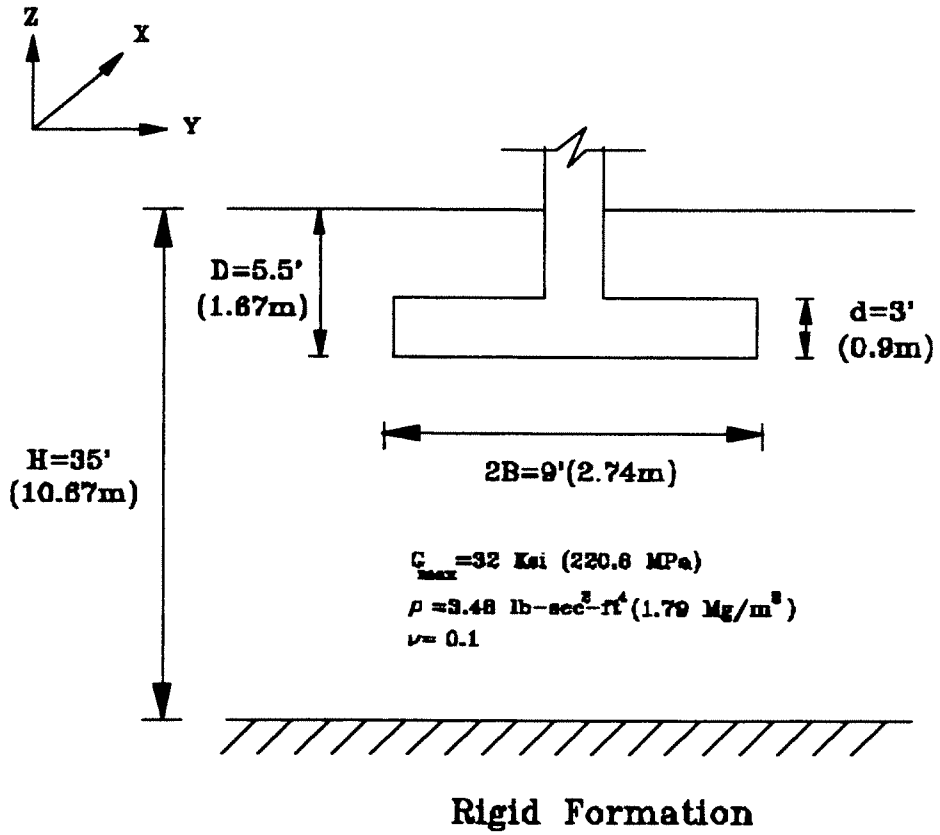

Figure D.1. Geometry of Footing II in the Short Direction and Measured Soil Properties under the Footing

To compute the stiffness of footing I tested in the short direction (Fig. 2.3), the design steps presented in Sec. 6.3 were followed. During the dynamic field test, footing II was subjected to a harmonic force of 19,500 lb (86.7 KN) in the short direction of the footing. The force was applied at a frequency (f) of 6.45 Hz. Figure D.1 shows a sketch of the footing and includes all the pertinent geometry and material properties of soil under the footing.

The equivalent radius (R) for the different modes of vibration of the rectangular footing can be determined using Eqs. 5.12 to 5.15 presented in Chapter 5. The following values are presented according to the coordinate system shown in Fig. D.1:

For translational modes:

$$R = \sqrt{\frac{4 * 4.5 * 6.5}{\pi}} = 6.1\,\text{ft} \quad (1.86\,\text{m}) \tag{D.1}$$

For Z-axis torsion:

$$R = \left[\frac{4 * 4.5 * 6.5 * \left(4 * 4.5^2 + 4 * 6.5^2\right)}{6 * \pi}\right]^{1/4} = 6.3\,\text{ft} \quad (1.9\,\text{m}) \tag{D.2}$$

For X-axis rocking:

$$R = \left[\frac{9 * 13^3}{3 * \pi}\right]^{1/4} = 6.76\,\text{ft} \quad (2.06\,\text{m}) \tag{D.3}$$

For Y-axis rocking:

$$R = \left[\frac{9^3 * 13}{3 * \pi}\right]^{1/4} = 5.63\,\text{ft} \quad (1.72\,\text{m}) \tag{D.4}$$

The footing stiffness corresponding to the applied dynamic force can be predicted using an iterative procedure. This is mainly due to the variation of the soil shear modulus with shear strain induced in the soil. As a first trial, G_{max} is used in the computation of footing stiffness. The static stiffness of the equivalent surface circular footing over bedrock can be computed as follow (Eqs. 5.18 to 5.21):

$$K_{Z,sur} = \frac{4*4608*6.1}{1-0.1}*\left(1+1.3*\frac{6.1}{35}\right) \quad \text{(C.5)}$$

$$= 1.53\times10^{5}\ \text{K/ft}\ \ (2.4\times10^{6}\ \text{KN/m})$$

$$K_{X,sur} = K_{Y,sur} = \frac{8*4608*6.1}{2-0.1}*\left(1+0.5*\frac{6.1}{35}\right) \quad \text{(D.6)}$$

$$= 1.30\times10^{5}\ \text{K/ft}\ \ (2.0\times10^{6}\ \text{KN/m})$$

$$K_{\theta Z,sur} = \frac{16}{3}*4608*6.3^{3}*\left(1+0.1*\frac{6.3}{35}\right) \quad \text{(D.7)}$$

$$= 6.26\times10^{6}\ \text{K-ft}\ \ (9.1\times10^{6}\ \text{KN-m})$$

$$K_{\theta X,sur} = \frac{8*4608*6.76^{3}}{3*(1-0.1)}*\left(1+0.17*\frac{6.76}{35}\right) \quad \text{(D.8)}$$

$$= 4.35\times10^{6}\ \text{K-ft}\ \ (6.4\times10^{6}\ \text{KN-m})$$

$$K_{\theta Y,sur} = \frac{8*4608*5.63^{3}}{3*(1-0.1)}*\left(1+0.17*\frac{5.63}{35}\right) \quad \text{(D.9)}$$

$$= 2.50\times10^{6}\ \text{K-ft}\ \ (3.6\times10^{6}\ \text{KN-m})$$

The stiffness of the equivalent circular footing that includes the embedment effect can be computed as follow (Eqs. 5.23 to 5.26):

$$K_{Z,emb} \cong 1.53\times10^{5}*\left(1+0.55*\frac{3}{6.1}\right)*\left[1+\left(0.85-0.28*\frac{5.5}{6.1}\right)*\frac{5.5}{35-5.5}\right] \quad \text{(D.10)}$$

$$\cong 2.16\times10^{5}\ \text{K/ft}\ \ (3.4\times10^{6}\ \text{KN/m})$$

$$K_{X,emb} = K_{Y,emb} \cong 1.3\times10^{5}*\left(1+\frac{3}{6.1}\right)*\left(1+1.25*\frac{5.5}{35}\right) \quad \text{(D.11)}$$

$$\cong 2.32\times10^{5}\ \text{K/ft}\ \ \ (3.6\times10^{6}\ \text{KN/m})$$

$$K_{\theta Z,emb} \cong 6.26\times10^{6} * \left(1+2.67*\frac{3}{6.3}\right) \cong 14.2\times10^{6}\ \text{K-ft}\ \ (20.8\times10^{6}\ \text{KN-m}) \tag{D.12}$$

$$K_{\theta X,emb} \cong 4.35\times10^{6} * \left(1+2*\frac{3}{6.76}\right)*\left(1+0.65*\frac{5.5}{35}\right) \cong 9.0\times10^{6}\ \text{K-ft}\ \ (13.0\times10^{6}\ \text{KN-m}) \tag{D.13}$$

$$K_{\theta Y,emb} \cong 2.50\times10^{6} * \left(1+2*\frac{3}{5.63}\right)*\left(1+0.65*\frac{5.5}{35}\right) \cong 5.7\times10^{6}\ \text{K-ft}\ \ (8.2\times10^{6}\ \text{KN-m}) \tag{D.14}$$

In order to correct for the foundation shape, the computed stiffness for an equivalent embedded circular footing should be multiplied by the shape factor α determined from Fig. 5.5. For L/B ratio equal to 1.44, the value of α for different modes of vibration is as follow:

$\alpha = 1.04$	(vertical translation, Z-direction)
$\alpha = 1.042$	(horizontal translation, X-direction)
$\alpha = 1.01$	(horizontal translation, Y-direction)
$\alpha = 1.056$	(rocking, X and Y-axes)
$\alpha = 1.056$	(torsion, Z-axis)

Therefore, the stiffness of footing II for the different mode of vibration is computed by multiplying α by the values determined from Eqs. D.10 to D.14:

$$K_{Z,emb} \cong 2.16\times10^{5} * 1.04 \cong 2.25\times10^{5}\ \text{K/ft}\ \ (3.5\times10^{6}\ \text{KN/m}) \tag{D.15}$$

$$K_{X,emb} \cong 2.32\times10^{5} * 1.042 \cong 2.42\times10^{5}\ \text{K/ft}\ \ (3.8\times10^{6}\ \text{KN/m}) \tag{D.16}$$

$$K_{Y,emb} \cong 2.32\times10^{5} * 1.01 \cong 2.34\times10^{5}\ \text{K/ft}\ \ (3.7\times10^{6}\ \text{KN/m}) \quad \text{(D.17)}$$

$$K_{\theta Z,emb} \cong 14.2\times10^{6} * 1.056 \cong 15.0\times10^{6}\ \text{K-ft}\ \ (21.9\times10^{6}\ \text{KN-m}) \quad \text{(D.18)}$$

$$K_{\theta X,emb} \cong 9.0\times10^{6} * 1.056 \cong 9.5\times10^{6}\ \text{K-ft}\ \ (13.7\times10^{6}\ \text{KN-m}) \quad \text{(D.19)}$$

$$K_{\theta X,emb} \cong 5.7\times10^{6} * 1.056 \cong 6.0\times10^{6}\ \text{K-ft}\ \ (8.7\times10^{6}\ \text{KN-m}) \quad \text{(D.20)}$$

It is important to know that the previous footing stiffness was computed using the measured G_{max}, which does not reflect the soil shear modulus corresponding to the applied dynamic load. Therefore, in order to determine the induced shear strain in the soil, a response history analysis was performed using a computer program *COSMOS/M*. As a first trial, the previous computed footing stiffness was used in the dynamic history analysis.

Since in the dynamic field test, only the soil in the near-field region is strained. Therefore, the calculated stiffness of the footing should be based on the soil shear modulus at the strain level induced in the near-field region (relative shear strain). At the base of footing II, a maximum displacement of approximately 8.0×10^{-4} in. (0.021 mm) was predicted along the short direction of the footing. By assuming a representative element in the soil at a depth of 4.5-ft (1372 mm) under the base of the footing, the induced shear strain was approximately 8×10^{-4} percent. This was determined using the computer program *COSMOS/M* as explained in Sec. 5.7.5. The value of G/G_{max} corresponding to that shear strain was 0.95 (Fig. 5.2 for sandy soils). This indicates that the soil shear modulus was

reduced to approximately 30.4 Ksi (209.6 MPa) at the maximum shear strain induced in the soil during the dynamic field test of the footing.

Finally, the stiffness of footing II corresponding to the applied dynamic load is computed by multiplying G/G_{max} by the values obtained from Eqs. D.15 to D.20:

$$K_{Z,emb} \cong 2.25\times10^{5} * 0.95 \cong 2.14\times10^{5} \text{ K/ft} \quad (3.4\times10^{6} \text{ KN/m}) \tag{D.21}$$

$$K_{X,emb} \cong 2.42\times10^{5} * 0.95 \cong 2.3\times10^{5} \text{ K/ft} \quad (3.6\times10^{6} \text{ KN/m}) \tag{D.22}$$

$$K_{Y,emb} \cong 2.34\times10^{5} * 0.95 \cong 2.22\times10^{5} \text{ K/ft} \quad (3.5\times10^{6} \text{ KN/m}) \tag{D.23}$$

$$K_{\theta Z,emb} \cong 15.0\times10^{6} * 0.95 \cong 14.25\times10^{6} \text{ K-ft} \quad (20.5\times10^{6} \text{ KN-m}) \tag{D.24}$$

$$K_{\theta X,emb} \cong 9.5\times10^{6} * 0.95 \cong 9.0\times10^{6} \text{ K-ft} \quad (13.0\times10^{6} \text{ KN-m}) \tag{D.25}$$

$$K_{\theta X,emb} \cong 6.0\times10^{6} * 0.95 \cong 5.7\times10^{6} \text{ K-ft} \quad (8.2\times10^{6} \text{ KN-m}) \tag{D.26}$$

Note that the computed footing stiffness was attained by using an iterative procedure, where several runs of the response history analysis was performed until the assumed shear modulus matched that predicted from the program.

LIST OF CENTER FOR CIVIL ENGINEERING EARTHQUAKE RESEARCH (CCEER) PUBLICATIONS

Report No.	Publication
CCEER-84-1	Saiidi, M., and R. Lawver, "User's Manual for LZAK-C64, A Computer Program to Implement the Q-Model on Commodore 64," Civil Engineering Department, Report No. CCEER-84-1, University of Nevada, Reno, January 1984.
CCEER-84-2	Douglas, B. and T. Iwasaki, "Proceedings of the First USA-Japan Bridge Engineering Workshop," held at the Public Works Research Institute, Tsukuba, Japan, Civil Engineering Department, Report No. CCEER-84-2, University of Nevada, Reno, April 1984.
CCEER-84-3	Saiidi, M., J. Hart, and B. Douglas, "Inelastic Static and Dynamic Analysis of Short R/C Bridges Subjected to Lateral Loads," Civil Engineering Department, Report No. CCEER-84-3, University of Nevada, Reno, July 1984.
CCEER-84-4	Douglas, B., "A Proposed Plan for a National Bridge Engineering Laboratory," Civil Engineering Department, Report No. CCEER-84-4, University of Nevada, Reno, December 1984.
CCEER-85-1	Norris, G. and P. Abdollaholiaee, "Laterally Loaded Pile Response: Studies with the Strain Wedge Model," Civil Engineering Department, Report No. CCEER-85-1, University of Nevada, Reno, April 1985.
CCEER-86-1	Ghusn, G. and M. Saiidi, "A Simple Hysteretic Element for Biaxial Bending of R/C Columns and Implementation in NEABS-86," Civil Engineering Department, Report No. CCEER-86-1, University of Nevada, Reno, July 1986.
CCEER-86-2	Saiidi, M., R. Lawver, and J. Hart, "User's Manual of ISADAB and SIBA, Computer Programs for Nonlinear Transverse Analysis of Highway Bridges Subjected to Static and Dynamic Lateral Loads," Civil Engineering Department, Report No. CCEER-86-2, University of Nevada, Reno, September 1986.
CCEER-87-1	Siddharthan, R., "Dynamic Effective Stress Response of Surface and Embedded Footings in Sand," Civil engineering Department, Report No. CCEER-86-2, University of Nevada, Reno, June 1987.
CCEER-87-2	Norris, G. and R. Sack, "Lateral and Rotational Stiffness of Pile Groups for Seismic Analysis of Highway Bridges," Civil Engineering Department, Report No. CCEER-87-2, University of Nevada, Reno, June 1987.
CCEER-88-1	Orie, J. and M. Saiidi, "A Preliminary Study of One-Way Reinforced Concrete Pier Hinges Subjected to Shear and Flexure," Civil Engineering Department, Report No. CCEER-88-1, University of Nevada, Reno, January 1988.
CCEER-88-2	Orie, D., M. Saiidi, and B. Douglas, "A Micro-CAD System for Seismic Design of Regular Highway Bridges," Civil Engineering Department, Report No. CCEER-88-2, University of Nevada, Reno, June 1988.
CCEER-88-3	Orie, D. and M. Saiidi, "User's Manual for Micro-SARB, a Microcomputer Program for Seismic Analysis of Regular Highway Bridges," Civil Engineering Department, Report No. CCEER-88-3, University of Nevada, Reno, October 1988.
CCEER-89-1	Douglas, B., M. Saiidi, R. Hayes, and G. Holcomb, "A Comprehensive Study of the Loads and Pressures

Exerted on Wall Forms by the Placement of Concrete," Civil Engineering Department, Report No. CCEER-89-1, University of Nevada, Reno, February 1989.

CCEER-89-2 Richardson, J. and B. Douglas, "Dynamic Response Analysis of the Dominion Road Bridge Test Data," Civil Engineering Department, Report No. CCEER-89-2, University of Nevada, Reno, March 1989.

CCEER-89-2 Vrontinos, S., M. Saiidi, and B. Douglas, "A Simple Model to Predict the Ultimate Response of R/C Beams with Concrete Overlays," Civil Engineering Department, Report NO. CCEER-89-2, University of Nevada, Reno, June 1989.

CCEER-89-3 Ebrahimpour, A. and P. Jagadish, "Statistical Modeling of Bridge Traffic Loads - A Case Study," Civil Engineering Department, Report No. CCEER-89-3, University of Nevada, Reno, December 1989.

CCEER-89-4 Shields, J. and M. Saiidi, "Direct Field Measurement of Prestress Losses in Box Girder Bridges," Civil Engineering Department, Report No. CCEER-89-4, University of Nevada, Reno, December 1989.

CCEER-90-1 Saiidi, M., E. Maragakis, G. Ghusn, Y. Jiang, and D. Schwartz, "Survey and Evaluation of Nevada's Transportation Infrastructure, Task 7.2 - Highway Bridges, Final Report," Civil Engineering Department, Report No. CCEER 90-1, University of Nevada, Reno, October 1990.

CCEER-90-2 Abdel-Ghaffar, S., E. Maragakis, and M. Saiidi, "Analysis of the Response of Reinforced Concrete Structures During the Whittier Earthquake 1987," Civil Engineering Department, Report No. CCEER 90-2, University of Nevada, Reno, October 1990.

CCEER-91-1 Saiidi, M., E. Hwang, E. Maragakis, and B. Douglas, "Dynamic Testing and the Analysis of the Flamingo Road Interchange," Civil Engineering Department, Report No. CCEER-91-1, University of Nevada, Reno, February 1991.

CCEER-91-2 Norris, G., R. Siddharthan, Z. Zafir, S. Abdel-Ghaffar, and P. Gowda, "Soil-Foundation-Structure Behavior at the Oakland Outer Harbor Wharf," Civil Engineering Department, Report No. CCEER-91-2, University of Nevada, Reno, July 1991.

CCEER-91-3 Norris, G., "Seismic Lateral and Rotational Pile Foundation Stiffnesses at Cypress," Civil Engineering Department, Report No. CCEER-91-3, University of Nevada, Reno, August 1991.

CCEER-91-4 O'Connor, D. and M. Saiidi, "A Study of Protective Overlays for Highway Bridge Decks in Nevada, with Emphasis on Polyester-Styrene Polymer Concrete," Civil Engineering Department, Report No. CCEER-91-4, University of Nevada, Reno, October 1991.

CCEER-91-5 O'Connor, D.N. and M. Saiidi, "Laboratory Studies of Polyester-Styrene Polymer Concrete Engineering Properties," Civil Engineering Department, Report No. CCEER-91-5, University of Nevada, Reno, November 1991.

CCEER-92-1 Straw, D.L. and M. Saiidi, "Scale Model Testing of One-Way Reinforced Concrete Pier Hinges Subject to Combined Axial Force, Shear and Flexure," edited by D.N. O'Connor, Civil Engineering Department, Report No. CCEER-92-1, University of Nevada, Reno, March 1992.

CCEER-92-2 Wehbe, N., M. Saiidi, and F. Gordaninejad, "Basic Behavior of Composite Sections Made of Concrete Slabs and Graphite Epoxy Beams," Civil Engineering Department, Report No. CCEER-92-2, University of Nevada, Reno, August 1992.

CCEER-92-3 Saiidi, M. and E. Hutchens, "A Study of Prestress Changes in A Post-Tensioned Bridge During the First 30 Months," Civil Engineering Department, Report No. CCEER-92-3, University of Nevada, Reno, April 1992.

CCEER-92-4 Saiidi, M., B. Douglas, S. Feng, E. Hwang, and E. Maragakis, "Effects of Axial Force on Frequency of Prestressed Concrete Bridges," Civil Engineering Department, Report No. CCEER-92-4, University of Nevada, Reno, August 1992.

CCEER-92-5 Siddharthan, R., and Z. Zafir, "Response of Layered Deposits to Traveling Surface Pressure Waves," Civil Engineering Department, Report No. CCEER-92-5, University of Nevada, Reno, September 1992.

CCEER-92-6 Norris, G., and Z. Zafir, "Liquefaction and Residual Strength of Loose Sands from Drained Triaxial Tests," Civil Engineering Department, Report No. CCEER-92-6, University of Nevada, Reno, September 1992.

CCEER-92-7 Douglas, B., "Some Thoughts Regarding the Improvement of the University of Nevada, Reno's National Academic Standing," Civil Engineering Department, Report No. CCEER-92-7, University of Nevada, Reno, September 1992.

CCEER-92-8 Saiidi, M., E. Maragakis, and S. Feng, "An Evaluation of the Current Caltrans Seismic Restrainer Design Method," Civil Engineering Department, Report No. CCEER-92-8, University of Nevada, Reno, October 1992.

CCEER-92-9 O'Connor, D., M. Saiidi, and E. Maragakis, "Effect of Hinge Restrainers on the Response of the Madrone Drive Undercrossing During the Loma Prieta Earthquake," Civil Engineering Department, Report No. CCEER-92-9, University of Nevada, Reno, February 1993.

CCEER-92-10 O'Connor, D., and M. Saiidi, "Laboratory Studies of Polyester Concrete: Compressive Strength at Elevated Temperatures and Following Temperature Cycling, Bond Strength to Portland Cement Concrete, and Modulus of Elasticity," Civil Engineering Department, Report No. CCEER-92-10, University of Nevada, Reno, February 1993.

CCEER-92-11 Wehbe, N., M. Saiidi, and D. O'Connor, "Economic Impact of Passage of Spent Fuel Traffic on Two Bridges in Northeast Nevada," Civil Engineering Department, Report No. CCEER-92-11, University of Nevada, Reno, December 1992.

CCEER-93-1 Jiang, Y., and M. Saiidi, "Behavior, Design, and Retrofit of Reinforced Concrete One-way Bridge Column Hinges," edited by D. O'Connor, Civil Engineering Department, Report No. CCEER-93-1, University of Nevada, Reno, March 1993.

CCEER-93-2 Abdel-Ghaffar, S., E. Maragakis, and M. Saiidi, "Evaluation of the Response of the Aptos Creek Bridge During the 1989 Loma Prieta Earthquake," Civil Engineering Department, Report No. CCEER-93-2, University of Nevada, Reno, June 1993.

CCEER-93-3 Sanders, D.H., B.M. Douglas, and T.L. Martin, "Seismic Retrofit Prioritization of Nevada Bridges," Civil Engineering Department, Report No. CCEER-93-3, University of Nevada, Reno, July 1993.

CCEER-93-4 Abdel-Ghaffar, S., E. Maragakis, and M. Saiidi, "Performance of Hinge Restrainers in the Huntington Avenue Overhead During the 1989 Loma Prieta Earthquake," Civil Engineering Department, Report No. CCEER-93-4, University of Nevada, Reno, June 1993.

CCEER-93-5 Maragakis, E., M. Saiidi, S. Feng, and L. Flournoy, "Effects of Hinge Restrainers on the Response of the San Gregorio Bridge During the Loma Prieta Earthquake," (in final preparation) Civil Engineering Department, Report No. CCEER-93-5, University of Nevada, Reno.

CCEER-93-6 Saiidi, M., E. Maragakis, S. Abdel-Ghaffar, S. Feng, and D. O'Connor, "Response of Bridge Hinge Restrainers During Earthquakes -Field Performance, Analysis, and Design," Civil Engineering Department, Report No. CCEER-93-6, University of Nevada, Reno, May 1993.

CCEER-93-7 Wehbe, N., Saiidi, M., Maragakis, E., and Sanders, D., "Adequacy of Three Highway Structures in Southern Nevada for Spent Fuel Transportation, Civil Engineering Department, Report No. CCEER-93-7, University of Nevada, Reno, August 1993.

CCEER-93-8 Roybal, J., Sanders, D.H., and Maragakis, E., "Vulnerability Assessment of Masonry Public Buildings in the Reno-Carson City Urban Corridor," Civil Engineering Department, Report No. CCEER-93-8, University of Nevada, Reno, May 1993.

CCEER-93-9 Zafir, Z. and Siddharthan, R., "MOVLOAD: A Program to Determine the Behavior of Nonlinear Horizontally Layered Medium Under Moving Load," Civil Engineering Department, Report No. CCEER-93-9, University of Nevada, Reno, August 1993.

CCEER-93-10 O'Connor, D.N., Saiidi, M., and Maragakis, E.A., "A Study of Bridge Column Seismic Damage Susceptibility at the Interstate 80/U.S. 395 Interchange in Reno, Nevada," Civil Engineering Department, Report No. CCEER-93-10, University of Nevada, Reno, October 1993.

CCEER-94-1 Maragakis, E., B. Douglas, and E. Abdelwahed, "Preliminary Dynamic Analysis of a Railroad Bridge," Report CCEER-94-1, January 1994.

CCEER-94-2 Douglas, B.M., Maragakis, E.A., and Feng, S., "Stiffness Evaluation of Pile Foundation of Cazenovia Creek Overpass," Civil Engineering Department, Report No. CCEER-94-2, University of Nevada, Reno, March 1994.

CCEER-94-3 Douglas, B.M., Maragakis, E.A., and Feng, S., "Summary of Pretest Analysis of Cazenovia Creek Bridge," Civil Engineering Department, Report No. CCEER-94-3, University of Nevada, Reno, April 1994.

CCEER-94-4 Norris, G.M. and Madhu, R., "Liquefaction and Residual Strength of Sands from Drained Triaxial Tests, Report 2," Civil Engineering Department, CCEER-94-4, University of Nevada, Reno, August 1994.

CCEER-94-5 Saiidi, M., Hutchens, E., and Gardella, D., "Prestress Losses in a Post-Tensioned R/C Box Girder Bridge in Southern Nevada," Civil Engineering Department, CCEER-94-5, University of Nevada, Reno, August 1994.

CCEER-95-1 Siddharthan, R., El-Gamal, M., and Maragakis, E.A., "Nonlinear Bridge Abutment Stiffnesses: Formulation, Verification, and Design Curves," Civil Engineering Department, CCEER-95-1, University of Nevada, Reno, January 1995.

CCEER-95-2 Norris, G.M., Madhu, R., Valceschini, R., and Ashour, M., "Liquefaction and Residual Strength of Loose Sands from Drained Triaxial Tests," Report 2, Civil Engineering Department, Report No. CCEER-95-2, University of Nevada, Reno, February 1995.

CCEER-95-3 Wehbe, N., Saiidi, M., Sanders, D., and Douglas, B., "Ductility of Rectangular Reinforced Concrete

Bridge Columns with Moderate Confinement,"Civil Engineering Department, Report No. CCEER-95-3, University of Nevada, Reno, July 1995.

CCEER-95-4 Martin, T., Saiidi, M., and Sanders, D., "Seismic Retrofit of Column-Pier Cap Connections in Bridges in Northern Nevada," Civil Engineering Department, Report No. CCEER-95-4, University of Nevada, Reno, August 1995.

CCEER-95-5 Darwish, I., Saiidi, M., and Sanders, D., "Experimental Study of Seismic Susceptibility of Tapered Bridge Column-Footing Connections," Civil Engineering Department, Report No. CCEER-95-5, University of Nevada, Reno, September 1995.

CCEER-95-6 Griffin, G., Saiidi, M., and Maragakis, E., "Nonlinear Seismic Response of Isolated Bridges and Effects of Pier Ductility Demand," Civil Engineering Department, Report No. CCEER-95-6, University of Nevada, Reno, November 1995.

CCEER-95-7 Acharya, S., Saiidi, M., and Sanders, D., "Seismic Retrofit of Bridge Footings and Column-Footing Connections," Report for the Nevada Department of Transportation, Civil Engineering Department, Report No. CCEER-95-7, University of Nevada, Reno, November 1995.

CCEER-95-8 Maragakis, E., Douglas, B., and Sandirasegaram, U., "Full-Scale Field Resonance Tests of a Railway Bridge," A Report to the Association of American Railroads, Civil Engineering Department, Report No. CCEER-95-8, University of Nevada, Reno, December 1995.

CCEER-95-9 Douglas, B., Maragakis, E., and Feng, S., "System Identification Studies on Cazenovia Creek Overpass," Report for the National Center for Earthquake Engineering Research, Civil Engineering Department, Report No. CCEER-95-9, University of Nevada, Reno, October 1995.

CCEER-96-1 El-Gamal, M.E. and Siddharthan, R.V., "Programs to Computer Translational Stiffness of Seat-Type Bridge Abutment," Civil Engineering Department, Report No. CCEER-96-1, University of Nevada, Reno, March 1996.

CCEER-96-2 Labia, Y., Saiidi, M., and Douglas, B., "Evaluation and Repair of Full-Scale Prestressed Concrete Box Girders," A Report to the National Science Foundation, Research Grant CMS-9201908, Civil Engineering Department, Report No. CCEER-96-2, University of Nevada, Reno, May 1996.

CCEER-96-3 Darwish, I., Saiidi, M., and Sanders, D., "Seismic Retrofit of R/C Oblong Tapered Bridge Columns with Inadequate Bar Anchorage in Columns and Footings," A Report to the Nevada Department of Transportation, Civil Engineering Department, Report No. CCEER-96-3, University of Nevada, Reno, May 1996.

CCEER-96-4 Ashour, M., Pilling, P., Norris, G., and Perez, H., "The Prediction of Lateral Load Behavior of Single Piles and Pile Groups Using the Strain Wedge Model," A Report to the California Department of Transportation, Civil Engineering Department, Report No. CCEER-96-4, University of Nevada, Reno, June, 1996.

CCEER-97-1 Maragakis, E., Douglas, B., and Sandirasegaram, U. "Full-Scale Field Resonance Tests of a Railway Bridge," A Report to the Association of American Railroads, Civil Engineering Department, University of Nevada, Reno, May, 1996.

CCEER-97-2 Wehbe, N., M. Saiidi, and D. Sanders, "Effects of Confinement and Flares on the Seismic Performance of Reinforced Concrete Bridge Columns," Civil Engineering Department, University of Nevada, Reno,

Report No. CCEER-97-2, September, 1997.

CCEER-97-3 Darwish, I., M. Saiidi, G. Norris, and E. Maragakis, "Determination of In-Situ Footing Stiffness Using Full-Scale Dynamic Field Testing," A Report to the Nevada Department of Transportation, Structural Design Division, Carson City, Nevada, Report No. CCEER-97-3, University of Nevada, Reno, October, 1997.

CCEER-97-4 Wehbe, N., and M. Saiidi, "RCMC- A Computer Program for Moment-Curvature Analysis of Confined and Unconfined Reinforced Concrete Sections," Center for Civil Engineering Earthquake Research, Department of Civil Engineering, University of Nevada, Reno, Nevada, Report No. CCEER-97-4, November, 1997.

CCEER-97-5 Isakovic, T., M. Saiidi, and A. Itani, "Influence of new Bridge Configurations on Seismic Performance," Department of Civil Engineering, University of Nevada, Reno, Report No. CCEER-97-5, September, 1997.

Kenny C. Guinn, Governor

Nevada Department of Transportation
Tom Stephens, P.E. Director
Prepared by Research Division
Alan Hilton, Research Manager
(775) 888-7803
ahilton@dot.state.nv.us
1263 South Stewart Street
Carson City, Nevada 89712

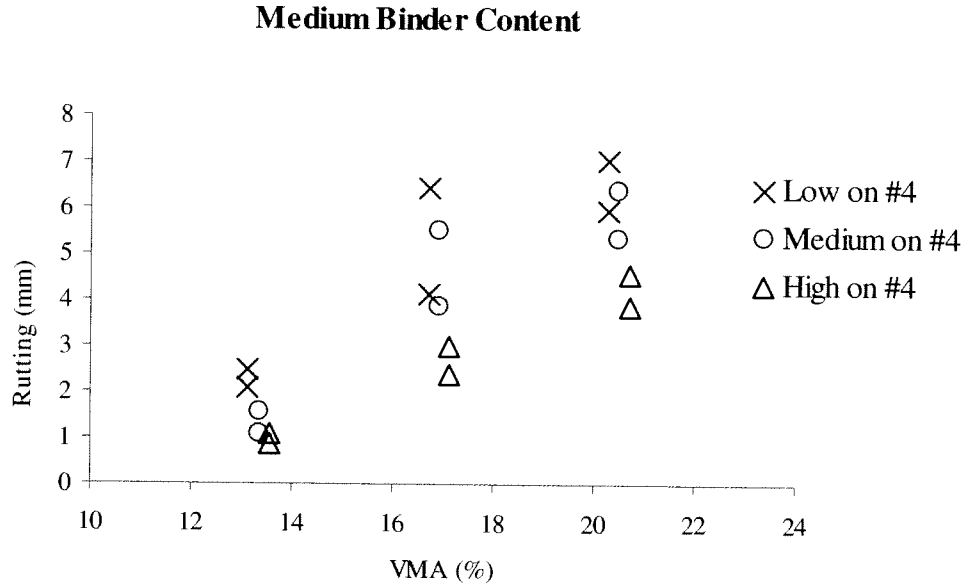

Figure 23 Rutting Vs. VMA for the Lockwood Aggregate Source at Medium %AC

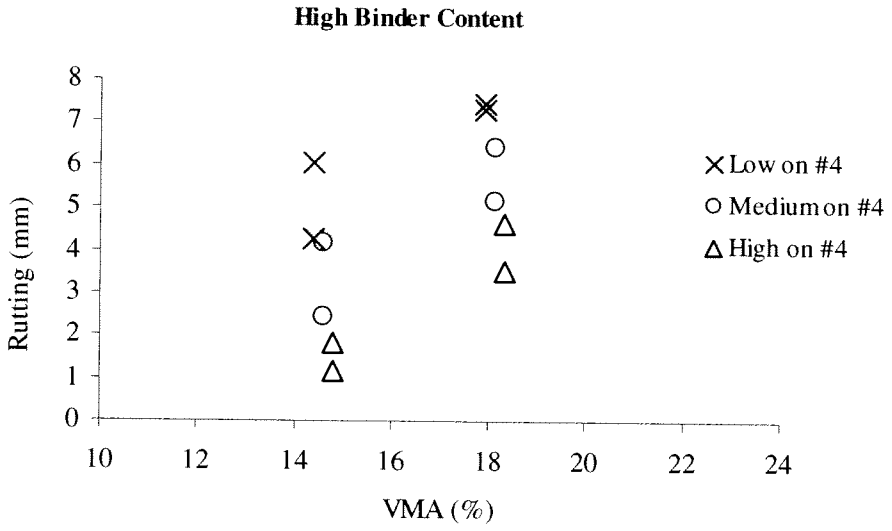

Figure 24 Rutting Vs. Percent VMA for the Lockwood Aggregate Source at High %AC

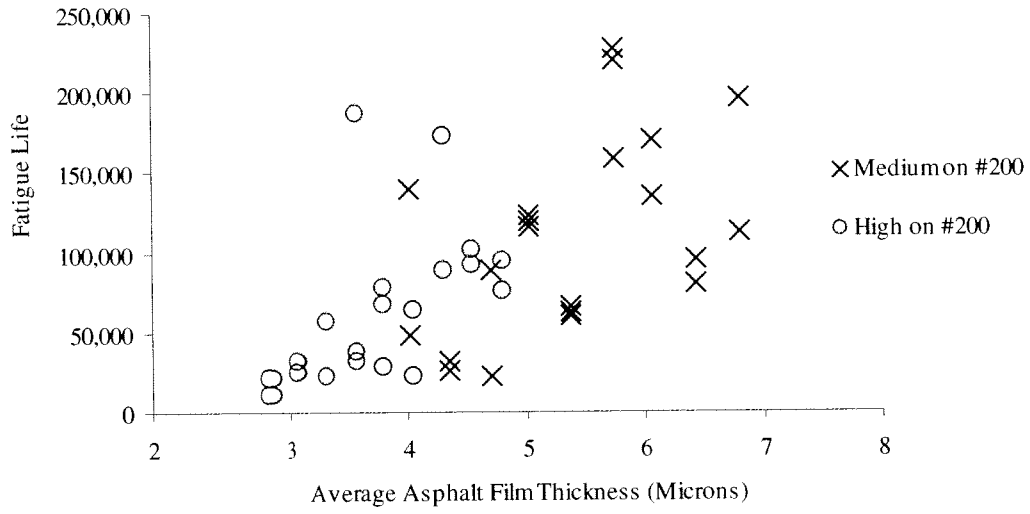

Figure 25 Fatigue Life Vs. Film Thickness for the Lockwood Aggregate Source.

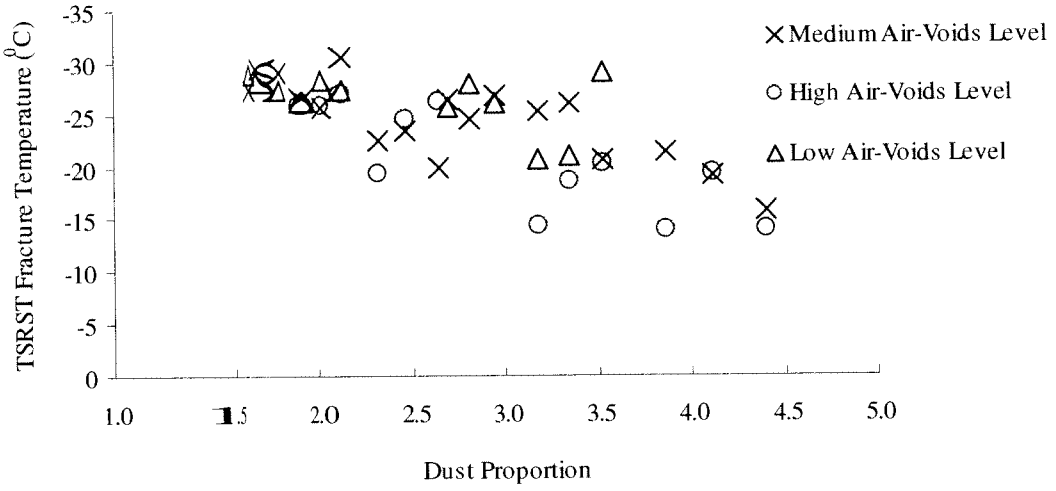

Figure 26 Fracture Temp Vs. Dust Proportion for the Lockwood Aggregate Source.

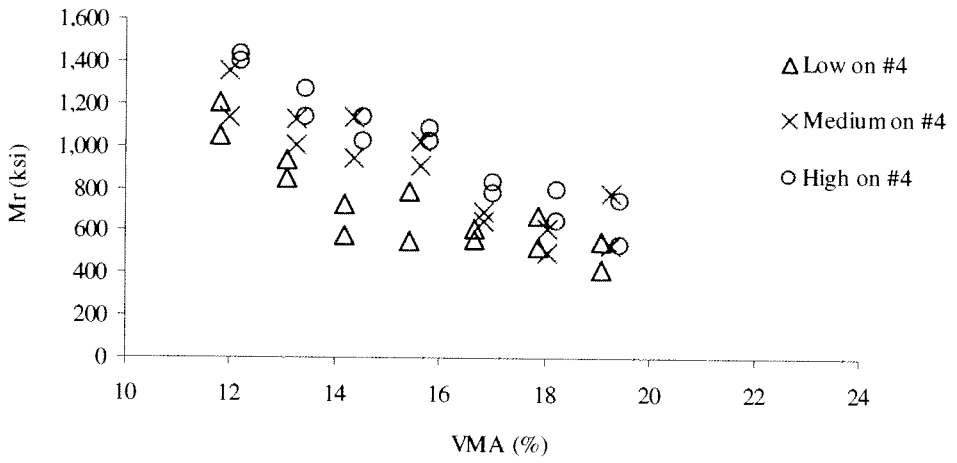

Figure 27 Resilient Modulus Vs. Percent VMA for the Sloan Aggregate Source.

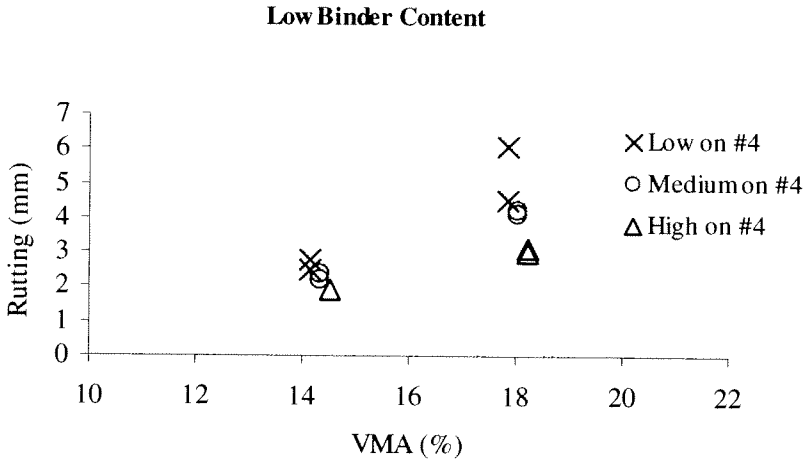

Figure 28 Rutting Vs. Percent VMA for the Sloan Aggregate Source at Low %AC

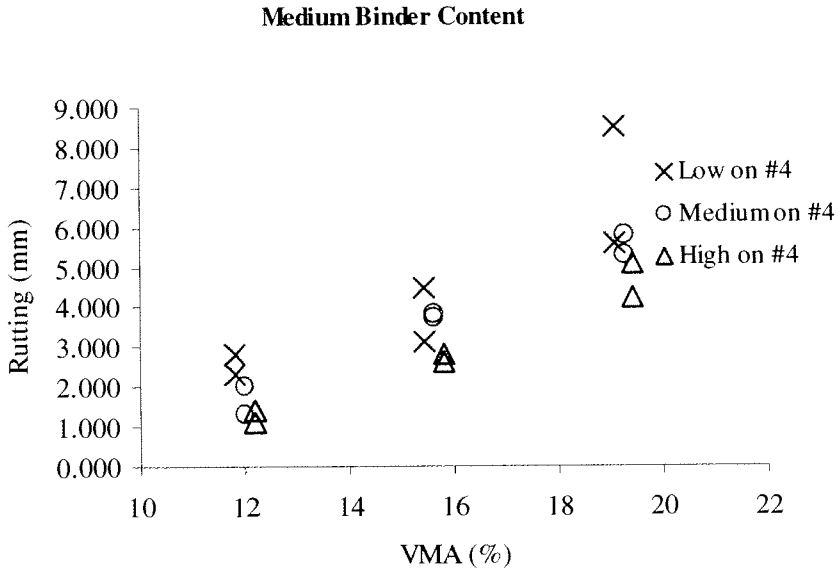

Figure 29 Rutting Vs. Percent VMA for the Sloan Aggregate Source at Medium %AC

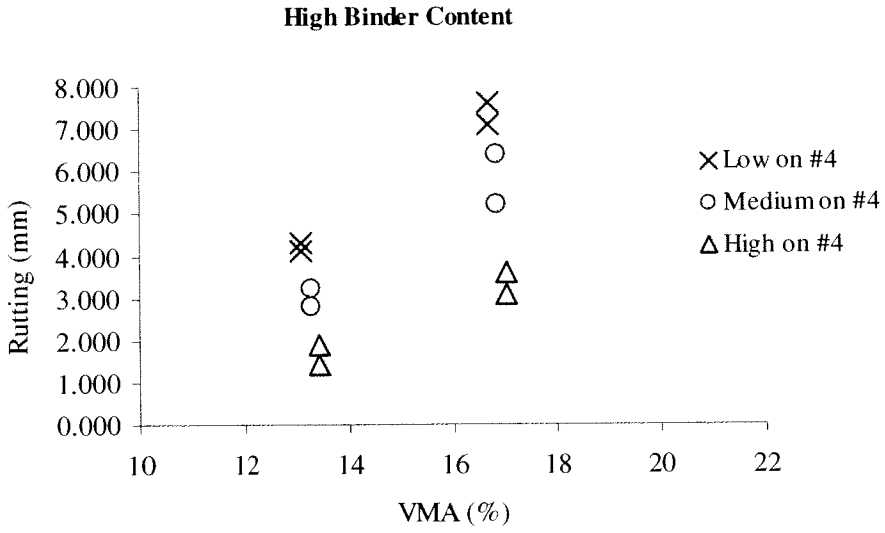

Figure 30 Rutting Vs. Percent VMA for the Sloan Aggregate Source at High %AC

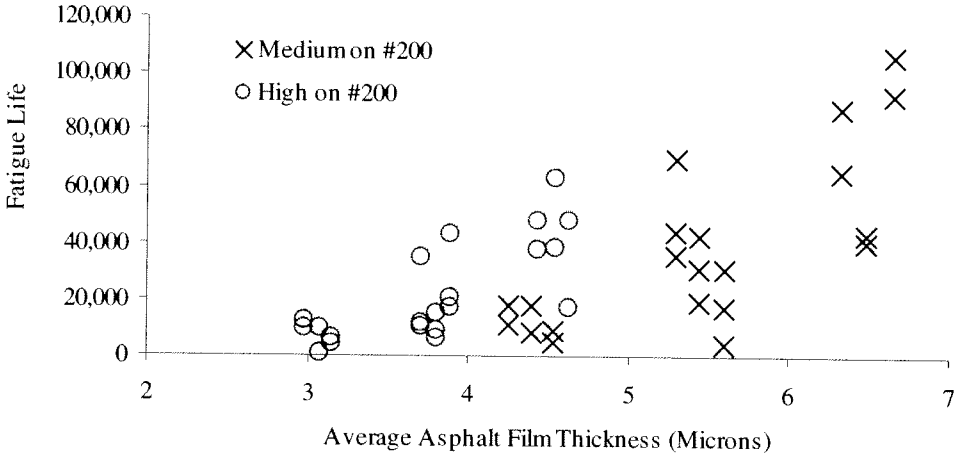

Figure 31 Fatigue Life Vs. Film Thickness for the Sloan Aggregate Source.

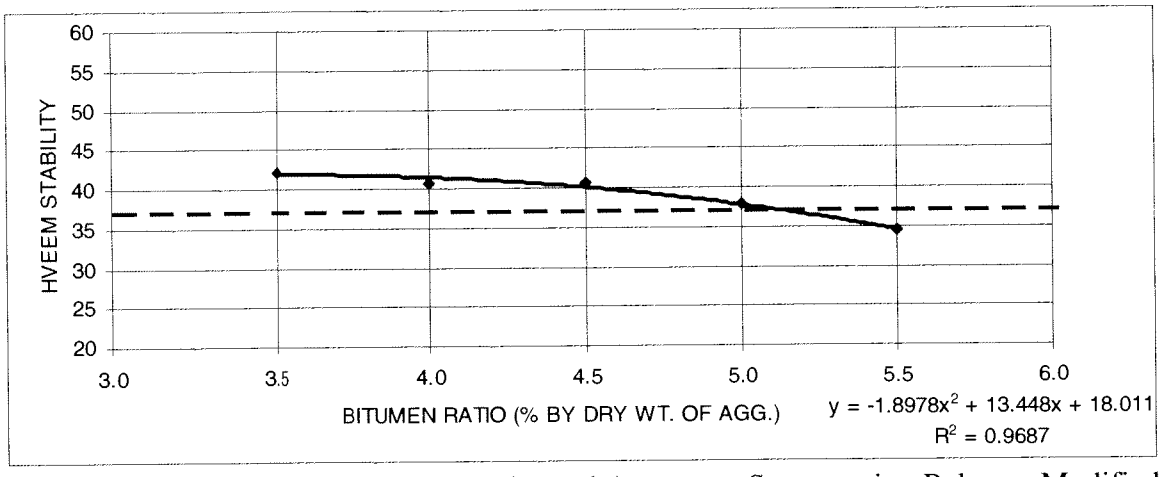

Figure 32 Hveem Stability for the Lockwood Aggregate Source using Polymer Modified Binder.

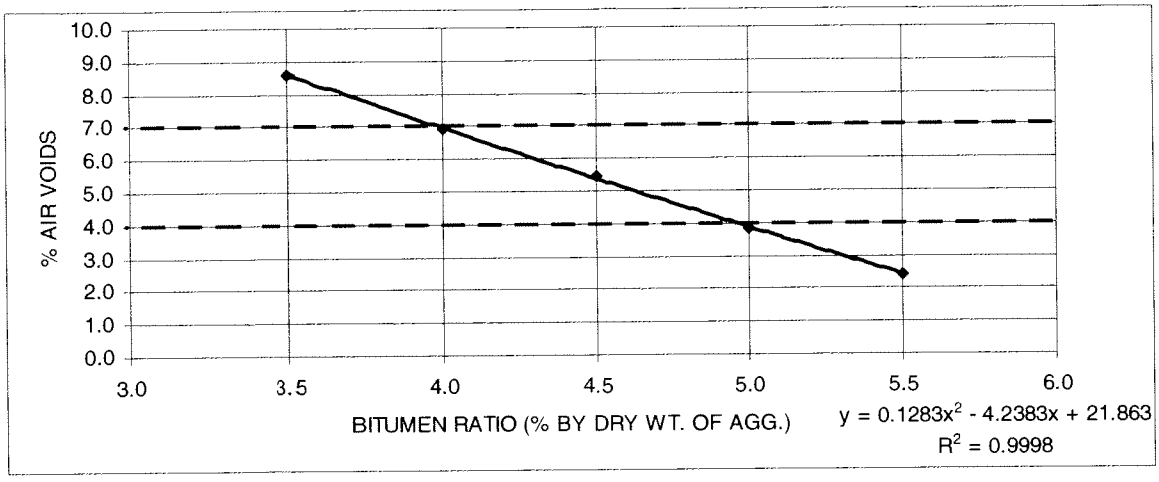

Figure 33 Percent Air-Voids for the Lockwood Aggregate Source using Polymer Modified Binder.

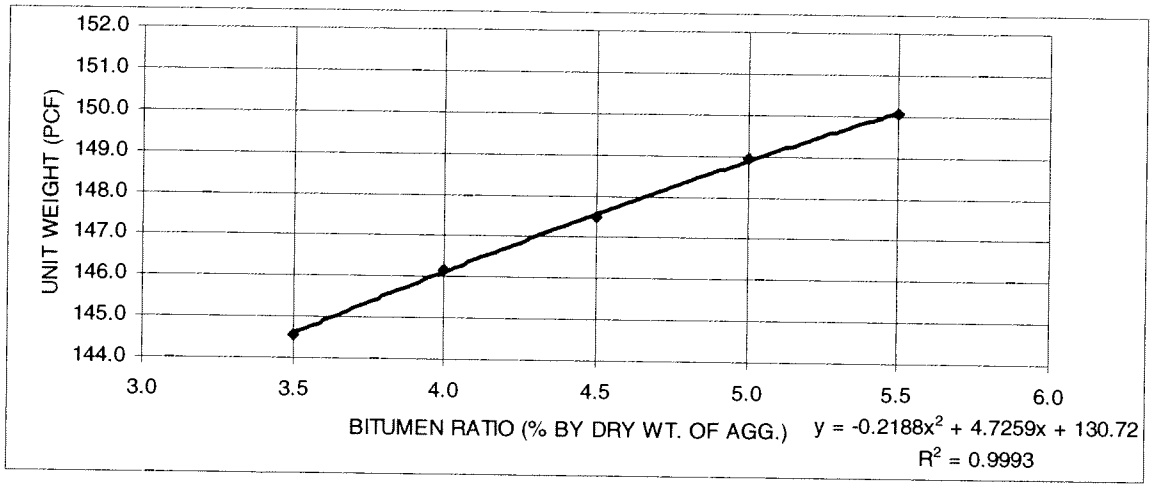

Figure 34 Unit Weight for the Lockwood Aggregate Source using Polymer Modified Binder.

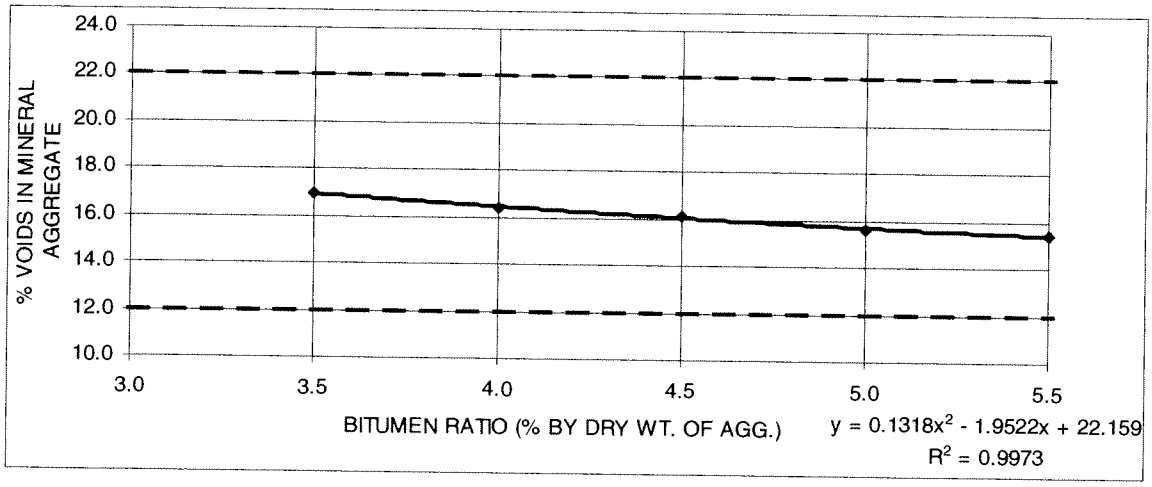

Figure 35 Percent VMA for the Lockwood Aggregate Source using Polymer Modified Binder.

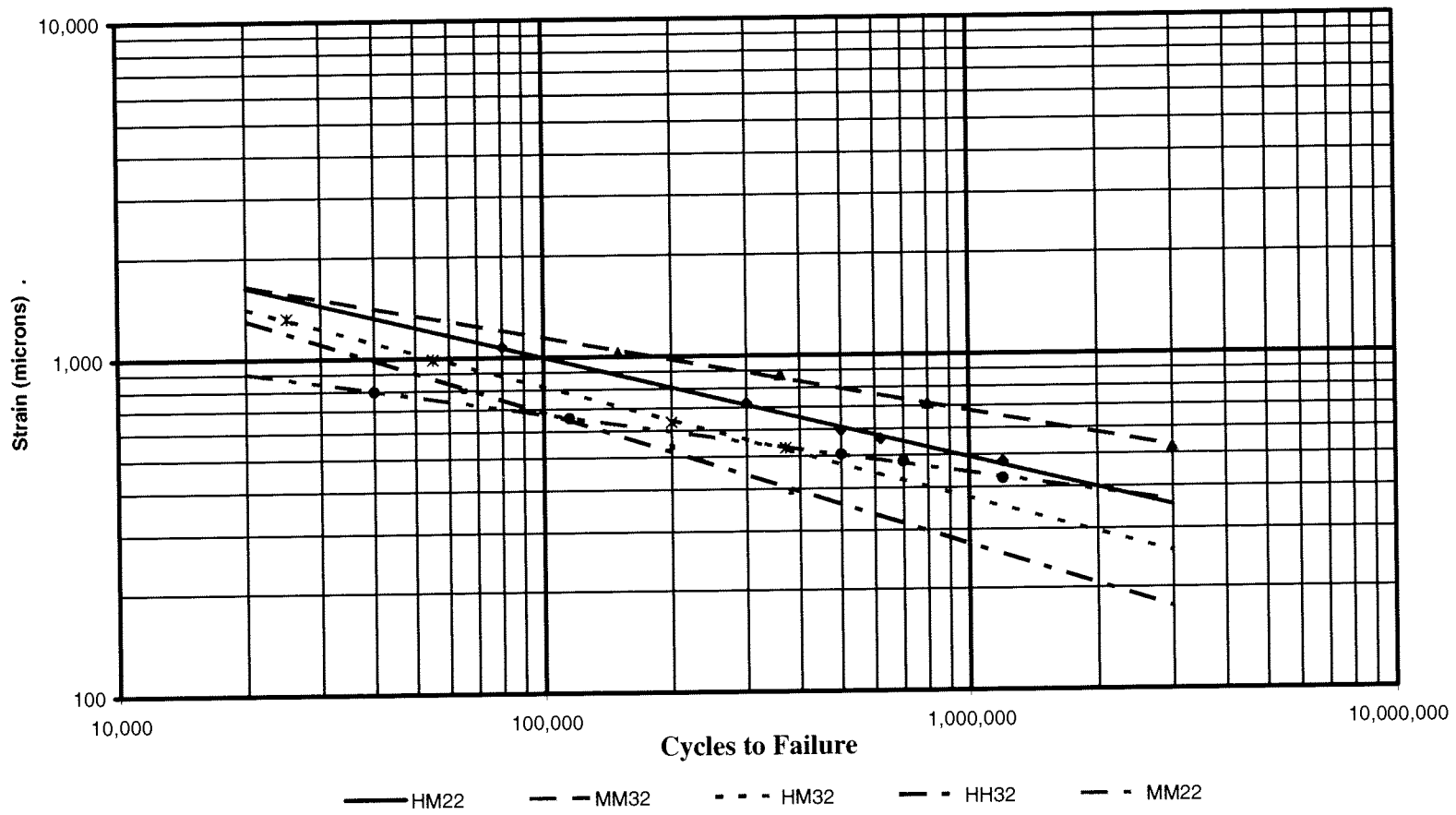

Figure 36 Fatigue Relationships of the Lockwood Aggregate Source using Polymer Modified Binder.

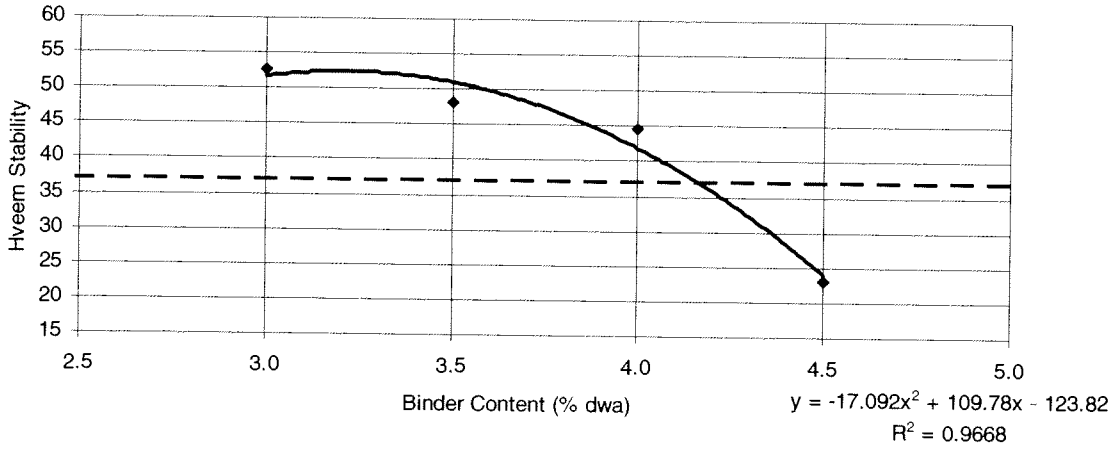

Figure 37 Hveem Stability for the Sloan Aggregate Source using Polymer Modified Binder.

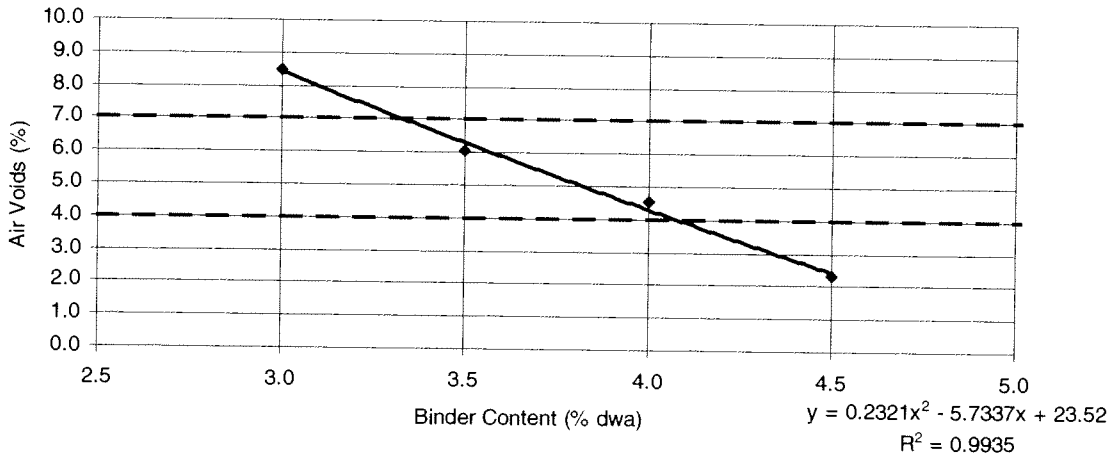

Figure 38 Percent Air-Voids for the Sloan Aggregate Source using Polymer Modified Binder.

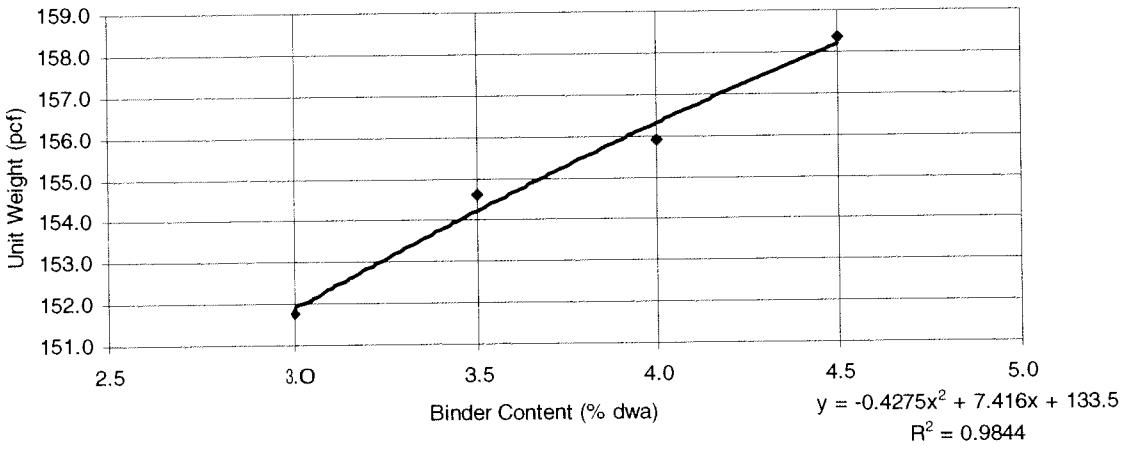

Figure 39 Unit Weight for the Sloan Aggregate Source using Polymer Modified Binder.

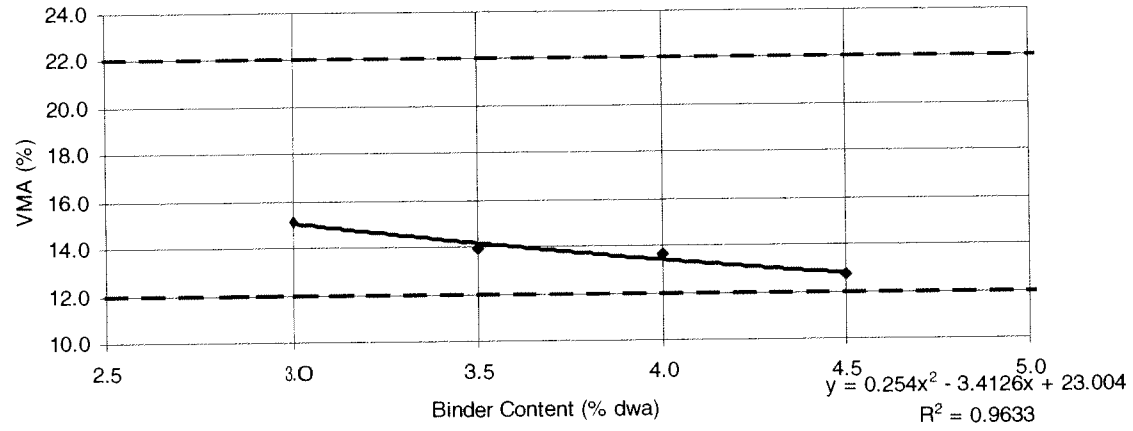

Figure 40 Percent VMA for the Sloan Aggregate Source using Polymer Modified Binder.

Kenny C. Guinn, Governor

Jeff Fontaine, P.E. Director
Prepared by Research Division
Tie He, Research Division Chief
(775) 888-7803
the@dot.state.nv.us
1263 South Stewart Street
Carson City, Nevada 89712